The Dissertation Committee for Michael Dean Stewart Certifies that this is the approved version of the following dissertation:

Catalyst Diffusion in Positive-Tone Chemically Amplified Photoresists

Committee:

C. Grant Willson, Supervisor

David T. Allen

John G. Ekerdt

Isaac C. Sanchez

Stephen E. Webber

Catalyst Diffusion in Positive-Tone Chemically Amplified Photoresists

by

Michael Dean Stewart, B.E.

Dissertation

Presented to the Faculty of the Graduate School of

The University of Texas at Austin

in Partial Fulfillment

of the Requirements

for the Degree of

Doctor of Philosophy

The University of Texas at Austin

December, 2003

Dedication

To my parents.

Acknowledgements

First, I would like to thank my dissertation committee members, Professors Allen, Ekerdt, Sanchez, Webber, and Willson for their help and suggestions. I would also like to thank the many other people who helped me through my course of graduate study. Special thanks must go to the undergraduate students who worked for/with me and actually performed many of the experiments gathered in this dissertation. They are Mark A. Nierode, Timothy B. Stachowiak, and Darren J. Becker. I also had the privilege to work a summer with Michael Graves, a Westlake High School student. I thank Sergei V. Postnikov, my predecessor on this project. I owe a tremendous debt of gratitude to my friend Sergei for showing the way forward on this project. The entire Willson group has always been a tremendous resource and I thank them all, past and present, collectively. Individually, I would like to thank former graduate students Hoang Vi Tran, Mark H. Somervell, Brian C. Trinque, Gerard M. Schmid, and Sean D. Burns all of whom were close collaborators on some aspect of this thesis. I also would like to especially thank Dr. Willson for being such a dedicated teacher and understanding friend. Finally, I must thank my parents, Tom and Joy, and my sister, Stacy, for putting up with, taking care of, and supporting me through the years. By far, they have done more for me than I ever deserved.

Catalyst Diffusion in Positive-Tone Chemically Amplified Photoresists

Publication No._____

Michael Dean Stewart, Ph. D.

The University of Texas at Austin, 2003

Supervisor: C. Grant Willson

The most advanced microelectronic devices of today are manufactured using photoresists that rely on the design concept of "chemical amplification". Rather than using exposure energy to directly cause a solubility switch, chemically amplified photoresists use exposure energy only to generate a catalytic species. The photogenerated catalyst then promotes a solubility-switching chemical reaction in the exposed regions of the photoresist. In this manner, lithographic imaging can be accomplished with very low exposure doses, saving time and money in manufacturing. While chemically amplified resists have many advantages, they have one potential limitation or drawback. It is possible in chemically amplified systems for catalyst generated in exposed regions to diffuse into unexposed regions, causing blurring of the deposited latent image. This blurring effect is an observed fact in microelectronic processing and becomes of

increasing concern as feature sizes shrink. The topic of catalyst diffusion (often referred to as "acid diffusion" because the catalyst in all practical systems has been an acid) has been of concern to microlithography community since the introduction of chemically amplified photoresists in the late 1980's. Since that time it has been a well studied, but poorly understood, phenomenon. This work is an attempt to develop a fundamental, mechanistic understanding of catalyst transport processes in chemically amplified photoresist. It is hoped that a better understanding of the fundamentals of resist performance will eventually lead to better photoresist designs and formulations and thus, faster and cheaper microelectronic devices.

Table of Contents

List of Tables

List of Figures

Chapter 1: Chemically Amplified Photoresists

MICROLITHOGRAPHY INTRODUCTION

Tremendous economic growth has been made possible by the availability of cheap and powerful semiconductor devices. Microchips are now an integral part of a great variety of devices ranging from the mundane to exotic, from wristwatches and cars to satellites and cruise missiles. And of course, the explosive growth of the Internet would never have been possible without the semiconductor industry's ability to continuously provide more computing power at lower prices. As an example of the industry's ability to improve performance while lowering costs one can look at the change in computer memory chips prices over the last decade. In 1993, a $1000 would buy 16 megabytes of computer memory; today over 1000 megabytes can be purchased for the same amount.

The improvement in performance and price of microelectronic devices is mainly the result of the continual shrinkage in the minimum feature dimension that can be printed or etched on a silicon wafer. Since wafer-processing time is essentially independent of feature dimension, printing smaller features allows greater numbers of devices to be printed on the wafer in the same amount of time, thus lowering device-manufacturing costs (at least on a per transistor basis). As well as improving manufacturing yields, smaller feature sizes also improve computing speed by decreasing the distance electrical signals must travel in the device.

There are many different steps necessary for the construction of an integrated circuit device, but it is the photolithographic step that has historically limited the minimum printable feature size. A schematic of the photolithographic process is presented in Figure 1.1. In this process a photomask, which contains a stencil representation of a device layer, is used to selectively block the transmission of exposure radiation. The light passing through the photomask is collected by a series of lenses and then projected onto a silicon wafer coated with a light sensitive material known as a photoresist. The photoresist undergoes a photochemical reaction that changes its solubility in developer solution. Treatment with a developer solvent produces a three-dimensional photoresist relief image of the photomask pattern on the silicon substrate. Figure 1.2 shows some actual resist images produced by the photolithography. Depending on whether exposure enhances or inhibits photoresist dissolution, the image maybe in either positive or negative tone. The relief image created by photolithography provides patterned access to the underlying substrate and can be used as a mask for other processing steps such as etching, ion implantation, or metal deposition that transfer some aspect of the circuit pattern into the underlying substrate. Typical integrated circuit designs require ten to twenty-five different, precisely patterned, layers stacked one upon the other, to create a functional device.

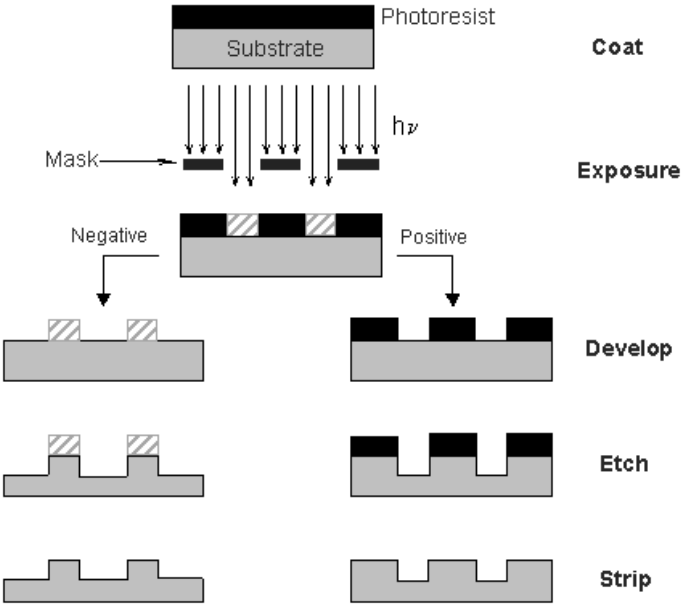

Figure 1.1: The photolithographic process: 1) Substrate is coated with photoresist. 2) Exposure through a mask generates a latent image in the photoresist. 3) Development removes soluble regions, in a positive tone system exposed regions become soluble. 4) Image is transferred into substrate with an etch process. 5) Any remaining photoresist is removed.

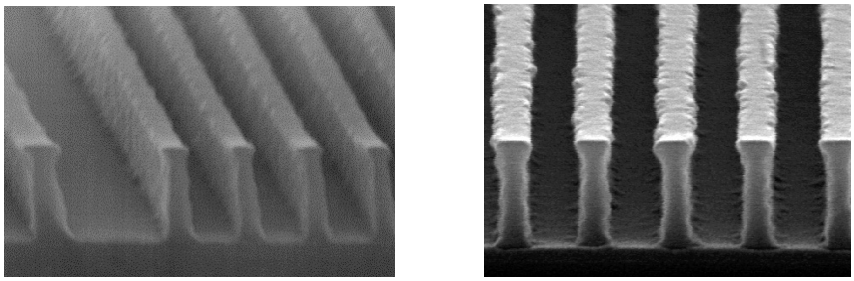

Figure 1.2: SEM micrographs of 3-D resist relief images produced by lithography.

HISTORY OF PHOTORESISTS

The early development of photoresist materials is tied to the development of photography in the early 19th century.[1] The first permanent "photographs" were in fact projection printed photolithographic images. Around 1826, Joseph Niépce pioneered photography by using a polished pewter plate coated with a tar-like photoresist called "bitumen of Judea" to record an image of his courtyard. Bitumen of Judea, which draws its name from its Dead Sea origins, is rendered less soluble by exposure to sunlight so development removes the unexposed regions and reveals the substrate. An image could be permanently recorded by etching into the exposed pewter surface with an acid. This process is an exact analogy with the processes used to manufacture even the most complex microelectronic devices today.

Bitumen of Judea is not an ideal photoresist material because it is not particularly light sensitive; several hours of exposure are required to record an image. A more sensitive photoresist system based on "dichromated gelatin" was developed, and an entire photolithographic industry based on this new photoresist arose in the middle of the 19th century. The reproduction of artwork and papers using printing plates produced by photolithography with this photoresist became a very important industry. Well into the 20th century, the production of printing plates was still almost the exclusive province of photolithography with dichromated gelatin photoresists.

It was dichromated gelatins that were first used as photoresist materials when the photolithography process developed for the printing plate industry was

adapted for manufacturing the first integrated circuit devices. Dichromated gelatins were generally very successful imaging materials, but they did not quite fulfill the demands of integrated circuit manufacturing. Gelatins lack the required resistance to certain acid etches required in IC construction and it became clear that new materials needed to be developed. Even prior to the advent of the IC industry, the printing plate industry had begun investigating alternatives to gelatin-based photoresists because of the presence of a so-called "dark reaction" in the formulated dichromated photoresist. Once formulated, dichromated gelatin photoresists undergo, even in complete darkness, a cross-linking reaction that renders the mixture useless after only a few hours of storage. This storage instability, along with the lack of etch resistance, led to a search for replacements for gelatin-based resists. The solution that emerged was the "bis-azide rubber" photoresists.

These bis-azide rubber photoresists are formulated by mixing photoactive bis-arylazides with low molecular weight synthetic rubbers. When exposed to light the biz-azides cross-link the rubber resin making it insoluble. The bis-azide compound mixed with cyclized poly(cis-isoprene) was the photoresist system of choice in semiconductor manufacturing for about 15 years, from the late 1950's to the early 1970's.

The lithographic resolution with biz-azide rubber photoresists was limited to about 2 microns; smaller features were not possible due to fundamental limitations of the photoresist material design. These resists work by simply cross-linking the rubber matrix resin, so swelling of the exposed regions during

development with organic solvents is an inescapable problem. The cross-linked regions are insoluble in developer solvent, but swelling of cross-linked areas due to solvent absorption still occurs and it is this swelling that limits resolution. Printing dimensions below 2 microns required new photoresists materials that did not suffer the inherent limitations of the bis-azide resists. These new materials were found already in use in the printing plate industry. A positive-tone photoresist consisting of diazonaphthoquinone (DNQ) molecules blended into novolac resin had been developed in the 1950's.[2] Figure 1.3 gives the chemical structure of the components in a DNQ/novolac system. The DNQ molecules inhibit dissolution of the novolac resin material in aqueous base solutions, but upon exposure to ultraviolet light the DNQ molecules undergo a rearrangement and react with water to produce a carboxylic acid photoproduct that enhances dissolution in aqueous base. There is an extremely large difference in dissolution rates between exposed and unexposed regions which, along with a lack of swelling during development, enables high-resolution imaging in DNQ/novolac systems. Photoresists based on this system were highly successful in the semiconductor industry[4] and are still in widespread use for several applications.

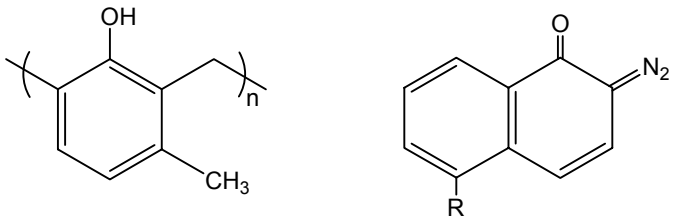

Novolac Resin **Diazonapthoquinone**

Figure 1.3: Generic components of a DNQ/novolac photoresist.

THE RISE OF CHEMICALLY AMPLIFIED PHOTORESISTS

While several factors influence the minimum feature size printable by photolithographic techniques, two of the most important are the wavelength of the exposure radiation and the numerical aperture of the projection lens system. The resolution of a projection-based photolithographic process is governed by the Rayleigh equation:

$$R = k_1 \frac{\lambda}{NA} \qquad \text{(Eqn. 1.1)}$$

where R is the minimum feature width, λ is the wavelength of the exposing radiation, NA is the numerical aperture of the imaging lens system, and k_1 is a process factor generally dependent on the photoresist. The k_1 factor ranges from 0.6 to 0.8 in a typical photolithography process. The numerical aperture (NA) is dependent on the diameter of the lens system and is defined for a given distance between photomask and lens as the sine of the maximum half-angle that the lens can capture, multiplied by the index of refraction of the surrounding media (typically air).

$$NA = \ell_{gap} \times Index \times Sin\left(\frac{\theta \max}{2}\right) \qquad \text{(Eqn. 1.2)}$$

As seen in equation 1.1, there are generally two paths to smaller features – shorter wavelengths and higher numerical apertures – and both paths have been and continued to be pursued, but neither of these pathways is without drawbacks. Larger lenses required for higher numerical aperture imaging systems are difficult to grind and therefore more expensive and moving to shorter wavelengths often means finding new exposure sources and/or photoresist materials, which can be costly and time consuming. Both pathways to higher resolution also negatively

affect process latitude by altering the depth of focus (DoF) of the optical imaging system. The depth of focus of a photolithographic system can be shown to vary according to the following equation:

$$DoF = \pm \frac{\lambda}{2(NA)^2} \qquad \text{(Eqn. 1.3)}$$

where the variables λ and NA are defined the same as in Eqn. 1.1. As can be seen in Eqn. 1.3, the penalty in DoF for moving to higher numerical apertures is greater than the penalty for the same improvement in resolution achieved by decreasing exposure wavelength.

Over its history, semiconductor lithography has progressively moved to shorter and shorter exposure wavelengths to improve imaging resolution. In the beginning of semiconductor lithography, high-pressure mercury arc lamps were the exposure source of choice. Figure 1.4 shows a typical output spectrum of a mercury arc lamp. These lamps provide high intensity light in the ultraviolet region at relatively low cost. Due to problems with chromatic aberration in lens imaging systems, it is necessary to use a fairly narrowly defined exposure band, so only a small portion of the exposure source output spectrum can be used at once. The output spectrum of a mercury arc lamp has several characteristic emission peaks and semiconductor lithography has systematically worked its way through these peaks to lower wavelengths to improve resolution. The last strong characteristic emission peak of a mercury arc lamp occurs at 365 nm (I-line). I-line lithography using DNQ/novolac photoresists is capable of printing sub-micron device features and this technology carried the semiconductor industry into the early 1990's.

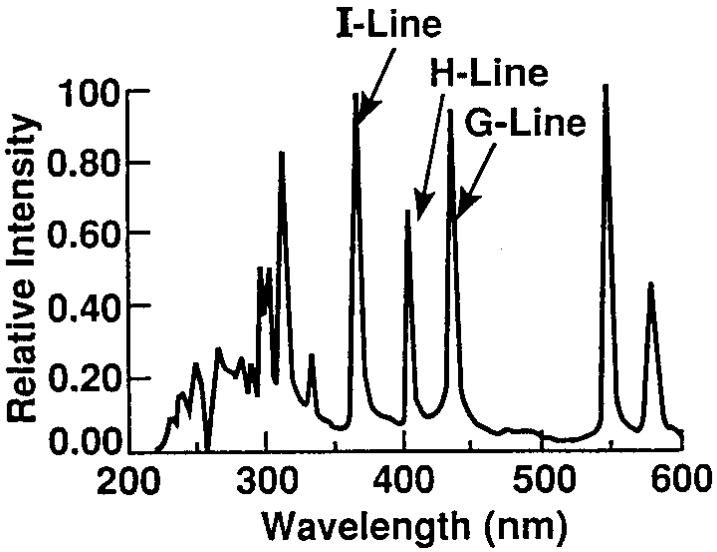

Figure 1.4: Typical output spectrum high-pressure mercury arc lamp.

As seen in Figure 1.4, the output intensity of a mercury arc lamp begins to drops off drastically in the "deep ultraviolet" region below about 300 nm. The output intensity of a mercury arc lamp in the deep ultraviolet region is about two orders of magnitude less than the mid-ultraviolet region. Improving resolution by moving into the deep ultraviolet exposure region required either brighter exposure sources or more sensitive photoresists if process throughput was to be maintained. Brighter sources were eventually developed in the form of excimer lasers, but it was found that high-sensitivity photoresists were still needed because high-intensity laser pulses damage the expensive optical components of production tools.[5,6] A high sensitivity photoresist helps increase the service lifetime of the expensive imaging optics.

One approach to designing a high sensitivity resist system is to use the principle of "chemical amplification". In a chemically amplified system, exposure photons do not directly cause a solubility switching reaction event; rather, they are used to generate a stable catalytic species. The photogenerated catalyst then initiates a chain reaction or promotes a cascade of reactions that changes resist solubility in exposed regions. The apparent quantum efficiency for the solubility switching reaction in such a resist system is the product of the quantum efficiency for catalyst generation and the catalytic chain length. Catalytic chain lengths in the many hundreds are common, so in effect the apparent quantum efficiency can be much, much greater than one. One photochemical conversion can cause several chemical reactions, and thus the exposure can be said to have been "chemically amplified".

The first chemically amplified systems for DUV photolithography were designed in the early 1980s.[7-10] These resist systems were based on the phenolic polymer poly(4-hydroxystyrene) (PHS) and its t-butyl carbonate (t-BOC) protected analog poly(4-t-butyloxycarbonyloxystyrene) (PTBOC). The principles behind this design have been used in the development of almost all subsequent photoresists. In this system imaging contrast was provided by the difference in dissolution rate of the t-BOC protected polymer and the unprotected polymer in certain solvents. By changing developer solvents the system could be imaged in either positive or negative tone. For example, in an aqueous base developer the protecting group slows dissolution allowing for positive tone imaging, while an organic solvent such as anisole gives negative tone imaging.

Imaging occurs by selectively removing protecting groups in exposed regions to modulate solubility. This deprotection is accomplished by exploiting the acid catalyzed thermolysis of the t-BOC group (Figure 1.5). Upon DUV exposure, catalytic amounts of acid are generated from a photoacid generator (PAG) dispersed in the polymer matrix. Exposure creates at latent image of acid and a short (1 - 2 minute) bake at a temperature around 100 ºC is required for the actual deprotection reaction to occur. The PAG used in this system can be any one of several onium salts, first reported by Crivello in the late 1970s[11] and recently reviewed[12]. Figure 1.6 shows the mechanism of photoacid generation from a typical onium salt (triphenylsulfonium). The catalytic chain length of in this "t-BOC" resist is extremely long, and can, therefore, be imaged at doses two order magnitudes lower than any previous systems.[13]

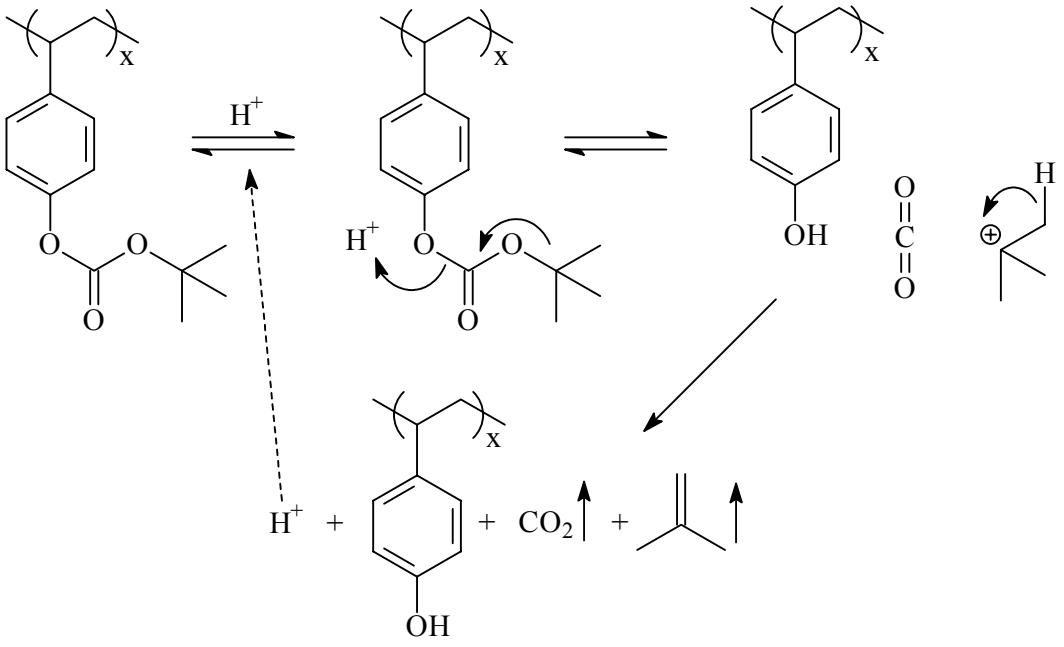

Figure 1.5: Catalytic deprotection reaction of tBOC-based photoresist.

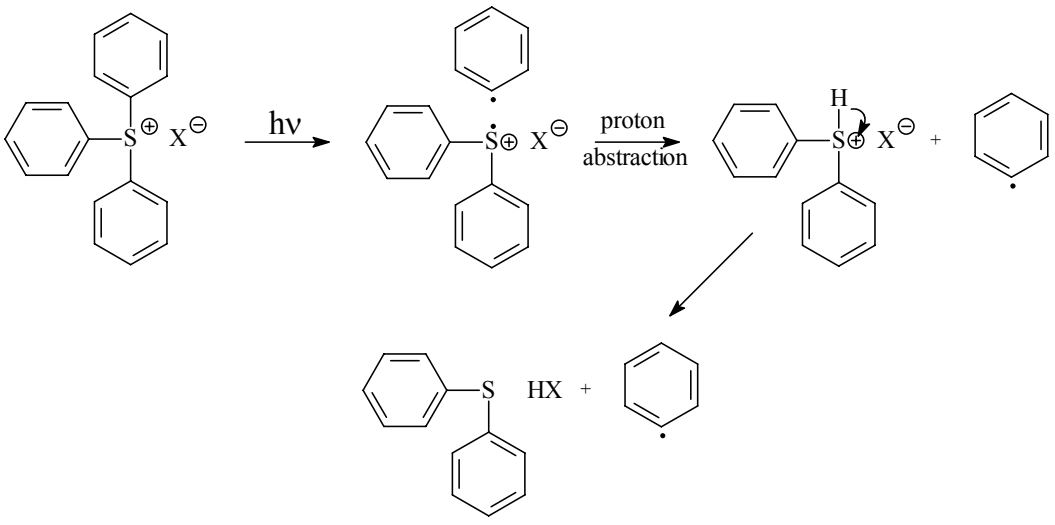

Figure 1.6: Mechanism of photoacid generation from onium salt.

ISSUES WITH CHEMICAL AMPLIFICATION

Chemical-amplification solves the sensitivity problem, but it can cause other problems. For example, the acid catalyst with its long catalytic chain length is susceptible to poisoning by base contaminates gettered from the atmosphere. Catalyst poisoning by atmospheric base contamination was a largely unforeseen problem, but it turned out to be very significant in early production. Even in the controlled atmosphere of a cleanroom with atmospheric base levels in parts per billion, contamination caused unacceptable processing variations in early t-BOC based systems.[14, 15] Atmospheric base contamination can also cause the more dramatic "T-topping" effect (Figure 1.7) when the acid generated in the resist's top layer is neutralized by contamination, preventing full deprotection at the resist-air interface. These contamination problems made it necessary to isolate resist-coated wafers from the regular cleanroom atmosphere and protect them with expensive filter and containment systems.

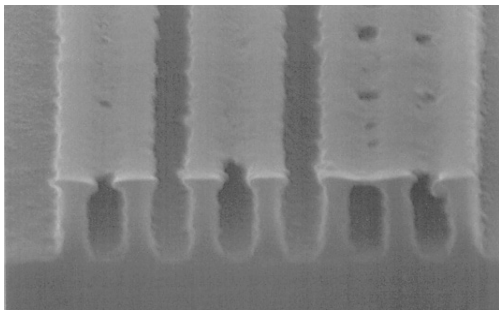

Figure 1.7: "T-topping" in a chemically amplified photoresist

Another way to avoid "T-Topping" is to tailor the background dissolution rate of the unexposed resist. In effect, by giving the matrix resin a finite dissolution rate, the base contaminated layer, which would normally cause the "T-topping", can just be dissolved away during development. The improvement in environmental stability more than compensates for small losses in resist thickness. The first resist system to incorporate a tailored background dissolution rate to improve environmental stability was IBM's APEX resist, which is simply a random copolymer of PHS and PTBOC.

These problems with atmospheric contamination caused several groups to begin development of new photoresists that would be less sensitive to their surroundings. The ESCAP resist developed in early 1990's was one particularly successful approach to lessening environmental sensitivity.[16, 17] Incorporation of *tert*-butyl acrylate to replace *tert*-butyloxycarbonyloxystyrene gave the resist a thermal decomposition temperature above its glass transition temperature (T_g). With a T_g below their thermal decomposition temperature, the ESCAP-class resists can be annealed above their T_g after spin-coating to remove excess free volume and densify the film. Removing free volume improves environmental stability by lowering the diffusion rate of contaminates into film. Previous systems thermally decomposed prior to reaching a glass transition temperature so no above-T_g annealing was possible. Changing to *tert*-butyl acrylate also improved environmental stability by lowering the solubility of base contaminates in the resist film.

Another potential problem for chemically amplified photoresist is the so called "critical dimension bias" problem or catalyst diffusion problem. The diffusion problem arises from the nature of the chemically amplified photoresists; a catalyst that is mobile enough to promote several hundred reactions can also move from nominally exposed regions into nominally unexposed regions and, thus, cause imaging resolution loss. Much effort is put forth in imaging system design to deposit light into as small as region as possible and any migration of the catalyst out of the regions of deposited light partly decouples the final developed image from the projected image. Many people predicted that the resolution in chemically amplified resists would be very poor due to catalyst diffusion, but this has not yet proven to be the case. Studies using extremely fine (2 nm) electron beam exposures have shown that the ultimate resolution of the t-BOC resist system is around 40 nm when processed in positive tone.[18,19] Other studies have shown that line-width spread by catalyst migration is self-limiting.[20,21] The reported self-limiting nature of line-width spread has led to debate about the actual mechanisms responsible for acid diffusion/transport in chemical amplified resist systems.[18-22] The work discussed in this dissertation thesis was done to develop an understanding of the transport mechanisms responsible for catalyst migration in chemically amplified systems.

LITHOGRAPHY AFTER OPTICAL LITHOGRAPHY

Production of the most commercially available microdevices is currently being carried out in the deep ultraviolet (DUV) at a 248 nm exposure wavelength,

which corresponds to the output a krypton-fluorine (KrF) excimer laser. Increasingly, certain critical device layers for advanced devices require the use of 193 nm exposure. Features not much larger than 100 nm are routinely being produced in manufacturing using 193 nm resists. This wavelength is expected to allow production of devices with features down to at least a 100 nm. Production of sub-100 nm devices is expected to require another wavelength decrease down to 157 nm exposure (fluorine excimer laser).

Many believe that photolithography with 157 nm light will be the last optical lithography technology developed. The industry is counting on one of the NGL (next generation lithography) alternatives such as extreme ultraviolet (EUV), or electron beam projection (i.e. SCALPEL) to emerge to replace optical lithography for sub-100 nm device production. The change over to any of these processes will require development of new high-resolution resist materials. As mentioned previously, the apparent resolution limit for the classical chemically amplified tBOC resist system was determined to be about 40 nm.[19] Printing a 50 nm feature in this material would be a difficult task for any NGL if there is already 40 nm of intrinsic resist bias. Other chemically amplified resist systems might have lower intrinsic bias, but interestingly it is exceedingly rare to see features (nested lines at least) printed by any lithographic method in a chemically amplified photoresist less than 30-50nm, suggesting perhaps a resolution barrier in this resist type. Even in if intrinsic bias is only 10nm, it might seriously affect manufacturing process latitude for sub-50nm lithography. Ways to improve resist resolution by limiting catalyst migration are under investigation, but to maintain

chemical amplification the catalyst must maintain some amount of mobility, and any amount of catalyst mobility will lead to some loss of resolution. This trade-off requires more study.

REFERENCES

1. C.G. Willson, R.A. Dammel, A. Reiser. *Proc. SPIE*, 1997; **3051**, 28.

2. R.A. Dammel, *Diazonapthoquinone-based Resists*, SPIE Optical Engineering Press: Bellingham, WA, 1993**.**

3. L.F. Thompson, C.G. Willson, M.J. Bowden, *Introduction to Microlithography*, American Chemical Society, Washington D.C., 1994.

4. A. Reiser, *Photoreactive Polymers – The Science and Technology of Resists*, J. Wiley & Sons, New York, 1989**.**

5. D.J. Ehrlich, M. Rothschild. *Microelectronic Eng.* 1989; **9**, 27.

6. R.E. Schenker, L. Eichner, H. Vaidya, S. Vaidya, W.G. Oldham. *Proc. SPIE*, 1995; **2440**, 118.

7. J.M.J. Fréchet, H. Ito, C.G. Willson. *Proc. Microcuit Eng*. 1982; 260.

8. H. Ito, C.G. Willson. *Polym. Eng. Sci.* 1983; **23**, 1012.

9. H. Ito, C.G. Willson, *Polymers in Electronics*; T. Davidson, Ed.; ACS Symposium Series 242, American Chemical Society, Washington D.C. 1984.

10. H. Ito, C.G. Willson, J. M. J. Fréchet. U.S. Patent 4,491,628, 1985.

11. J.V. Crivello, J. H. Lam. *J. Polym. Sci.: Polym Chem. Ed.* 1979; **17**, 977.

12. J.V. Crivello. *J. Polym. Sci. A,* 1999; **37***,* 4241.

13. S.A. MacDonald, C.G. Willson, J.M.J. Fréchet. *Accounts Chem. Res.* 1994; **27**, 150.

14. O. Nalamasu, E. Reichmanis, J.E. Hanson, R.S. Kanga, L. A. Heimbrook, A.B. Enerson, F.A. Baiocchi, S. Vaidya. *Polym. Eng. Sci.* 1992; **32**, 1565.

15. S.A. MacDonald, W.D. Hinsberg, H.R. Wendt, N.J. Clecak, C.G. Willson, C.D. Snyder. *Chem. Mater*. 1993; **5**, 348.

16. H. Ito, G. Breyta, D. Hofer, R. Sooriyakunaran, K. Petrillo, D. Seeger. *J. Photopolym. Sci. Technol.* 1994; **7**, 433.

17. G. Breyta, D.C. Hofer, H. Ito, D. Seeger, K. Petrillo, H. Moritz, T. Fischer. *J. Photopolym. Sci. Technol.* 1994; **7**, 449.

18. C.P. Umbach, A.N. Broers, C.G. Willson, R. Koch, R.B. Laibowitz. *J. Vac. Sci. Technol. B,* 1988; **6**, 319.

19. C.P. Umbach, A.N. Broers, C.G. Willson, R. Koch, R.B. Laibowitz. *IBM J. Res. Dev.* 1988; **32**, 454.

20. M. Zuniga, G. Wallraff, E. Tomacruz, B. Smith, C. Larson, W.D. Hinsberg, A.R. Neureuther. *J. Vac. Sci. Technol. B*, 1993; **11**, 2862.

21. S.V. Postnikov, M.D. Stewart, H.V. Tran, M. A. Nierode, D.R. Medeiros, T. Cao, J. Byers, S.E. Webber, C.G. Willson. *J. Vac. Sci. Technol. B*, 1999; **17**, 3335.

22. G.M. Wallraff, W.D. Hinsberg, F.A. Houle, M. Morrison, C.E. Larson, M. Sanchez, J. Hoffnagle, P.J. Brock, G. Breyta. *Proc.* SPIE, 1999; **3678**, 138.

23. E. Croffie, M. Cheng, A. Neureuther. *J. Vac. Sci. Technol. B*, 1999; **17**, 333.

Chapter 2: Diffusion in Polymers

Understanding diffusion in polymers begins with a more general understanding of transport phenomena. At the most basic level, diffusion results from random molecular motion. Consider, for example, a simple gas phase system in which thermal energy manifests itself largely as translational motion of the individual gas molecules. For a given system temperature, the statistical distribution of molecular velocities can be calculated, but the velocity of any specific molecule in the system is incalculable. The velocity (speed and direction) of each individual gas molecule is random and unpredictable except in a general, statistical sense. In a homogeneous system, molecules, on average, have no directional preference. The path taken by an individual molecule is often referred to as a "random walk". In the gas phase a molecule's random walk results from collisions with other molecules in the system and all molecules in the system are simultaneously taking there own random walks. In an isotropic system, since molecules do not have preferred travel directions, no net transport (of mass, heat, or momentum) occurs. When the system is inhomogeneous all molecules still take random walks, but now the net result will be transport in directions that remove system inhomogeneities (in mass, heat, or momentum). In an inhomogeneous system, individual molecules still do not have directional preferences, but because of an uneven initial distribution net transport will occur over time in directions that tend towards a homogeneous system. That is gradients in concentration will tend to disappear in time.

FICKIAN DIFFUSION MATHEMATICS

In the case of mass transfer, the concept of concentration-driven diffusion was first formalized by Fick in 1855. In an analogy with the process of heat transfer, as first mathematically described by Fourier, Fick stated that the net rate of mass transfer of a substance through a given unit area is proportional to concentration gradient of the substance measured normal to a unit area. Often referred to as Fick's First Law, the equation that follows is the mathematical basis for most diffusion analysis:

$$F = -D\left(\partial C \diagup \partial x\right) \qquad \text{(Eqn. 2.1)}$$

where F is the net rate transfer of material across a given unit area, known as the flux, C is the concentration of a given substance, x is the coordinate direction normal to the plane of interest, and D is a proportionality constant most often referred to as the diffusion coefficient.

When Equation 2.1 is combined with a general material balance on rectangular coordinates a version of what is usually called Fick's Second Law results:

$$\frac{\partial C}{\partial t} = D\left(\frac{\partial^2 C}{\partial x^2} + \frac{\partial^2 C}{\partial y^2} + \frac{\partial^2 C}{\partial z^2}\right) \qquad \text{(Eqn. 2.2)}$$

where C and D are as above and t is time.

Fick's Laws are very powerful and together can be used to solve a vast number of transport problems. In fact, many problems have already been solved and solutions are available standard textbooks.[1] In a later chapter experimental results will be compared to some common textbook solutions.

DIFFUSION IN GASES, LIQUIDS, AND SOLIDS

Diffusion in the gas phase is conceptually the simplest to understand as most intermolecular interactions present in other phases can be ignored. Collisions between gas molecules are comparatively rare and can often be well modeled as simple "hard sphere" interactions. In the liquid phase, diffusion processes are very similar to gas phase diffusion in that even while liquid molecules are strongly interacting, the motion and arrangement of liquid molecules is random (or at least chaotic). Diffusion in solids is more difficult to understand than diffusion in gas or liquid phase and several theories concerning diffusion in solids have been put forth. The close packed atoms of a solid present much less opportunity for significant translational motion and diffusion in solids often occurs extremely slowly. The simplest type of solid is the crystalline solid and for conceptual simplicity all types of solids are often modeled as rigid crystal lattices. In a crystalline solid the presence of lattices defects (especially vacancies) is considered to be a main diffusion pathway. As seen in Figure 2.1, diffusion in the crystalline case can be thought of as process of vacancy or "hole" hopping. The vacancies can be either fixed or mobile depending on the conditions. Another pathway available for atoms or very small molecules is interstitial diffusion, where, as shown in Figure 2.2, the smaller molecule moves through the space between lattice sites. Even in amorphous, non-crystalline solids, diffusion can be thought of analogous to the crystalline case, only with a non-uniform, irregular quasi-lattice configuration.

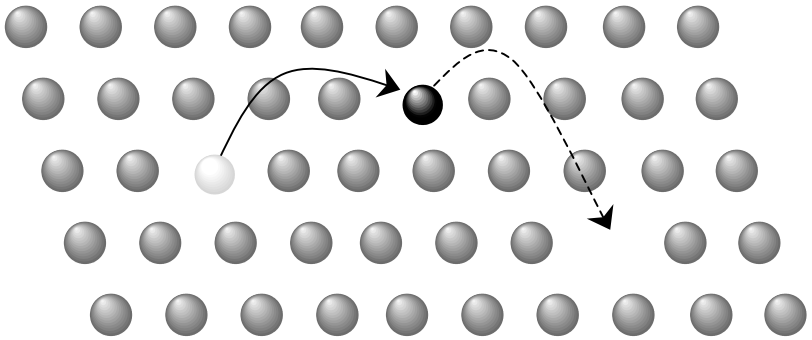

Figure 2.1: "Hole hopping" crystal lattice diffusion

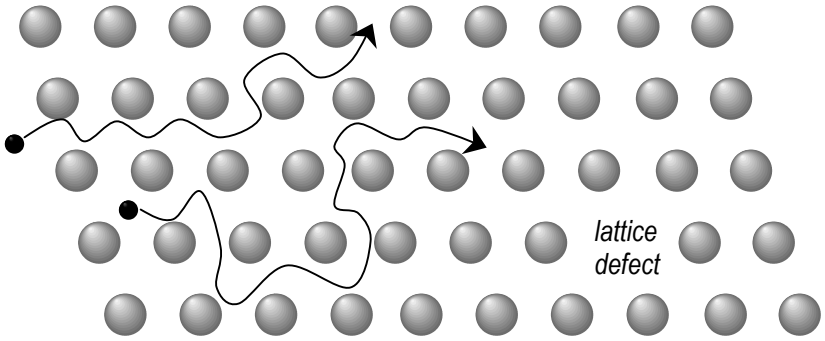

Figure 2.2: Interstitial diffusion in a crystal lattice by small molecules

DIFFUSION IN POLYMERS

Polymers are often considered a special topic in diffusion analysis since polymers are an intermediate case between liquids and solids. A polymer above its glass transition temperature is in a rubbery, pseudo-liquid state, while a glassy

polymer, a polymer below its glass transition temperature, behaves much like a solid. Higher mobility of polymer segments in a rubber creates many more opportunities for a penetrant molecule to make its way through the polymer. A rubbery polymer in many respects can be thought of as a highly viscous liquid, but a rubbery polymer is not a liquid and as such molecular motion is not as free as in a liquid phase or polymer melt. Even in a rubbery condition, molecular motion is still restricted such that connected polymer segments must coordinate their motion to allow a penetrant to diffuse. A variety of coordinated moves are available such as chain-end flexing and reptation, but the move that is usually considered to separate the glassy state from the rubbery state is *crank-shaft rotation* depicted in Figure 2.3.

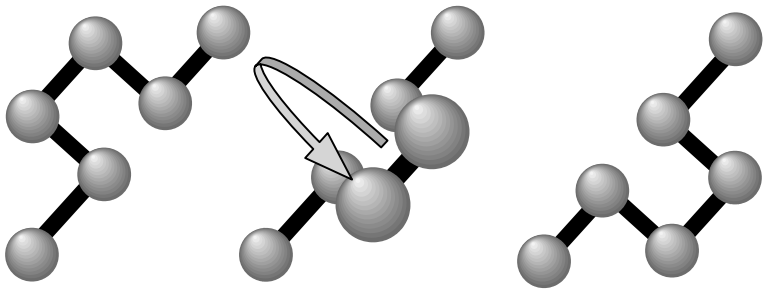

Figure 2.3: Crank-shaft rotation in polymers.

In a glassy polymer with restricted segmental mobility, it is not completely clear how penetrant diffusion should be best understood. Barrer[2] suggested the *hole theory* of diffusion in amorphous polymers. In this concept, much like lattice vacancies in a crystal lattice, discrete voids or holes exist in a polymer matrix through which penetrants must travel. Generated by thermal vibrations in the

polymer matrix, these discrete holes may be either fixed or mobile. Another perhaps more subtle way to consider diffusion in polymers involves the concept of free volume, initially conceptualized as *microvoids*.[3] It is not necessarily best to think of polymer free volume as discrete holes in the polymer matrix; it is probably more correct to think of free volume, especially in rubbery polymers, as the ability of the polymer to temporarily form voids or holes in the matrix. Free volume includes both the interstitial volume and the void volume found in a lattice system, but, unlike in a rigid crystal lattice, its location and size may fluctuate throughout the polymer matrix with time. The location and size distribution of free volume is a statistically determined function of temperature. The inherent flexibility of the polymer chain, the mobility of chain side groups, the thermal history of the polymer matrix, and the temperature are all known to affect the amount of free volume in a polymer system and, thus, the system's transport properties. Figure 2.4 illustrates the concept of free volume in an amorphous polymer. Total volume is shown to be the sum of occupied volume and free volume. Free volume is further broken down as interstitial volume and hole volume. Free volume is also shown to increase with increasing temperature.

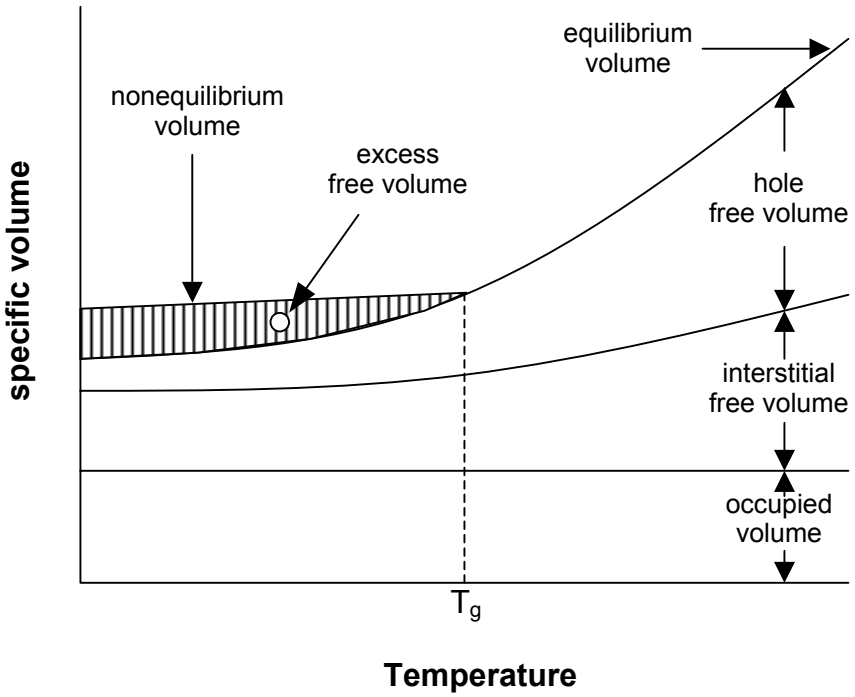

Figure 2.4: Free volume in polymers by component (adapted from Ref. 4 – Kumar 1998)

THE GLASS TRANSITION

Also shown in Figure 2.4 is a temperature, designated T_g, below which non-equilibrium hole volume starts being created. This temperature (T_g) is the glass transition temperature and, as mentioned previously, is temperature at which the polymer switches from glassy to rubbery. The extra, non-equilibrium free volume trapped in a glassy polymer is referred to as *excess free volume*. Annealing glassy polymers can remove excess free volume and change apparent polymer properties. The glass transition is a very important concept in polymer science as many polymer properties are highly dependent on whether the polymer

is glassy or rubbery. Glass transition is often referred to as a *second-order transition*[4], but many believe that this terminology tends to overstate the thermodynamic importance of the glass transition. The glass transition is not a thermodynamic phase change like melting or vaporization (*first order transitions*). The glass transition results from the kinetics of polymer chain rearrangement. There is actually not a sharply defined transition from glass to rubber at one specific temperature; rather, there is a temperature range of transition. The reported T_g value is usually the midpoint of a transition range. The breadth of the range and its midpoint are also actually a function of the cooling or heating rate the polymer sample experiences. Despite the presence of a measurable "glass transition" temperature, both rubbery and glassy polymers are thermodynamically in the same phase state.[5] All polymer molecular rearrangement moves available in rubbery polymers are available in glassy polymers, but the activation energy requirements make some moves less likely below certain temperatures.

CASES OF DIFFUSION

In polymers, diffusion can often be described by the traditional Fickian mathematics of Eqn. 2.1 and Eqn. 2.2. This is especially true in rubbery polymers when segmental motion is fast relative to diffusive motion. Fickian penetration distances change according to the following equation:

$$L = (2Dt)^{1/2} \qquad \text{(Eqn. 2.3)}$$

where L is the penetration distance, D is the diffusion coefficient, and t is time. This normal Fickian diffusion in polymeric systems has been termed *Case I*

diffusion, but there are also many examples of polymer-penetrant combinations that do not exhibit normal Fickian diffusion. For example, toluene diffusing into glassy polystyrene behaves very unlike what is predicted by Case I diffusion. Deviations from Case I behavior can occur because some penetrants cause changes to the surrounding polymer matrix like swelling or plasticization. Swelling or plasticization can change the diffusion properties of the polymer sample and the penetrant may not demonstrate typical Fickian behavior in a macroscopic sense.

When polymer relaxation processes are slow relative to the rate of penetrant diffusion, a situation referred to as *Case II* diffusion can occur. In Case II diffusion, as penetrant molecules sorb into the glassy polymer, the polymer swells and becomes rubbery. Diffusion in a swollen polymer is typically much faster than diffusion in a still glassy polymer. The penetrant concentration gradient across the swollen region is flat and a sharp front between swollen and glassy polymer develops. In Case II diffusion the penetrant front advances according to the following equation:

$$L = kt \qquad \text{(Eqn. 2.4)}$$

where L is the front penetration distance, k is a material dependent constant, and t is time. The physical existence of the Case II front is well documented.[6-8] The definitional features of a Case II front are its sharpness and its constant rate of advancement. The Case II front advances as a linear function of time, while Case I penetration occurs proportional to the square-root of time. Shown in Figure 2.5 is a diagram of Case II diffusion into a polymer membrane. Many penetrant-

polymer combinations produced results that are intermediate between the extremes of clear Case I or Case II diffusion. These intermediate cases are referred to as anomalous diffusion cases and occur when polymer relaxation rates are comparable to penetrant diffusion rates.

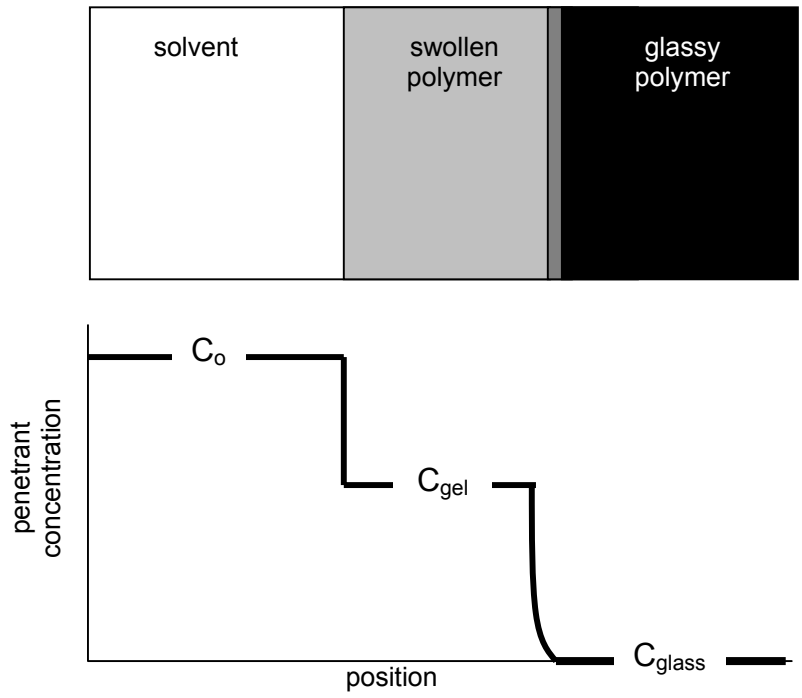

Figure 2.5: Case II diffusion front: Swollen polymer region separated from the glassy polymer region by a very narrow transition zone. Penetrant concentration is constant in all regions other than transition zone.

DESCRIPTION OF PROBLEM

Many types of diffusion problems have been previously solved and solutions for many general problem types have been published. The first thing to

do is to characterize our particular problem to see if it can be classified as one of the previously solved diffusion problems. The specific system of concern to photolithography (and this thesis) involves diffusion which is accompanied by a chemical reaction. Reaction-diffusion problems are also staples of textbooks on transport and kinetics, but our system is not a standard problem type. In the system of our concern, the diffusing molecule is a catalyst and is not a consumed reactant. As the catalyst diffuses, it promotes a reaction which chemically changes the surrounding polymer. The chemical changes in the matrix also change the diffusion properties of the surrounding matrix. The next chapter will demonstrate that for the system under study the reacted polymer matrix has a substantially lower diffusion coefficient than the unreacted matrix. If the reacted matrix had a larger diffusion coefficient than the unreacted matrix, a situation very similar to Case II diffusion would result, but that is not this case.

Because of the change in material properties upon reaction, simple Fickian diffusion with a single diffusion coefficient does not make phenomenological sense. It also does not account for all experimental observations. A non-constant diffusion coefficient, or at least two separate diffusion coefficients for reacted and unreacted polymer, would seem to be required. The possibility of a non-constant diffusion coefficient and its required functional form is a topic in later chapters. It must also be decided which factors to include in the functional description of a non-constant coefficient. Clearly, extent of reaction should be included, but the details of the matrix changing reaction include generation of small molecule, gaseous by-products. The generation of these by-products brings the possibility

of a transient presence of small molecule plasticizers (*i.e*. isobutylene and carbon dioxide) in the polymer matrix. If these by-products do act as plasticizers, then it is possible that the diffusion coefficient will be time dependent because the local concentration of gas by-products may change due to differences in generation and desorption rates. Investigation of the transient presence of reaction by-products in the polymer film will be discussed later in Chapter 5.

PREVIOUS ACID DIFFUSION EXPERIMENTS

Image blur caused by acid diffusion has been a topic of concern to semiconductor industry since the introduction chemically amplified photoresists. Several researchers have investigated aspects of acid catalyst diffusion in various photoresist systems over the last two decades. The majority of early work inferred diffusion coefficients from lithographic results[9-13]; that is the dimensions of printed features were compared to the nominal mask size and any differences between the two were attributed to acid diffusion. The drawback to this approach is that the lithographic process is fairly complex, involving several steps, making it difficult to separate and distinguish contributions to image bias resulting from the different process factors. Diffusion coefficients obtained by these litho-based methods are typically estimated by assuming a simple Fickian relation and rearranging Eqn. 2.3 to give:

$$D = \frac{L^2}{2t} \qquad \text{(Eqn. 2.5)}$$

where D is again the diffusion coefficient, L is the measured diffusion distance, and t is the length of time of diffusion. This is not, *a priori*, a poor assumption,

but experiment has shown that in the some photoresists, different diffusion coefficients will result for different diffusion time scales[14-16]. For short time scales of diffusion (≤ 2 minutes) the apparent diffusion coefficient is relatively large, but with increasing diffusion times the apparent coefficient gets smaller and smaller. A non-constant coefficient suggests the system is more complex than just normal Fickian diffusion. For short or fixed diffusion times, the simplicity of using a single, constant diffusion coefficient may outweigh any problems resulting from inaccuracy in the underlying physical model; for industrial applications it is often more important to have a workable solution than to understand why the solution works or to worry about whether a workable solution truly represents the underlying chemistry and physics of the phenomenon.

Despite the fact normal Fickian diffusion does not explain all experimental observations, several researchers have reported single diffusion coefficients for a variety of photoresists systems. Several researchers have reported diffusion measurements using lithography based measurements, but comparison between data sets is complicated by differences in choices for processing conditions and materials. Several researchers[9-13,17-19] have studied acid diffusion in negative-tone, cross-linking photoresists using measurements of lithographically generated features. Some have used other methods to measure acid diffusivity in negative-tone resists such as scanning probe microscopy on latent resist images[20] and generation of layered structures via sequential spin casting[21,22]. These negative-tone papers generally agree that diffusion coefficients in negative tone resists are a function of extent of reaction (cross-link density), with diffusion decreasing

with increasing cross-linking, but there is not full agreement on the functional form this dependence takes.

Other researchers[15,16,23-26] have used lithographic methods to study acid diffusion in positive-tone photoresists, estimating diffusion coefficients by the Fickian relation of Eqn. 2.5. Another popular method for estimating diffusion coefficients in positive-tone systems is based on ion conductivity measurements[24,25,27,-29]. Other experiments use layered film stacks to study acid diffusion. Layered films may be generated by sequential spin casting[21,30-33], physical stacking (top-to-top) of separately generated films[34,35], or by the film floating techniques[14] (also discussed in detail in Chapters 3 and 4). The diffusion measurements from film stack experiments are usually determined by measuring remaining layer thickness after a development step[21,30-35], but ellipsometric modeling[14] and IR spectroscopy (as discussed in this work) have also been used. A related method that can be used to generated pseudo-stacks from a single film layer was advanced by researchers at IBM[36]. In the IBM method, a single resist layer is exposed at a wavelength that the resist absorbs strongly. The exposure energy attenuates very quickly with film depth, such that only a thin layer at the top of the resist receives significant exposure, so acid is generated only in a thin, upper layer of the resist. The pseudo-stack does not have a sharp boundary between exposed and unexposed layers, but the deposition of exposure energy as a function of depth into the resist can be modeled very accurately. Other experimental methods developed have included fluorescence probe methods, both *in situ*, on-wafer imaging of latent profiles[37-40] and a variation on film stack

experiments[41] used to measure acid vapor diffusion in resist polymers. And a few researchers have simply estimated diffusion coefficients by modeling photoresist reaction kinetics.[42,43]

IONIC CONDUCTIVITY MEASUREMENTS

In the ion conductivity method, diffusion coefficients are measured by coating photoresist films onto interdigitated, micro-sized electrodes to obtain the film's ion conductivity. The ion conductivity of the film is related to the diffusion coefficient of the charged species (presumed to be the acid) in the film by the following equation:

$$D = \frac{\sigma kT}{[H^+]q^2} \qquad \text{(Eqn. 2.6)}$$

where D is the diffusion coefficient, σ is the measured ion conductivity, k is the Boltzmann constant, T is the temperature, q is the diffusing species' ionic charge, and $[H^+]$ is the acid concentration in the film. This method is fairly easy to apply, but often the assumption that the acid is the only ionic species in a photoresist is not actually true. For example, many photoresist formulations, for a variety of reasons, purposely include additives which are basic in nature. Also, ion conductivity measurements can be sensitive to atmospheric base contamination. The requirement to know or measure the concentration of acid in the film is also a complicating factor. Accurately measuring acid concentrations in resist films is extremely difficult because of the very small (nanomolar) quantities involved. Whether because of experimental difficulties or problems with some underlying

physical assumptions, diffusion coefficient values measured by ionic conductivity seldom agree with values obtained by other methods.[24,25]

DIFFERENT PHYSICAL MODELS FOR ACID DIFFUSION

While diffusion coefficients estimated by ionic conductivity measurements and changes in lithographic features tend to disagree, the two methods share common assumptions about the underlying physics of a reacting photoresist. Both methods assume normal Fickian diffusion and that the chemical reaction does not change transport properties of the photoresist. Many researchers realized these simplifying assumptions limited the usefulness and general applicability of results and began to consider more complex, realistic physical models. Perhaps the biggest problem with the physical model represented by a single, constant Fickian coefficient is it does not explicitly take into account changes in materials properties caused by the deprotection reaction. This, intuitively, seems wrong as the starting material (unreacted photoresist) clearly differs significantly from the final product (if the two differed not at all, imaging would be impossible). The protected resin and the unprotected resin differ in, among other things, solvent solubility, glass transition temperature, and hydrophobicity, so why should acid diffusivity be the same in both? A constant coefficient also does not cleanly explain all experimental observations. Changes in feature line width were shown to increase linearly with bake time over short times ($\leq$ 60 sec.).[15,16] This result can be explained with constant Fickian diffusion, but the magnitude of the coefficient must be large. The short time

behavior does not continue indefinitely, in fact, after 60-90 sec. line width change begins to slow rather drastically. This slowing can also be explained by Fickian analysis by including some acid loss mechanism to deplete acid concentration, but then the acid loss mechanisms must be investigated and explained.

An alternative to the constant coefficient is Fickian diffusion with a non-constant coefficient. Equations 2.1 and 2.2 were presented for the case of a non-varying, isotropic diffusion coefficient, but they can be rewritten and considered in more generalized forms. For example, *D* might be a function of time such that Eqn. 2.1 could be written:

$$F = -D(t)\frac{\partial C}{\partial x} \qquad \text{Eqn. 2.7)}$$

where *F*, *C*, and *x* are as before. The question arises, what functional form does *D(t)* take? Most often reaction kinetics are coupled to diffusion such that *D(t)* becomes a function of extent of reaction and not directly time. Researchers have proposed various functions for the diffusion coefficient's dependence on extent of reaction. Linear variation has been suggested[44,45] as has simple exponential variation[35,44,45], but these simple mathematical models lack a compelling physical rational. They can be used to reasonably fit experimental results, but they do not fundamentally explain the system. A reasonably simple model with a physical rational is the Fujita-Doolittle model[46]:

$$D = D_o \exp\left(\frac{\alpha x}{1+\beta x}\right) \qquad \text{(Eqn. 2.8)}$$

where D_o is intrinsic diffusivity of the unreacted photoresist, α and β are experimentally determined, temperature dependent constants, and *x* is the extent

of reaction. This model can be derived from assumptions concerning polymer free volume and has been used previously to explain solvent diffusion in photoresists[47]. Unfortunately, the Fujita-Doolittle model does not explicitly take reaction into account, so it requires modification to represent the system of interest.

Zuniga *et al*. proposed using Case II mathematics to represent reaction and diffusion in photoresists.[16] This was based on one, critically wrong, assumption. Zuniga *et al*. assumed the reacted photoresist had a much higher diffusivity than the unreacted material. Later experiments have determined this is not, in fact, the case. The Case II model also does not explain observed slowing of diffusion at longer times adequately.

Sergei Postnikov[48,49] proposed a variation on the Case II model which has been termed the *Reaction Front Propagation model*. In the Reaction Front model, as in Case II, a relatively sharp boundary between acid containing and non-containing regions is maintained. The reaction is assumed to be rapid such that the photoresist is quickly and completely deprotected in regions where acid is located. Thus, a sharp boundary between regions with acid and without acid implies a sharp boundary between reacted and unreacted regions and therefore the existence of a Case II like front. Unlike Zuniga, Postnikov assumed that reacted regions had lower, not enhanced, diffusivity. The slow diffusivity of reacted regions is used to explain the slowing of the front at longer times. Since the reaction front becomes separated from the main reservoir of acid by band of low-

diffusivity, reacted material the concentration in the front eventually dies out. The Reaction Front Propagation model is depicted schematically in Figure 2.6.

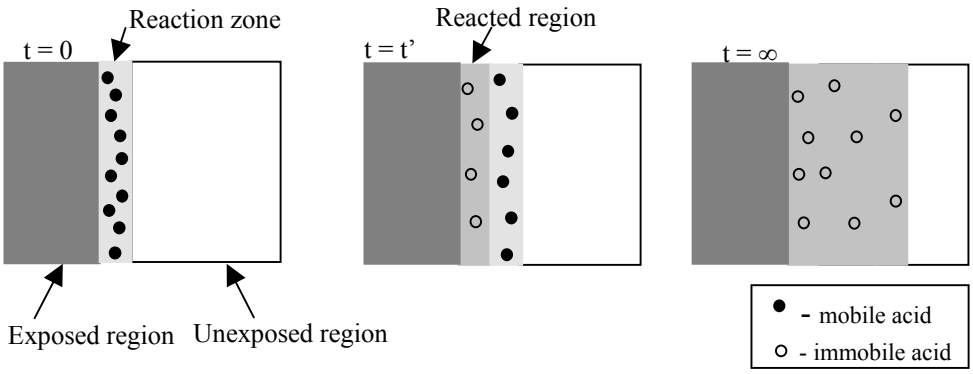

Figure 2.6: Reaction Front Propagation model

Another postulate of the reaction front model is that the deprotection reaction causes a local, transient enhancement to acid diffusivity. The transient enhancement was thought necessary to explain the high initial rates of observed diffusion and feature width changes. Local diffusion enhancement mechanisms might be excess free volume generated by the evolution of gaseous deprotection by-products or plasticization of the polymer caused by lingering gaseous by-products. Another possible, but hard to test, enhancement mechanism could be the exothermic deprotection reaction locally raising the polymer above its glass transition temperature. Of course, some combination of these factors might be jointly responsible.

The Reaction Front model is an attempt to understand the photoresist at a microscopic scale. The concept of reaction enhanced mobility, key to the Reaction Front model, has been implemented in mesoscale computer simulations[50] which have been shown to be in good agreement with experiment. Researchers at IBM have separately come to a concept very similar to reaction enhanced diffusion. They have postulated that acid has a local rate of diffusion and global rate of diffusion which are separate and perhaps result from different mechanisms[43]. In form, this is very similar to suggesting that acid in a reacting photoresist has locally enhanced mobility. The mechanisms of enhancement remain in their analysis unnamed and unexamined. One of the drawbacks of the Reaction Front model is it complexity. It suggests that not only is the diffusion coefficient a function of extent of concentration, but it is also time dependent (and maybe position dependent as well). The complexity makes it very difficult to solve the related reaction-diffusion equations, but researchers at UC-Berkeley have developed a mathematical model based on Moving Boundary Transport that successfully represents the key aspects of the Reaction Front model.[51] With a few simplifying assumptions the resulting system of equations can be solved fairly easily and used to simulate photoresist performance.

DISSERTATION STRUCTURE

This dissertation concentrates on experimental work performed to understand acid transport in positive tone chemically amplified photoresists. While experiments often use polymers of specific interest to the microlithography industry, to some extent, results are more widely applicable to polymer science in

general. Early chapters concentrate on basic diffusion experiments while later chapters apply the understanding gained from early work to more advanced, lithography specific issues. Much of the experimental effort presented in this thesis was done to test the assumptions upon which the reaction front propagation model is based. Chapter 3 describes experiments used determine the acid diffusivity in fully reacted photoresist materials. Chapter 4 describes experiments designed to investigate acid transport in unreacted and reacting photoresists. Chapter 5 investigates the mechanisms thought to cause transient enhancement to acid mobility in a reacting photoresist. Chapter 6 describes experiments that attempt to demonstrate whether a sharp front exists between reacted on unreacted regions. Chapter 7 investigates the more complex lithographic issues of line-end shortening (LES) and line-edge roughness (LER) using experimental methods similar to those developed in earlier chapters. Chapter 8 is a preliminary investigation into whether the reaction front model can be applied to a different, less well understood, photoresist type. The final chapter summarizes conclusions and suggests future work in the areas of molecular transport and photoresist technology.

REFERENCES

1. J. Crank, *The Mathematics of Diffusion*, 2nd ed., Oxford University Press: Oxford, UK, 1975.

2. R.M. Barrer, *Diffusion in and through Solids*, Cambridge University Press: London, 1951.

3. P.J. Meares. *J. Am. Chem. Soc.* 1954; **76**, 3415.

4. A. Kumar, R.K. Gupta, *Fundamentals of Polymers*, McGraw-Hill: New York, 1998, p383.

5. F.W. Billmeyer, *Textbook of Polymer Science, 3rd ed.*, John Wiley & Sons: New York, 1984, p321.

6. F.A. Long, D. Richman. *J. Am. Chem. Soc.* 1960; **82**, 513.

7. N.L Thomas, A.H. Windle. *Polymer*, 1978; **19**, 255.

8. T.E. Alfrey, E.F. Gurnee, W.G. Lloyd. *J. Polym. Sci.* 1966; **C12**, 249.

9. T.H. Fedynyshyn, M.F. Cronin, C.R. Szmanda. *J. Vac. Sci. Technol. B*, 1991; **9**, 3380.

10. T. Yoshimura, Y. Nakayama, S. Okazaki. *J. Vac. Sci. Technol. B*, 1992; **10**, 2615.

11. T.H. Fedynyshyn, C.R. Szmanda, R.F. Blacksmith, W.E. Houck. *Proc. SPIE*, 1993; **1925**, 2.

12. T.H. Fedynyshyn, J.W Thackeray, J.M. Mori. *Microelectron. Eng.* 1994; **23**, 315.

13. P. Zandbergen, H.J. Dijkstra. *Microelectron. Eng.* 1994; **23**, 299.

14. D.S. Fryer, S. Bollepali, J.J. de Pablo, P.F. Nealey. *J. Vac. Sci. Technol. B*, 1999; **17**, 3351.

15. J. Sturtevant, S. Holmes, P. Rabidoux, *Proc*. *SPIE*, 1992; **1672**, 114.

16. M.A. Zuniga, G. Wallraff, E. Tomacruz, B. Smith, C. Larson, W.D. Hinsberg, A.R. Neureuther. *J. Vac. Sci. Technol. B,* 1993; **11**, 2862.

17. I. Raptis. *Jpn. J. Appl. Phys*. 1997; **36**, 17.

18. T. Yoshimura, H. Shiraishi, T. Terasawa, S. Okazaki. *J. Vac. Sci. Technol. B,* 1996; **14**, 4216.

19. N. Glezos, G.P. Patsis, I. Raptis, P. Argitis, M. Gentili, L. Grella. *J. Vac. Sci. Technol. B,* 1996; **14**, 4252.

20. L.E. Ocola, F. Cerrina, T. May. *J.Vac. Sci. Technol. B*, 1997; **15**, 2545.

21. H. Watanabe, H. Sumitani, T. Kumada, M. Inoue, K. Marumoto, Y. Matsui. *Jpn. J. Appl. Phys*. 1995; **34**, 6780.

22. S. Uchino, J. Yamamoto, S. Migitaka, K. Kojima, M. Hashimoto, F. Murai, H. Shiraishi. *J. Photopolym. Sci. Technol.* 1998; **11**, 555.

23. M.A. Zuniga, A.R. Neureuther. *J. Vac. Sci. Technol. B*, 1996; **14**, 4221.

24. T. Fedynyshyn, J. Thackeray, J. Georger, M. Denison, *J. Vac. Sci. Technol. B*, 1994; **12**, 3888.

25. D. Kang, E.K. Pavelchek, C. Swible-Keane. *Proc. SPIE,* 1999; **3678**, 877.

26. J. Nakamura, H. Ban, K. Deguchi, A. Tanaka. *Jpn. J. Appl. Phys. Part 1*, 1991; **30**, 2619.

27. T. Itani, H. Yoshino, M. Fujimoto, K. Kasama. *J. Vac. Sci. Technol. B*, 1995; **13**, 3026.

28. T. Itani, H. Yoshino, S. Hashimoto, M. Yamana, N. Samoto, K. Kasama. *J. Vac. Sci. Technol.* B, 1996; **14**, 4226.

29. T. Itani, H. Yoshino, S. Hashimoto, M. Yamana, N. Samoto, K. Kasama. *J. Vac. Sci. Technol. B*, 1997; **15**, 2541.

30. K. Asakawa. *J. Photopolym. Sci. Technol.* 1993; **6**, 505.

31. D.L. Goldfarb, M. Angelopoulos, E.K. Lin, R.L. Jones, C.L. Soles, J.L. Lenhart, W. Wu. *J. Vac. Sci. Technol. B*, 2001; **19**, 2699.

32. J. Kim, J. Choi, Y. Kwon, M. Hung, K. Chang. *Polymer*, 1999; **40**, 1087.

33. M.D. Stewart, G.M. Schmid, D.L. Goldfarb, M. Angelopoulos, C.G. Willson. *Proc. SPIE,* 2003; **5039**, 415.

34. L. Schlegel, T. Ueno, N. Hayashi, T. Iwayanagi. *Jpn. J. Appl. Phys.* 1991; **11B**, 30; L. Schlegel, T. Ueno, N. Hayashi, T. Iwayanagi. *J. Vac. Sci. Technol. B*, 1991; **9**, 278.

35. M. Zuniga, A.R. Neureuther. *J. Vac. Sci. Technol. B*, 1995; **13**, 2957.

36. G.M. Wallraff, W.D. Hinsberg, F.A. Houle, M. Morrison, C.E. Larson, M. Sanchez, J. Hoffnagle, P.J. Brock, G. Breyta. *Proc. SPIE*, 1999; **3678**, 138.

37. P.M. Dentinger, B. Lu, J.W. Taylor, S.J. Bukofsky, G.D. Feke, D. Hessman, R.D. Grober. *J. Vac. Sci. Technol. B*, 1998; **16**, 3767.

38. B. Lu, J.W. Taylor, F. Cerrina, C.P. Soo, A.J. Bourdillon. *J. Vac. Sci. Technol. B*, 1999; **17**, 3345.

39. C. Coenjarts, J. Cameron, N. Deschamps, D. Hambly, G. Pohlers, C. Scaiano, R. Sinta, S. Virda, A. Zampini. *Proc. SPIE*. 1999; **3678**, 1062.

40. P.L. Zhang, S.E. Webber, J. Mendenhall, J.D. Byers, K. Chao. Proc. SPIE, 1998; **3333**, 794.

41. P.L Zhang, A.R. Eckert, C.G. Willson, S.E. Webber, J.D. Byers. *Proc. SPIE*, 1997; **3049**, 898.

42. A.A. Krasnoperova, M. Khan, S Rhyner, J.W. Taylor, Y. Zhu, F. Cerrina. *J. Vac. Sci. Technol. B,* 1994; **12**, 3900.

43. F.A. Houle, W.D. Hinsberg, M. Morrison, M.I. Sanchez, G.M. Wallraff, C. Larson, J. Hoffnagle. *J. Vac. Sci. Technol. B*, 2000; **18**, 1874.

44. C.A. Mack, *Inside Prolith*, Finle Technologies: Austin, Texas, 1997.

45. J.S. Petersen, C.A. Mack, J. Sturtevant, J.D. Byers, D.A. Miller. *Proc. SPIE*, 1995; **2438**, 167.

46. H. Fujita, A. Kishimoto, K. Matsumoto, *Transactions Faraday Soc*. 1960; **56**, 424.

47. Katherine E. Mueller, *Ph.D. Dissertation*, The University of Texas at Austin, 1998

48. S.V. Postnikov, M. D. Stewart, H.V. Tran, M. A. Nierode, D. R. Medeiros, T. Cao, J. Byers, S. E. Webber, C. G. Willson. *J. Vac. Sci. Technol. B*, 1999; **17**, 3335.

49. Sergei V. Postnikov, *Ph.D. Dissertation*, The University of Texas at Austin, 1999.

50. Gerard M. Schmid, *Ph.D. Dissertation*, The University of Texas at Austin, 2003.

51. E. Croffie, M. Cheng, A. Neureuther, *J. Vac. Sci. Technol. B*, 1999; **17**, 3339.

Chapter 3: Trilayer Diffusion Experiments

An FT-IR "sandwich" or trilayer approach to determining acid diffusion coefficients in thin polymer films has been reported previously.[1,2] The "sandwich" technique has been used by others to study diffusion of various penetrants in thin polymer films with methods other than IR spectroscopy. For example, Torkelson *et al.* used a sandwich structure and fluorescence non-radioactive energy transfer to measure diffusion of small dye molecules in various polymer films.[3] Lin *et al.* used the sandwich technique and neutron reflectometry for measuring interdiffusion of isotopically labeled PMMA and unlabeled PMMA.[4]

In this work the sandwich, or polymer film stack, consists of the polymer being studied (*e.g.* PHS) sandwiched between a photoacid feeder layer and an acid detector layer. The film stack is created on a mirror backed silicon wafer, which allows for real-time FT-IR monitoring of the stack while it bakes on a hotplate. Acid is generated in the feeder layer by exposing the stack to ultraviolet light. Once the acid traverses the analyzed polymer layer and reaches the detector layer, it catalyzes a reaction that alters the IR absorbance of the sample and the acid arrival time can thereby be determined. Diffusion coefficients can then be calculated from the Fickian relation:

$$D = L^2 / 2t_{diffusion} \qquad \text{(Eqn. 3.1)}$$

where L is the thickness of the analyzed layer and $t_{diffusion}$ is acid transit time. Figure 3.1 presents a schematic diagram of the film stack as typically constructed

in these experiments. While Figure 3.2 provides an example of an experimental result that demonstrates acid arrival after some time delay and the measurement of the acid transit time ($t_{diffusion}$). Figure 3.2 is an example of an experiment with PTBOC as the detector layer, but other polymers can also be used and in particular another polymer is necessary for high-temperature (>130 °C) measurements.

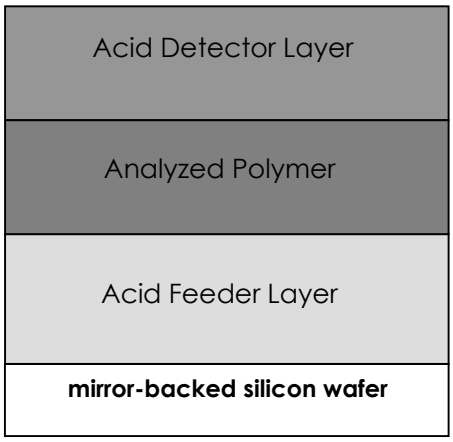

Figure 3.1: Schematic of trilayer film stack as typically constructed.

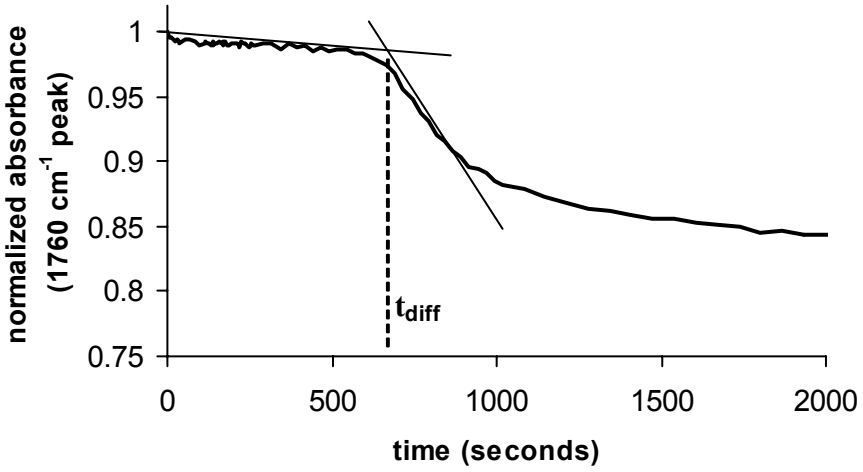

Figure 3.2: Determination of acid transit time with a PTBOC based acid detector layer.

EXPERIMENTAL - HIGH TEMPERATURE METHOD

Materials:

Poly(4-hydroxystyrene) (PHS) used in this experiment was synthesized from the base-catalyzed hydrolysis of poly(4-acetoxystyrene) (Mw = 8,000), which was made from the free-radical (AIBN) polymerization of 4-acetoxystyrene monomer supplied by Triquest Chemical Co. Poly(4-methoxystyrene) (PMOS) was synthesized from the reaction of PHS, potassium carbonate, and methyl iodide in acetone. A high-temperature detector layer, poly(4-(1,2-dihydroxy-1,2-dimethylpropyl)styrene) (PSDIOL) was prepared from the free-radical (AIBN) polymerization of the corresponding monomer. This

monomer was synthesized from the Grignard reaction between freshly prepared 4-chloromagnesiostyrene (2 equivalents) and 3-hydroxy-3-methyl-2-butanone in THF. A fuller description of the synthesis of PSDIOL can be found in Reference 5. The structure and the acid-catalyzed rearrangement of PSDIOL are shown in Figure 3.3. The photoacid generator used in this study was bis(4-t-butylphenyl)iodonium perfluorobutane-1-sulfonate (nonaflate) The nonaflate PAG was obtained from Midori Kagaku Co. The spin-casting solvent for the PMOS and PSDIOL layers was propylene glycol methyl ether acetate (PGMEA), which was obtained from Aldrich Chemical Co. Reagent-grade ethanol was used as the casting solvent for PHS.

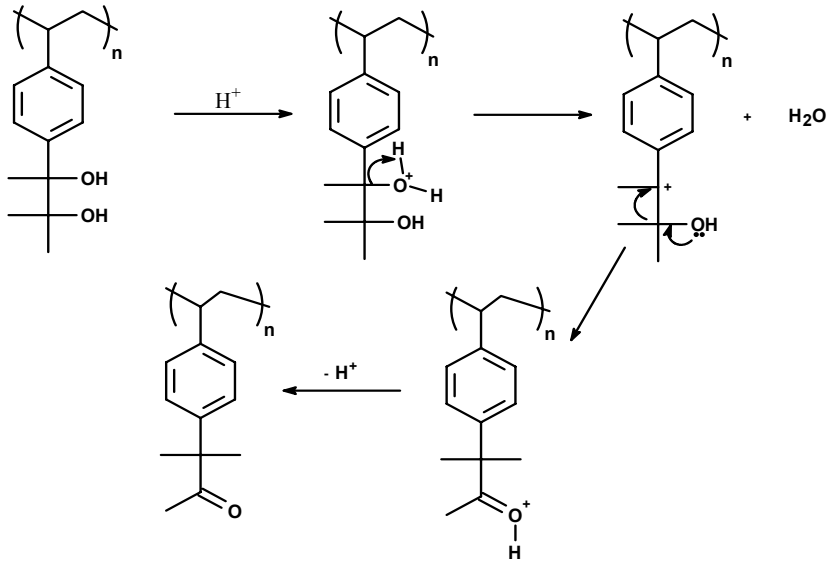

Figure 3.3: Acid catalyzed Pinacol rearrangement reaction of PSDIOL which serves as the basis for a high-temperature acid detector layer

Sample preparation:

Films stacks for PHS trilayer experiments were prepared on double-polished silicon wafer pieces, one side of which had been coated with approximately 100 nanometers (nm) of aluminum or gold metal to facilitate collection of IR data in mirror-backed reflection mode. Film stacks were created on the silicon side of the wafer piece. The first layer formed on the wafer piece was the acid feeder layer. The acid feeder layer consisted of PMOS and nonaflate PAG in a 20:1 weight ratio. The feeder layer was spin cast at 2500 rpm, then baked on a hotplate for two minutes at 90 ºC to yield a film 550 nm thick. The PHS layer was spin cast from ethanol directly onto the feeder layer. PHS layers were spin cast at speeds ranging from 4500 rpm to 1500 rpm to give the various thicknesses required by the experimental design. After coating with PHS, the wafer piece was baked at 90 ºC for two minutes. The third layer, the detector layer, consisted of the PSDIOL polymer. PSDIOL was spin cast onto a glass microscope slide substrate and, after a ten second bake on a 90 ºC hotplate, was floated from its glass substrate onto the surface of de-ionized water. The floating detector layer was then picked up onto the silicon substrate coated with the previous two layers. A two-minute bake at 40 ºC was used to remove water caught between the PHS and detector layers. After the 40 ºC bake, a two-minute bake at 90 ºC was used to drive off residual casting solvent. Completed samples were then exposed with 60 mJ/cm^2 of 248 nm ultraviolet light. Exposed samples were then placed on a hotplate attached to a Fourier-transform infrared spectrometer.

Results shown later in Chapter 6 demonstrate that layers formed by this floating method are distinct layers. A series of control experiments[6] were performed to test "leaching" of photoacid generator from the acid feeder layer during the floating process. No significant amount of leaching was detected.

Apparatus:

The FT-IR setup used for real-time monitoring of the bake process consists of a Nicolet MagnaIR 550 FT-IR with an attached liquid nitrogen cooled MCT/B external IR detector from Axiom Analytical. A nitrogen purged sample chamber attached to a temperature controlled hotplate allows sample spectra to be collected at elevated bake temperatures. Samples were exposed using a JBA High Performance collimated UV light source either though an Acton Research Corp. 248 nm interference filter or broadband (no filter).

RESULTS AND DISCUSSION – HIGH TEMPERATURE METHOD

Previous attempts[6] to use the sandwich FT-IR experimental method to directly measure acid migration times through PHS films with PTBOC detector layers were limited to temperatures below 125 ºC. Above this temperature, the PTBOC acid detector layer begins to rapidly decompose due to uncatalyzed thermolysis. This decomposition occurs whether acid is present or not and thus makes PTBOC useless as an acid detector layer at temperatures above 125 ºC. A new detector layer had to be found to investigate the transport properties of PHS at higher temperatures, say near its glass transition temperature (T_g) of 170 ºC. Several different polymers were tried before finally settling upon the PSDIOL

polymer. PSDIOL was found to be stable up to at least 200 ºC and acid reactive at temperatures above 160 ºC. Arrival of acid at the PSDIOL layer can been seen in the IR as an increase in the carbonyl signal at 1710 cm^{-1}, caused by the Pinacol rearrangement of the diol into a ketone.

Once a suitable high-temperature acid detector layer was found, acid transport could be investigated at temperatures above 125 ºC. The first set of PSDIOL experiments measured the acid transit time for nonaflate acid through PHS films of varying thickness at 180 ºC. (Thickness was varied from 0.3 microns to 1.1 microns.) As shown in Figure 3.4, the time it took for acid to traverse the intermediate PHS layer scales linearly ($R^2 = 0.96$) with the square of layer thickness. This is behavior to be expected from classical Fickian diffusion. The diffusion coefficient for nonaflate acid determined from this method is $5x10^{-5}$ $\mu m^2/s$. A diffusion coefficient of this magnitude would give around 50 nm of acid displacement during a ninety-second post exposure bake. This rapid diffusion rate can be explained by noting that PHS is ten degrees above its glass transition temperature and is, therefore, in a rubbery state where segmental polymer chain motion can occur.

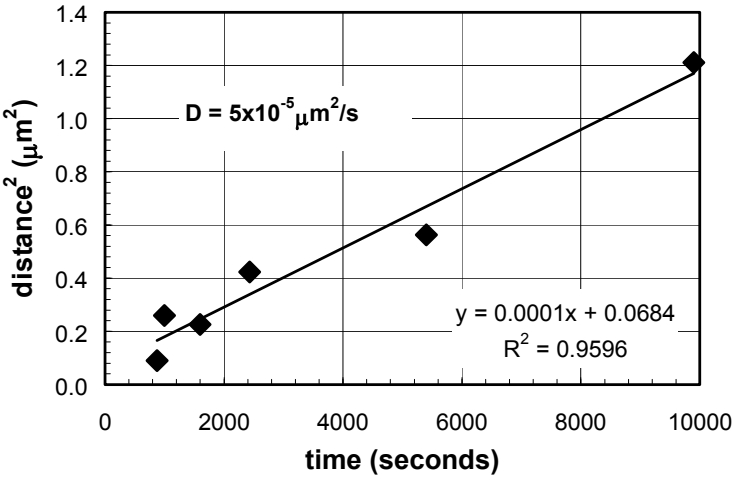

Figure 3.4: Measured times required for nonaflate acid to diffuse through PHS layers of various thickness at 180 ºC.

Experiments at 180 ºC were able to show that the trilayer method is a valid approach for measuring diffusion coefficients in PHS, but diffusion properties of PHS at 180 ºC are not particularly useful in microlithographic practice since most post exposure bakes are carried out at much lower temperatures. To get results of more interest to microlithography, another set of experiments using the PSDIOL detector layer were performed to investigate the effect of bake temperature on acid transport times through PHS layers of a fixed thickness. Acid transit times were determined at post exposure bake temperatures of 185 ºC, 180 ºC, 175 ºC, 170 ºC and 165 ºC for samples with a 510 nm thick intermediate PHS layer. Figure 3.5 shows the results of this series of measurements. The mid-point glass transition temperature of 170 ºC for PHS, as measured by differential scanning calorimetery on the dry polymer powder, was used in the generation of Figure 3.5.

These results show that molecular transport time has a sharp dependence on the relationship of the bake temperature to the glass transition temperature. This strong dependence on T_g is a widely observed phenomenon in polymer science. In Figure 3.5 the difference between the bake temperature (T_{bake}) and the glass transition temperature (T_g) is used as the x-coordinate. Data was collected on film stacks which consisted of 680 nm of PSDIOL over 510 nm PHS on 425 nm of PMOS + 5wt% nonaflate PAG.

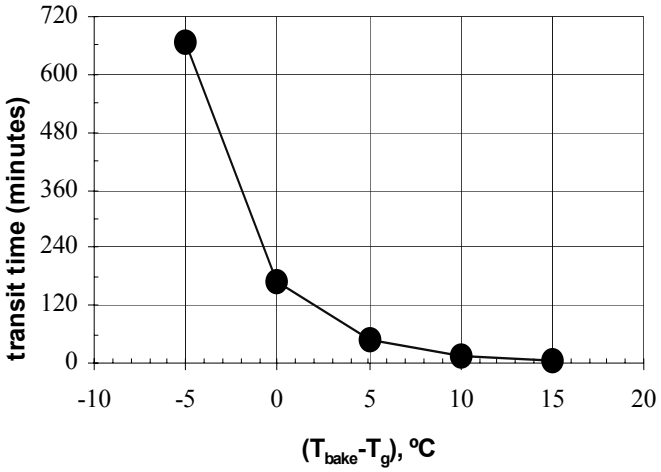

Figure 3.5: Acid transit time through 510 nm of PHS at different bake temperatures.

The lowest bake temperature presented in Figure 3.5 is still significantly higher than that typically used for a photoresist post exposure bake. When experiments where carried out at 160 ºC, no acid arrival was detected even through the samples were monitored for over twenty-four hours. It is likely that

the acid did arrive, but the response of the detector layer was not great enough to register above the random noise limit of the FT-IR. A simple linear extrapolation from gathered data suggests acid arrival should occur after some fourteen hours, but no acid arrival was detected over the course of a twenty-four hour experiment. The lower temperature limit for PSDIOL as an acid detector layer is likely limited by its own diffusion properties and reaction kinetics. PSDIOL does not rearrange noticeably below 165 °C.

Even though diffusion data were not collected below 165 ºC, methods of extrapolation exist that can estimate diffusion coefficients for lower temperatures. One such extrapolation method is the Williams-Landel-Ferry (WLF) equation originally developed to describe the kinetics of relaxation in polymers.[7] WLF analysis takes into account the change in rotational mobility of polymer chain segments occurring at the glass transition. Using the WLF analysis, diffusion data can be plotted using the following equation:

$$\ln\left(\frac{t_{diffusion}}{t_{Tg}}\right) = \frac{-C_1\left(T - T_g\right)}{\left(C_2 + \left(T - T_g\right)\right)} \qquad \text{(Eqn. 3.2)}$$

where $t_{diffusion}$ is the acid transit time, t_{Tg} is the acid transit time at the glass transition temperature, T is the bake temperature, and T_g is the midpoint glass transition temperature. The value of constant C_2 is usually taken to be 50 ºC. The slope of the fitted line gives C_1, but the typical C_1 value for most polymers is reported to be near 17.4.[8] As seen in Figure 3.6, the experimentally determined value of C_1 for PHS is 14.9 which is within fifteen percent of the typical value.

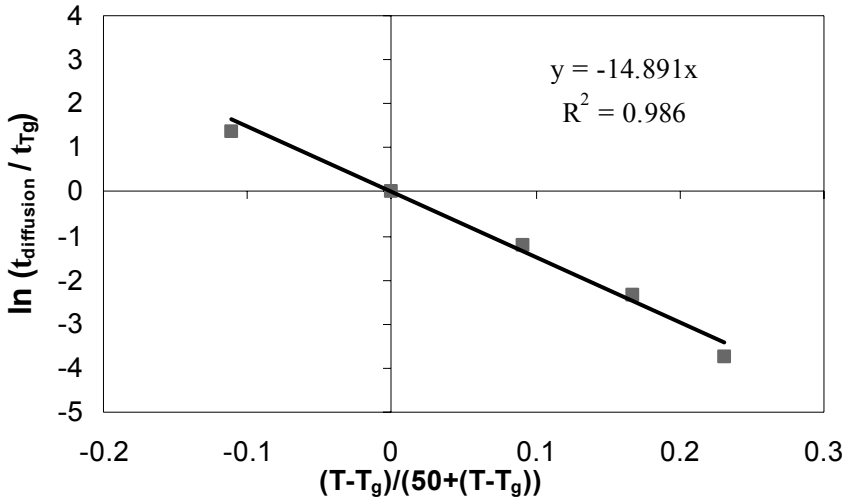

Figure 3.6: WLF fit for nonaflate acid in PHS.

Tabulated results for both the experimentally measured and WLF extrapolated diffusion coefficients are given in Table 3.1. The WLF extrapolation was carried with both the experimentally determined C_1 value and the reported generic C_1 value. It can be seen in Table 3.1 that both C_1 values give diffusion coefficients with roughly the same order of magnitude over most of the extrapolated range. As seen in Table 3.1, at 150 ºC (20 ºC below the glass transition temperature), the magnitude of the nonaflate acid diffusion coefficient in PHS is estimated to be 10^{-10} $\mu m^2/s$. A diffusion coefficient with this order of magnitude would lead to only 0.26 nm to 0.80 nm of total line width spread during a 90 seconds post exposure bake. Previously, IBM researchers have reported a diffusion coefficient of nonaflate acid in PHS at 85 ºC with a magnitude of 10^{-8} $\mu m^2/s$. [9] This value, which was extracted from simulation, is

dramatically higher than the extrapolated values reported here. For example, the WLF extrapolated value at 155 ºC (just 10 ºC below the last measured value) is already of the same magnitude as the IBM reported value at 85 ºC. According to WLF analysis, the change in segmental mobility occurring at glass transition is the controlling factor in penetrant mobility; so for equivalent differences between T and T_g, it would be expected that acid diffusion coefficients in any polymer system would be similar in magnitude to those estimated for PHS. Acid mobility in any non-reactive polymer matrix will be extremely low when the bake temperature is significantly (more than 10 ºC) below the glass transition temperature of the polymer. Similar values were in fact observed for the polymers poly(ethyl methacrylate) and poly(methyl methacrylate) using the same experimental method.[6]

Table 3.1: Measured and extrapolated diffusion coefficients for nonaflate acid in PHS.

Temperature (ºC)	$D_{measured}$ ($\mu m^2/s$)	D_{WLF} ($C_1 = 14.9$) ($\mu m^2/s$)	D_{WLF} ($C_1 = 17.4$) ($\mu m^2/s$)
185	5.4×10^{-4}	4.0×10^{-4}	7.1×10^{-4}
180	1.3×10^{-4}	1.5×10^{-4}	2.3×10^{-4}
175	4.3×10^{-5}	5.0×10^{-5}	6.2×10^{-5}
170	1.3×10^{-5}	1.3×10^{-5}	1.3×10^{-5}
165	3.3×10^{-6}	2.5×10^{-6}	1.9×10^{-6}
160	-	3.1×10^{-7}	1.7×10^{-7}
155	-	2.2×10^{-8}	7.4×10^{-9}
150	-	6.3×10^{-10}	1.2×10^{-10}
145	-	4.4×10^{-12}	3.6×10^{-13}
140	-	2.6×10^{-15}	5.9×10^{-17}

An extensive effort[6] was previously made to directly measure acid diffusion coefficients in PHS. This was effort was generally unsuccessful as no positive results were obtained from the various methods attempted. One possible inference that can be drawn from the lack of a positive response was that acid diffusion in PHS was extremely slow at the attempted experimental temperatures. This inference was somewhat supported by results in other polymers (specifically poly(ethyl methacrylate) and poly(methyl methacrylate)) that demonstrated that the trilayer method worked - at least for these other polymers near their glass transition temperature. Previous attempts to measure acid diffusion in PHS had taken place at temperatures much lower than its glass transition of approximately 170 °C. With the completion of these high temperature experiments in PHS it is much clearer that the inference that diffusion was very slow in PHS at normal post exposure bake temperatures was correct. At the least, these high temperature results can be taken as support for one of the reaction front propagation model's main assumptions, namely, acid diffusion in the reacted material is extremely slow.

PTBOC ANALOGUES

This work focuses on "APEX-like" positive tone CA resists that were described in Chapter 1. As previously stated, APEX resists were the first successful CA photoresists and most current 248 nm photoresists are derived in part from the APEX system. Even 193 nm and 157 nm photoresists, while derived from different materials, are very similar in design concept to the original

APEX resist. Most positive tone CA photoresists modulate solubility by using photogenerated acid to catalyze removal of pendant protecting groups from the base polymer resin. In the APEX system the polymer resin consists of polyhydroxystyrene (PHS) with a certain fraction of the phenolic sites protected with an acid-labile tBOC-protecting group. An onium salt photoacid generator is added as the catalyst source. After generation of the photoacid a post exposure bake is carried out to promote the deprotection reaction. It is typically during the post exposure bake that the majority of catalyst migration occurs. During the post exposure bake step the catalyst is both diffusing and reacting, complicating the analysis of the diffusion process.

The complexity of the reaction-diffusion process makes it extremely difficult to develop a full understanding of what is occurring at the molecular level in the baking photoresist. As the acid molecule diffuses, the reactivity and diffusion properties of the surrounding polymer matrix are constantly changing. The exposed areas of photoresist change chemical identity over the course of the post exposure bake and this can result in a drastic change in diffusivity from initial state to final state. In addition to the overall change in composition, it is possible that the resist goes through a transient material state as deprotection by-products leave the film. This means that the diffusion coefficient of the acid molecule is at least a function of bake temperature and local extent of reaction. In addition, because temperature, extent of reaction, and by-product concentration are changing over the course of the bake, the overall mobility of acid molecule is not constant over time.

Ignoring transient effects, the reaction-diffusion system can be expressed in equation form as the following coupled differential equations for a one-dimensional case[10]:

$$\frac{\partial C_{ps}}{\partial t} = -k_{ps} C_{ps} C_a^n$$

$$\frac{\partial C_a}{\partial t} = \frac{\partial}{\partial z}\left(D_a \frac{\partial C_a}{\partial z} \right) \qquad \text{(Eqn. 3.3a \& 3.3b)}$$

where C_a is concentration of catalyst, C_{ps} is the concentration of protected sites, D_a is the acid diffusion coefficient and k_{ps} is the deprotection reaction rate constant. Solution of this system is straightforward if D_a is either constant or a known function of extent of reaction. Unfortunately, D_a is likely not constant and its dependence on extent of reaction is not yet fully understood. Also, as mentioned previously, a transient material state is possible, so D_a could be a time dependent function.

While many functional forms are possible, for illustration purposes consider the simple assumption that diffusivity follows a simple linear mixing rule like the following:

$$D_a = (1 - x) D_{ao} + x D_{af} \qquad \text{(Eqn. 3.4)}$$

where x is extent of reaction, D_{ao} is the diffusivity in the unreacted resist and D_{af} is the diffusivity in the completely reacted resist. D_{af} in an APEX-like resist is simply the acid diffusion coefficient in polyhydroxystyrene, and is, in principle, measurable. In practice, D_{af} in PHS is so small that it is difficult to directly

measure at typical post exposure bake temperatures (90 - 130 ºC), but it has been measured at certain elevated bake temperatures (165 - 190 ºC) as discussed above. It is not possible to directly measure $\boldsymbol{D_{ao}}$, as it is impossible to prevent reaction while diffusion is measured. It might be possible to estimate $\boldsymbol{D_{ao}}$ by measuring the diffusivity of unreactive "model acid" molecules in photoresist resin. The "model acid" molecule could be designed not to promote the deprotection reaction in the resist film, but might mimic a photoacid molecule in size or ionic character. The problem with using the model acid approach is the difficulty of finding a molecule that has all the essential characteristics of a real acid molecule except catalytic activity. Other approaches[11-13] treat $\boldsymbol{D_{ao}}$ as a fitting parameter in a reaction-diffusion simulation which is then tuned to fit experimental data. This route is very useful, but it does tend to convolve multiple factors into one number and gives little insight into the process at the molecular level. Also, since $\boldsymbol{D_{ao}}$ is only one of several fitting parameters in the model, questions about solution uniqueness are raised.

Direct experimental measurement of diffusion coefficients is ideal, but not always possible, except in specially designed model systems. The use of model systems avoids the uncertainties of data fitting and simulation while bringing other uncertainties in to the analysis. Of course questions of how closely the model system represents reality are of prime importance. For example, if a model acid is not ionic, it can not capture all the interactions that occur between the polymer and a real acid. Rather than finding an appropriate model acid molecule, it is perhaps easier to find a polymer that can act as an unreactive "model

polymer" so an actual acid molecule can be used. The experimental work discussed here includes the measurement acid diffusion coefficients in unreactive model polymers which are very close structural analogues to protected APEX resin. This data is intended to provide as direct as possible estimate of D_{ao}. Instead of tBOC-protected PHS, the polymers used in this work are shown below in Figure 3.7. Polymer B is poly(4-isopropyloxycarbonyloxystyrene) (IPOCST), and differs from the tBOC-protected PHS (Polymer A) by having one less methyl group in the protecting group. Polymer C is poly(4-neopentyloxycarbonyloxystyrene) (NPOCST), and differs from PTBOC by only a methylene spacer group between the tertiary carbon group and the final oxygen.

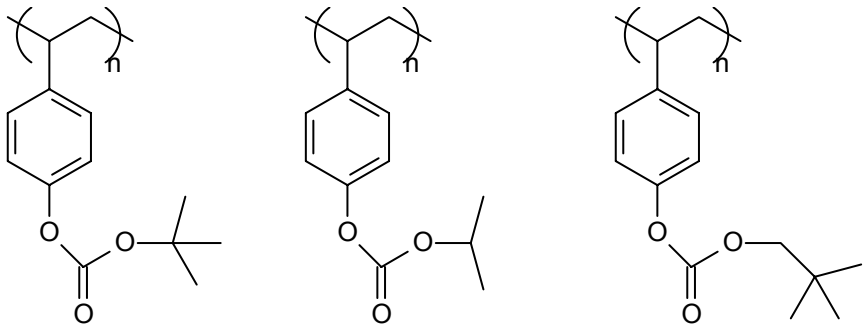

A) PTBOC B) IPOCST C) NPOCST

Figure 3.7: Structure of PTBOC and analogues

Structurally these polymers are all very similar, but they react with acid molecules very differently. The polymer PTBOC is rapidly converted into PHS when heated in the presence of even fairly weak acids. Even the phenol group of PHS is acidic enough to speed the tBOC deprotection reaction.[7] The isopropyl-

protecting group of IPOCST is acid-labile, but only with extremely strong acids and at very high temperatures.[8] Hexafluoroantimonatic acid ($HSbF_6$) will catalyze IPOCST deprotection, but perfluorobutanesulfonic acid ($HSO_3C_4F_9$) will not, even at temperatures up to 180 ºC. The neopentyl-protecting group of NPOCST is entirely unaffected by even strong acids at temperatures below 185 ºC, and according to thermogravimetric analysis, is thermally stable to very high temperatures when no acid is present.

EXPERIMENTAL - PTBOC ANALOGUES

Materials:

Poly(4-methoxystyrene) (PMOS) used as the acid generator layer in trilayer experiments was synthesized from the reaction of poly(4-hydroxystyrene), potassium carbonate, and methyl iodide in acetone. The photoacid generator used in this section was bis(4-t-butylphenyl)iodonium perfluorobutane-1-sulfonate (nonaflate) obtained by donation from Midori Kagaku Co. Poly(4-t-butyloxycarbonyloxystyrene) (PTBOC) used as the acid detector layer in trilayer experiments was prepared from the polymerization of 4-t-butyloxycarbonyloxystyrene monomer using AIBN. This monomer was obtained by donation from Triquest Chemical Co. Poly(4-ispropyloxycarbonyloxystyrene) (IPOCST) and poly(4-neopentyloxycarbonyloxystyrene) NPOCST were prepared by reaction of poly(4-hydroxystyrene) (MW 12,300 Pd 1.93) with the appropriate chloroformate in the presence of triethylamine. The PHS polymer was dissolved in tetrahydrafuran (THF) and the chloroformate was diluted in toluene. The

polymer-chloroformate mixture was stirred at room temperature overnight (~20 hours), then neutralized with added base and precipitated into methanol. Both neopentyl chloroformate and isopropyl chloroformate were purchased from Aldrich Chemical Co. and used as received. The PHS starting material was obtained by donation from Triquest. The spin-casting solvent for all polymer layers, propylene glycol methyl ether acetate (PGMEA), was also obtained from Aldrich Chemical Co. and used as received.

Glass transition temperatures were obtained for the IPOCST and NPOCST polymers by means of temperature scanning spectroscopic ellipsometery. The spectroscopic ellipsometer is a J.A. Woollam M-2000 modified with a heated sample stage. The sample stage was designed in our research group and is controlled with a LabView (National Instruments) program written in house. The sample stage is capable of constant temperature or scanning operation. When measuring glass transition temperatures, the stage temperature was ramped at rate of 5 ºC/min. The measured T_g's for IPOCST and NPOCST were 88 ºC and 82 ºC respectively.

Sample Preparation:

Films stacks for trilayer experiments were prepared on double-polished silicon wafer pieces with one side coated with approximately 100 nm of aluminum metal to allow collection of IR data in mirror reflection mode. The first layer spin cast onto the silicon side of the wafer piece was the acid feeder layer. The acid feeder layer consisted of PMOS and a nonaflate PAG in a 20:1 weight ratio. The feeder layer was spin cast, and then baked at 90 ºC on a

hotplate for two minutes, giving a film approximately 400 nm thick. The remaining layers in the trilayer film stack must be applied using a floating process. With the float method the subsequent layers were spin cast onto glass microscope slides, then floated off the slide onto the surface of deionized water. Once the layer was floating on the water surface, it was picked up onto the wafer piece containing the previously applied stack layers. The intermediate layer and the detector layer were spin cast at speeds ranging from 4500 rpm to 1500 rpm to give the various required thicknesses. After each new layer was applied by floating the film stack is dried for two minutes at 50 ºC. A two-minute bake at 90 ºC was used to drive off residual casting solvent. Completed samples were exposed to more than 60 mJ/cm^2 of 248 nm ultraviolet light. Exposed samples were then placed on a hotplate attached to a Nicolet Magna IR 550 Fourier-transform infrared spectrometer. Acid arrival is determined by monitoring the PTBOC carbonyl peak (1756 cm^{-1}) for a decrease in absorbance, indicating cleavage of the tBOC protecting group. IPOCST and NPOCST both have carbonyl peaks that overlap the PTBOC peak, which a places an upper limit on how thick the intermediate layer may be while maintaining acceptable IR signal to noise ratio to notice the change in absorbance caused by acid arrival at the detector layer. The FT-IR setup used for real-time monitoring of the bake process is the same as discussed in the previous section.

RESULTS AND DISCUSSION – PTBOC ANALOGUES

The goal of this work was to obtain an estimate of $\boldsymbol{D_{ao}}$ in PTBOC by measuring $\boldsymbol{D_a}$ in nonreactive analogue polymers. Diffusivity measurements in the model polymers IPOCST and NPOCST are useful only for the information they provide about the more important PTBOC system. As seen above in Figure 3.7, the model polymers are very similar in chemical structure, but often small structural differences make a tremendous difference in chemical properties. But other than different responses to acid, the model polymers appear to be fairly similar to PTBOC. All three polymers display similar solubility in such common solvents as THF, toluene, and PGMEA, and are insoluble in water, methanol, and hexane. The chemically important carbonyl group is present in all three polymers. No shifting was observed in the location of the characteristic carbonyl peak in IR spectra of any of the three polymers. The glass transition temperatures of the three polymers do differ, especially between the model compounds and PTBOC. The glass transition temperatures of IPOCST and NPOCST are both in the range between 80 – 90 ºC, while the glass transition of PTBOC has been measured by ellipsometry as 120 ºC. This difference in glass transition temperature means that values for $\boldsymbol{D_a}$ of the model polymers at a given temperature should not be taken as $\boldsymbol{D_{ao}}$ of PTBOC at that the same temperature. Because of the large impact glass transition has on diffusivity in polymers, the correct analogy is between $\boldsymbol{D_a}$ and $\boldsymbol{D_{ao}}$ for equivalent differences in polymer glass transition temperature and bake temperature. For example, the estimate for $\boldsymbol{D_{ao}}$ at 105 ºC (15 ºC below PTBOC T_g) would come from IPOCST $\boldsymbol{D_a}$ at 73 ºC.

IPOCST Polymer:

The IPOCST polymer is probably as close in chemical properties to PTBOC as any possible compound while still being unreactive with perfluorobutanesulfonic acid at normal post exposure bake conditions. IPOCST does react with acid, but it requires much harsher conditions than those used in this study. The lesser reactivity of IPOCST results from the lesser stability of the carbocation that must be formed as the isopropyl group is cleaved. The deprotection reaction of IPOCST goes through a secondary carbocation intermediate while PTBOC goes through a more stable tertiary carbocation.

Figure 3.8 presents the measured diffusion coefficients for IPOCST over the temperature range 65 – 95 ºC as measured in films with 150 nm nominal thickness. The plotted line is for exponential fit to the data and is shown only to demonstrate trend. As the experimental temperature traverses the glass transition temperature region for this polymer, it is expected that $\boldsymbol{D_a}$ will change dramatically. Measured $\boldsymbol{D_a}$'s range in magnitude from 10^{-14} cm^2/s at the lowest temperature to 10^{-12} cm^2/s at the highest temperature. As seen below in Table 3.2, IPOCST, in comparison with other polymers, seems to have relatively fast (about an order of magnitude faster) diffusion rates at the glass transition temperature. It is not fully clear why this should be the case.

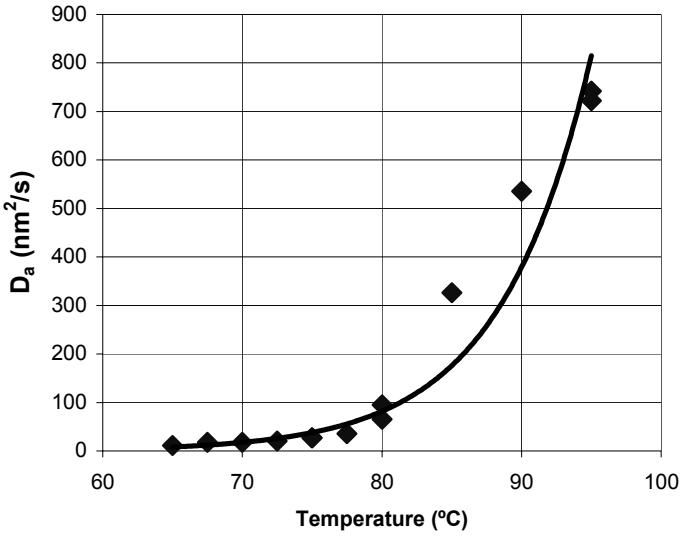

Figure 3.8: Measured acid diffusion coefficients for IPOCST polymer. Nominal film thickness = 150 nm. (1 nm^2/s = 10^{-14} cm^2/s)

NPOCST Polymer:

The NPOCST polymer is as close structurally to PTBOC as IPOCST, but it is less chemically similar. Under harsh conditions IPOCST does eventually deprotect, but NPOCST is extremely inert. For NPOCST to deprotect it must go through a primary carbocation intermediate which is even less stable than the secondary carbocation of IPOCST. Lesser stability translates into less likelihood of formation, which translates into less overall reactivity. No conditions were found under which NPOCST was reactive. The glass transition temperature of PTBOC drops more than 30 ºC with the addition of the methylene spacer group of NPOCST. The change in T_g suggests the spacer group must significantly enhance

pendant end group mobility. NPOCST also has a slightly lower glass transition temperature than IPOCST despite the bulkier end group. The mobility imparted by the methylene spacer group appears to more than compensate for the additional methyl unit in the end group.

Figure 3.9 shows the measured diffusion coefficients for NPOCST over the temperature range 70 – 95 ºC as measured in films with 320 nm nominal thickness. The plotted line is for exponential fit to the data and is shown only to demonstrate trend. As the experimental temperature traverses the glass transition temperature region for this polymer, it is expected that $\boldsymbol{D_a}$ will change dramatically. Measured $\boldsymbol{D_a}$'s for NPOCST cover the same magnitude range as IPOCST, with diffusion in NPOCST generally slower at every temperature despite NPOCST's lower glass transition temperature. As seen below in Table 3.2, NPOCST has acid diffusion rates that are more in line with the previously measured polymers PHS and poly(ethyl methacrylate).

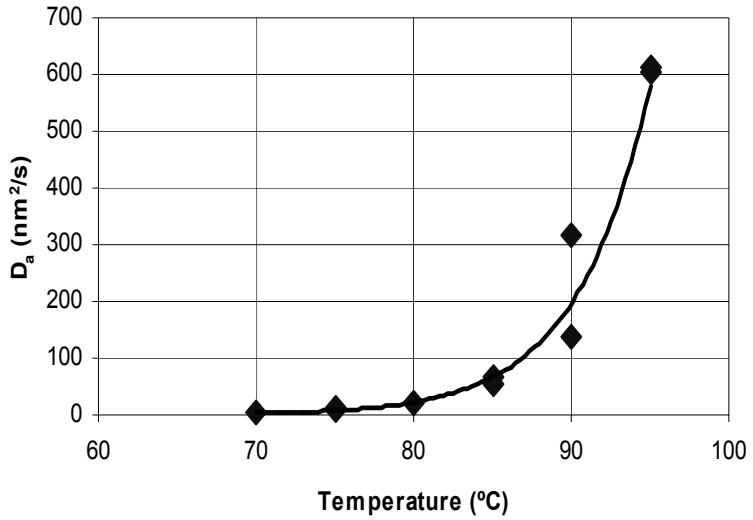

Figure 3.9: Measured acid diffusion coefficients for NPOCST polymer. Nominal film thickness = 320 nm. (1 $nm^2/s = 10^{-14}$ cm^2/s)

Table 3.2: Acid Diffusivity measured in polymers near T_g.

$T-T_g$ (ºC)	D_a (cm^2/s) IPOCST	D_a (cm^2/s) NPOCST	D_a (cm^2/s) PHOST	D_a (cm^2/s) PEMA* (Ref 14)
10	--	6.1×10^{-12}	1.3×10^{-12}	1.1×10^{-12}
5	3.7×10^{-12}	1.4×10^{-12}	4.3×10^{-13}	1.8×10^{-13}
0	2.7×10^{-12}	6.0×10^{-13}	1.3×10^{-13}	3.5×10^{-14}
-5	1.6×10^{-12}	2.0×10^{-13}	3.3×10^{-14}	1.6×10^{-14}
-10	3.5×10^{-13}	9.2×10^{-14}	--	3.4×10^{-15}
-15	1.3×10^{-13}	2.5×10^{-14}	--	--
-20	8.8×10^{-14}	--	--	--

*PEMA = poly(ethyl methacrylate)

ESTIMATES FOR PTBOC FROM ANALOGUE RESULTS

As stated previously, the goal of this work is to provide estimates for acid diffusion coefficients in reactive PTBOC polymer films. The following table gives estimates for the initial acid diffusivity (D_{ao}) of PTBOC based on measured values from the two analogue polymers. Estimates at each given temperature were obtained by substituting the glass transition temperature of PTBOC for the analogue polymers glass transition temperature. When values from both polymers are available an average value is also reported. Estimated values from the isopropyl polymer are on average larger than the neopentyl polymer by almost a factor of five.

Previous researchers have reported estimated diffusion coefficients for similar systems. IBM researchers have reported diffusion coefficients for the same acid (perfluorobutanesulfonic acid) in PTBOC at temperatures in the range of 65 - 105 ºC.[13] Their estimates range from $5x10^{-16}$ cm^2/s at 65 ºC up to $1.5x10^{-13}$ cm^2/s at 105 ºC. At the only point of overlap (105 ºC) in the two data sets, the D_{ao} estimate from IPOCST is $1.3x10^{-13}$ cm^2/s and the average estimate differs from the IBM value by only a factor of two. The IBM estimate comes from simulation fits to experimental results, but seems to be in good agreement with our estimates. Another estimate from simulation fits to experimental data comes from Zuniga and Neureuther. They measured diffusion in APEX-E and report an initial diffusion coefficient of $5.6x10^{-14}$ cm^2/s at 90 ºC as a fitting parameter.[11] The comparison here is not direct as APEX-E consists of only partially protected PHS polymer and the acid structure is not reported and is not likely the same as

these experiments. Other researchers have reported[14] diffusion coefficients in PTBOC in the temperature range 90 - 130 ºC for perfluorooctanesulfonic (PFOS) acid, rather than the perfluorobutanesulfonic (PFBS) acid used in these experiments. PFOS acid is a rather larger molecule than PFBS acid, and the reported diffusion coefficients reflect this as they range for PFOS from 2.6×10^{-16} cm^2/s at 90 ºC to 1×10^{-14} cm^2/s at 130 ºC, approximately two orders of magnitude smaller than PFBS.

Table 3.3: Estimated PTBOC acid diffusivity as function of temperature.

Temperature (ºC)	D_{ao} (cm^2/s) (IPOCST)	D_{ao} (cm^2/s) (NPOCST)	D_{ao} (cm^2/s) (Average)
130	--	6.1×10^{-12}	--
125	3.7×10^{-12}	1.4×10^{-12}	2.6×10^{-12}
120	2.7×10^{-12}	6.0×10^{-13}	1.7×10^{-12}
115	1.6×10^{-12}	2.0×10^{-13}	9.0×10^{-13}
110	3.5×10^{-13}	9.2×10^{-14}	2.2×10^{-13}
105	1.3×10^{-13}	2.5×10^{-14}	7.8×10^{-14}
100	8.8×10^{-14}	--	--

TRILAYER EXPERIMENT CONCLUSIONS

Acid diffusion coefficients for the PTBOC analogue polymers IPOCST and NPOCST were experimentally determined for temperature ranges near their glass transition temperatures. Based on these results, acid diffusion coefficients for PTBOC homopolymer were estimated for the temperature range 100 - 130 ºC. Estimates provided by the analogue polymers are in close agreement with estimates provided by other researchers using different methods for

determination. The high temperature experiments support the assumption that diffusion is very slow in PHS at normal post exposure bake temperatures. Taken together the results of the trilayer experiments support the conclusion that simple Fickian diffusion can not fully explain observed behavior, it appears that some reaction enhanced diffusion is required to fit the experimental data.

REFERENCES

1. S.V. Postnikov, M.D. Stewart, H.V. Tran, M.A. Nierode, D.R. Medeiros, T. Cao, J. Byers, S.E. Webber, C.G. Willson. *J. Vac. Sci. Technol. B*, **17(6)**, 3335, 1999

2. M.D. Stewart, S.V. Postnikov, H.V. Tran, D. R. Medeiros, M. A. Nierode, T. Cao, J. Byers, S. E. Webber, C. G. Willson. *ACS Polymeric Mat. Sci. Eng*. **81**, 58, 1999.

3. D. Hall, J. Torkelson. *Macromolecules*, 1998, **31**, 8817-8825.

4. E. Lin, W. Wu, S. Satija. *Macromolecules***,** 1997**, 30,** 7224-7231.

5. Hoang Vi Tran, *Ph.D. Dissertation*, The University of Texas at Austin 2002.

6. Sergei V. Postnikov, *Ph.D. Dissertation*, The University of Texas at Austin, 1999.

7. M.L Williams, R.F Landel, J.D. Ferry. *J. Am. Chemical Soc*. **77**, 1955.

8. P. Munk, *Introduction to Macromolecular Science*, John Wiley & Sons, New York, 1989.

9. G.M. Wallraff, W.D. Hinsberg, F.A. Houle, M. Morrison, C.E. Larson, M. Sanchez, J. Hoffnagle, P.J. Brock, G. Breyta. *Proc. SPIE*, **3678**, 138, 1999.

10. Notation adapted from *Inside PROLITH: A Comprehensive Guide to Optical Lithography Simulation*, Chris A. Mack, Finle Technologies, Inc., Austin, TX , 1997.

11. M. Zuniga, G. Wallraff, E. Tomacruz, B. Smith, C. Larson, W.D. Hinsberg, A.R. Neureuther; *J. Vac. Sci. Technol. B*. **11(6)**, 2862, 1993.

12. E. Croffie, M. Cheng, A. Neureuther; *J. Vac. Sci. Technol. B*. **17(6)**, 3339, 1999.

13. F.A. Houle, W.D. Hinsberg, M. Morrison, M.I. Sanchez, G. Wallraff, C. Larson, J. Hofnagle; *J. Vac. Sci. Technol. B*, **18(4)**, 1874, 2000.

14. D.L. Goldfarb, M. Angelopoulos, E.K. Lin, R.L. Jones, C.L. Soles, J.L. Lenhart, W. Wu. *J. Vac. Sci. Technol. B*, **19(6)**, 2699, 2001.

Chapter 4: Bilayer Diffusion Experiments

In the previous chapter, a method of studying acid transport in non-reactive polymer films with a "sandwich" or trilayer film stack experiment was discussed. In this chapter, acid transport in a reactive polymer film will be discussed. The experimental method used to study reactive diffusion is a variation on the sandwich experiment, using two polymer layers instead of three. The film stack is constructed as before, with the only difference being that the intermediate layer separating the acid reservoir layer from the detector layer is not included. In some sense, the bilayer stack can be considered a special, limiting case of a trilayer experiment with an intermediate layer of zero thickness.

For the purpose of these experiments, it is perhaps best to think of the bilayer as a simulant of a resist feature sidewall. The bilayer mimics a post exposure acid distribution generated by an ideal, step function aerial image. Figure 4.1 shows how the bilayer stack can be related to a lithographic image. A main advantage of the bilayer method over lithography-based methods is that it allows the effects of acid diffusion to be isolated from the complexities of a full lithographic process. The bilayer experimental approach allows resist performance to be isolated from aerial image formation and other processing variables. In general, the complexities of the full lithographic process make it difficult to cleanly assign causes to any observed variation without multiple control experiments.

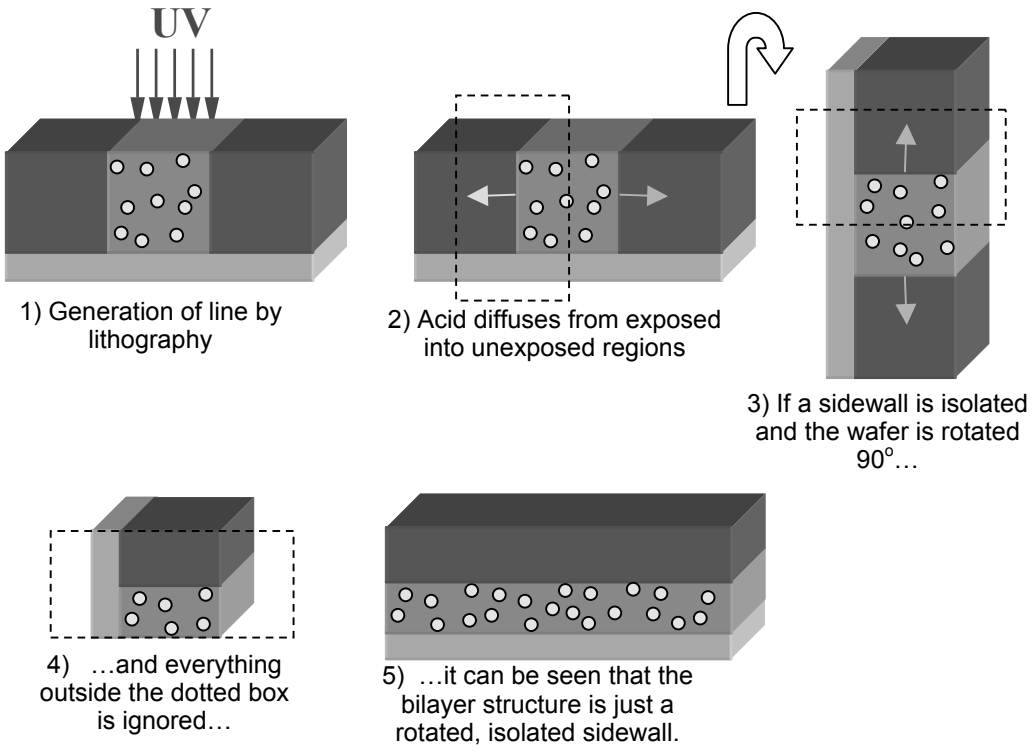

Figure 4.1: Resist feature sidewall relationship to bilayer sample

MATERIALS

The t-BOC polymer (PTBOC) used as detector layer in this study was prepared by free radical (AIBN) polymerization of t-butyloxycarbonyloxystyrene monomer from Triquest Chemical. Polymerization was carried out overnight (approximately 18 hours) in toluene at 70 °C with an overall concentration 1 molar with an AIBN initiator mole ratio of, approximately, 1:100. The resulting polymer was precipitated into hexanes, then dried in a vacuum oven at 50 °C for

one day. Poly(4-methoxystyrene) (PMOS) was synthesized from poly(4-hydroxystrene) (PHS), methyl iodide and base. The starting polymer was dissolved in tetrahydrofuran. The other components were added and the resulting solution was stirred at room temperature overnight. Product polymer was precipitated into methanol, and then dried in a vacuum oven at 50 °C. Photoacid generators, unless otherwise noted, were provided by Midori Kagaku, Co. The casting solvent for PTBOC and PMOS was propylene glycol methyl ether acetate (PGMEA) purchased from Aldrich Chemical Co. and used as received.

APPARATUS

The apparatus was as described in Chapter 3.

SAMPLE PREPARATION

Samples were prepared on double-polished silicon substrates coated with gold or aluminum on one side. The metal coating allowed IR measurements to be made in reflection mode. Bilayer film stacks were constructed using methods similar to those described in Chapter 3. A feeder layer of PMOS/PAG was spin cast onto a silicon substrate and then post apply baked at 90 ºC for two minutes. The PTBOC detector layer was spin cast on a glass microscope slide, then floated onto de-ionized water after a ten second, 90 ºC bake. The floating film was then picked up on a silicon substrate coated with the feeder layer. A two-minute bake a 50 ºC was used to evaporate residual water. The bilayer stack consisting of both feeder and detector layer was then baked at 90 ºC for two minutes. Samples were

then exposed to UV light, typically to very high doses (~100 mJ/cm^2) to give maximum acid generation. After exposure, samples were placed on the IR monitored hotplate and the experiment begun, usually within 10 minutes of initial exposure. A series of control experiments has been conducted to verify the float process does not leach a significant amount of PAG from the feeder films or cross-contaminate the layers[1] and the interface has been studied by neutron scattering[2] and SEM with the layers being shown to be distinct (below the detection limit).

CONSTRUCTING FILM STACKS

Creating polymer film stacks with a floating technique is not an unheard of procedure in polymer science; other researchers[3-6] have used it in the past to study other topics. Film floating is an unusual method in semiconductor-related research, though at least one other group[7] has used it in photoresist related research. The advantage to film floating is that it allows film stacks to be created even when mutually exclusive casting solvents can not be found for the proposed film stack layers, but the method has several drawbacks. First among the drawbacks is that a limited number of polymers float well. For a polymer to float well, it must cleanly release from the casting substrate and have enough flexibility to maintain film integrity when buffeted by surface vibrations. By careful selection of the casting substrate, almost any polymer film can be made to release from some substrate. Glass microscope slides work well for non-polar, hydrophobic polymers like PTBOC, but not very well for polymers like PHS.

Another option is to use dissolving release layers. These layers can be used to generate floating films of almost any polymer. Sucrose coated substrates and polished salt disks can be used for especially sticky polymers. The substrate (or its soluble coating) can be dissolved away leaving behind the free standing polymer film. Polymer brittleness is the factor most likely to prevent successful film floating. A polymer like PHS will typically shatter into unusable fragments when floating is attempted with sub-micron thick films. Another drawback to film floating is that it takes much longer than sequential spin casting. A float-solvent evaporation bake must be incorporated to remove float solvent (water) that gets trapped between layers. A second post apply bake is typically used as well, so the first coated layer receives extra bake time. The floating technique also requires some level of manual dexterity to be successfully completed. The dexterity level is fairly easily achieved with a few practice attempts, but, even with much practice, a significant percentage of potential samples are ruined by operator error.

As discussed briefly in Chapter 2, there are other methods available to construct film stacks. Sequential spin casting (spin cast one layer, then spin another directly over the first) of polymer films is the preferred method, but as the second casting solvent must not dissolve the first cast layer some polymer combinations are not possible. Later, in Chapter 7, experiments will be described that use the sequential casting method to construct samples to investigate line edge roughness. Those samples consist of a PTBOC underlayer spin cast from PGMEA and a PHS/PAG overlayer spin cast from an alcohol. This method has

been used by researchers at IBM[7] and NIST[2] to study acid diffusion. Perhaps, the simplest way to create film stacks is to simply spin cast films on separate substrates and then stack the films "top-to-top". This has been done previously to study acid diffusion in photoresists[9], but top-to-top stacking is not without limitations. When the films are on two rigid substrates, contact between the two layers is not necessarily complete or uniform across the entire film. Also, the top-to-top method introduces a variation not normally seen in photoresist systems – the polymers are effectively enclosed in a gas impervious case. A photoresist that releases gas by-products will have those by-products trapped in the film stack instead of released into the atmosphere. A clever variation on the top-to-top method is the "foil method" described by Schlegel *et al.*[10]. In this method a film is spin cast onto a normal, rigid substrate, and then the second layer is spin cast onto a foil coated substrate. The film is then either peeled from the foil or, if the polymer is glassy and rigid, the foil is bent and the film cracked off in pieces. Pieces of the polymer film can be collected and placed in contact with the first cast film to generate a film stack.

EXPERIMENTAL RESULTS

In general, experimental results from bilayer experiments all look very similar to one another. Figure 4.2 shows a typical IR response seen in a bilayer experiment. In Figure 4.2 the carbonyl absorbance (1756 cm^{-1}) of the film stack has been normalized against its initial (t = 0) absorbance and the normalized absorbance has been plotted versus bake time. The majority of the change in

absorbance seen over the course of the experiment occurs quickly at the beginning of the experiment, then the rate of change slows and a fairly constant, slow rate of deprotection continues until the conclusion of the bake.

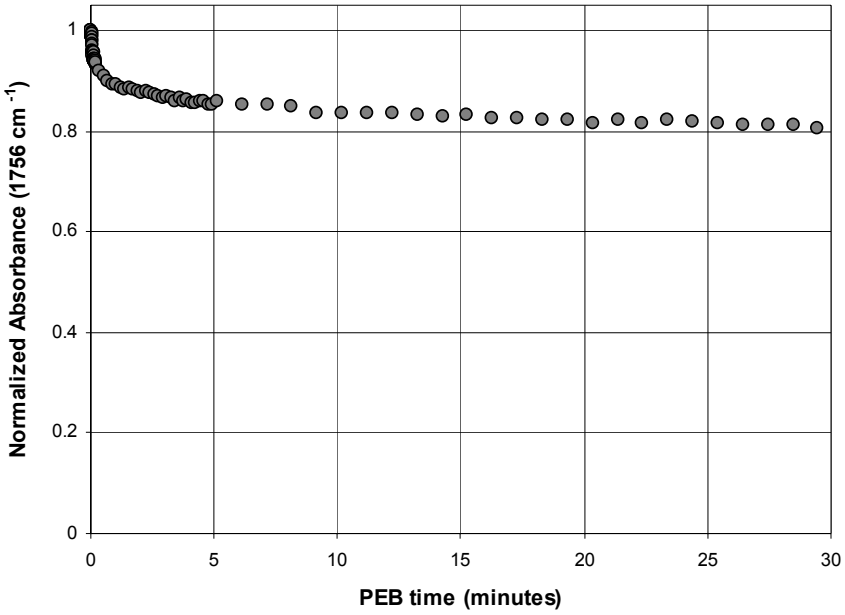

Figure 4.2: Normalized absorbance change with PEB time. T_{PEB} = 90 °C, PTBOC: 320 nm, PMOS: 420 nm, PAG: 10wt% $\phi_3S^+{}^-O_3SC_4F_9$

To be useful for our purposes, changes in normalized absorbance versus bake time must somehow be converted into diffusion distances versus time. This can be done by making some simplifying approximations. If it is assumed that the reaction goes to completion where ever a threshold acid concentration has been reached, then it can be assumed that the deprotection is confined to definite band and the change in absorbance is a result of a decrease in sample path length and not a change in concentration distributed throughout the entire layer. A look

at the deprotection kinetics of PTBOC makes the assumption that the reaction is fast and complete for even fairly low acid concentrations seem quite reasonable. Also, Chapter 6 will provide details of experiments using scanning electron microscopy that show deprotection does appears confined to a definite region and not distributed through the entire layer. Making the assumption that absorbance occurs layer by layer allows diffusion distances to be calculated according to the following equation:

$$Diffusion\ Distance = T_{film} \times \left(1 - \frac{Abs(t)}{Abs_o}\right) \qquad \text{(Eqn. 4.1)}$$

where T_{film} is the initial thickness of the upper layer, $Abs(t)$ is the sample's IR absorbance at time t, and Abs_o is the initial IR absorbance of the sample.

When the absorbance data is converted into diffusion distance data and plotted against bake time, a curve such as seen in Figure 4.3 results. Figure 4.3 shows the diffusion distance of perfluorobutanesulfonic acid against time at 90 °C. It shows that acid diffuses rapidly for the first few minutes, then slows significantly. The change in diffusion distances with bake time agrees very closely with changes in actual feature linewidths observed in lithographic experiments[11,12]. Because the bilayer experiment simulates just one line edge, the change in linewidth predicted by bilayer experiments is twice the reported bilayer diffusion distance.

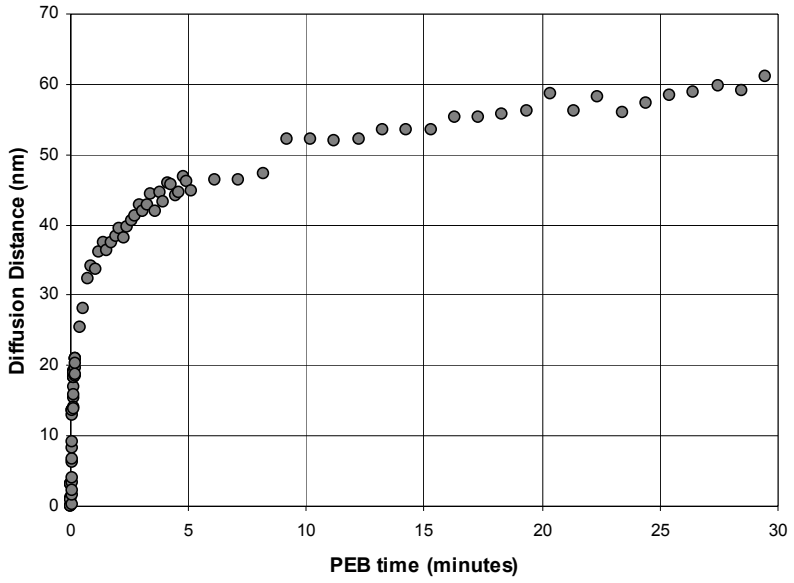

Figure 4.3: Diffusion Distance increase with PEB time. T_{PEB} = 90 °C, PTBOC: 320 nm, PMOS: 420 nm, PAG: 10wt% $\phi_3S^{+-}O_3SC_4F_9$

The shape of the curve in Figure 4.3 is particularly interesting – the fast then slow rate is difficult to explain. When the curve in Figure 4.3 is replotted along with the results of an unexposed control sample, the difference in short and long time diffusion rates is shown to be even more pronounced. Figure 4.4 shows the diffusion distance curve of Figure 4.3 along with the apparent diffusion distance curve for an unexposed sample. Some small portion of the initial drop seen in the exposed sample occurs in the control sample, this can be attributed to either some small amount of acid in the unexposed resist or perhaps evaporation of some residual casting solvent (PGMEA has an overlapping carbonyl peak). The long time change is not completely flat for the unexposed sample. This can

mostly like be attributed to the presence of small amount of uncatalyzed PTBOC thermolysis. PTBOC has an uncatalyzed thermolysis reaction pathway that results in background deprotection of PTBOC which likely accounts for the changes observed in the unexposed sample in Figure 4.4. Background thermolysis is distributed randomly throughout the PTBOC layer and not confined to a definite band, thus the long time slope of the diffusion distance curve for the exposed sample should be, to be completely accurate, corrected for the non-specific background deprotection. This would make the long time diffusion rate even slower, and therefore the change from the fast initial diffusion rate to long-time rate slightly more drastic than depicted.

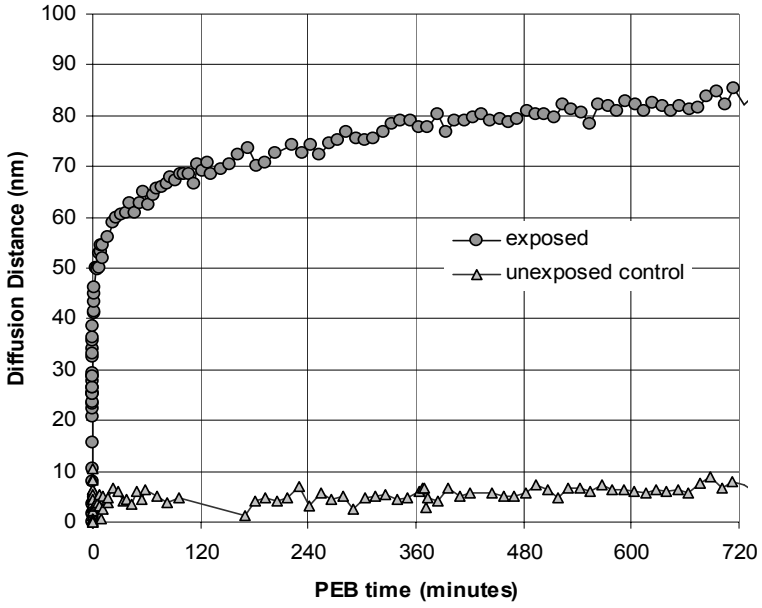

Figure 4.4: Long PEB data with unexposed control sample. T_{PEB} = 90 °C, PTBOC: 320 nm, PMOS: 420 nm, PAG: 10wt% $\phi_3S^{+}{}^{-}O_3SC_4F_9$

TEMPERATURE DEPENDENCE

In addition to just watching composition changes as function of time for fixed processing conditions, other parameters can be varied to probe the nature of acid transport in a reacting photoresist. Perhaps the simplest parameter to vary is the bake temperature. In the following temperature variation experiments sample construction parameters were fixed with a PTBOC layer of 320 nm thickness floated on to PMOS/PAG layer that was 420 nm thick. The PAG was triphenylsulfonium perfluorobutanesulfonate (TPS-nonaflate) synthesized in our labs. PAG loading was 10:1 weight ratio of polymer to PAG. That loading weight ratio works out to about 2 mol% acid in the film if full photochemical conversion of the PAG is obtained. Figure 4.5 below shows the results of several sample measurements made over the course of a 30 minute bake at temperatures of 75 °C, 90 °C, 100 °C and 110 °C. As expected, increases in bake temperature result in longer acid diffusion distances, and the shapes of the curves are all very similar.

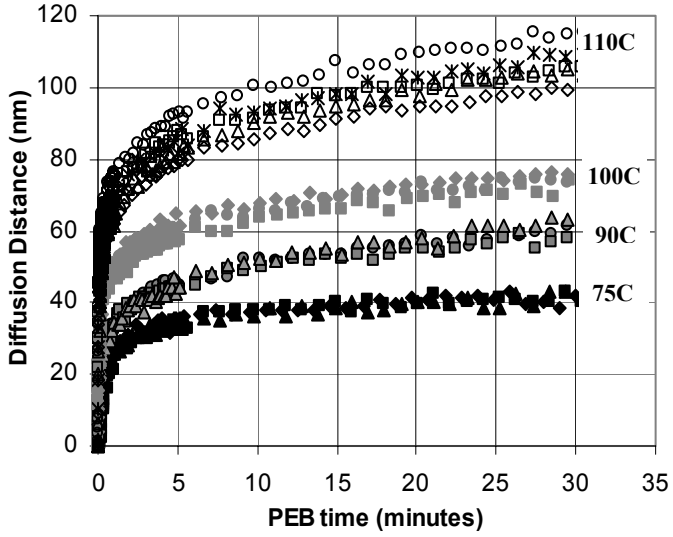

Figure 4.5: Diffusion Distance at various temperatures. PTBOC: 320 nm, PMOS: 420 nm, PAG: 10wt% $\phi_3S^{+}{}^{-}O_3SC_4F_9$.

For a given bake time it is possible to calculate a Fickian diffusion coefficient using Eqn. 2.5 ($D = L^2/2t$) that would correspond to the measured diffusion distance. This was done using the data in Figure 4.5 for bakes times of 1, 3, 5, 7, and 10 minutes and the results are summarized below in Table 4.1. The calculated diffusion coefficient increases with increasing temperature, but decreases when calculated for longer times. The time dependence of the diffusion coefficient suggests it is not just simple diffusion that is being measured, but something more complex. The implications of the apparent time dependence of the diffusion coefficient will be discussed later.

Table 4.1: Diffusion coefficients (nm^2/s) for different times and temperatures.

	Bake Time				
Temperature	1 minute	3 minute	5 minute	7 minute	10 minute
75C	5.6	2.6	1.9	1.7	1.1
90C	8.6	4.7	3.3	2.7	2.0
100C	20.0	8.7	6.1	4.8	3.6
110C	46.9	18.5	12.6	9.6	7.4

The temperature dependence of diffusion coefficients in polymers is a well studied topic. Several models have been put forth to explain this observed behavior such as the Eyring expression.[13] The Eyring equation is based on transition state theory, with the transition state in this analysis occurring when the penetrant is midway between microvoids, and is as follows:

$$D = e\lambda^2 \frac{kT}{h} e^{\Delta S^{\ddagger}/R} e^{-E_D/RT} \qquad \text{(Eqn. 4.2)}$$

where e is the exponential constant, λ is the length of the diffusive jump, k is Boltzmann's constant, h is Planck's constant, T is the absolute temperature, $\Delta S^{\ddagger}$ is the *entropy of activation for diffusion*, E_D is the *activation energy of diffusion*, and R is the universal gas constant. This model, derived from theory, is fairly complex, but at its core it is basically a modified Arrhenius relation. The Arrhenius equation, typically used to explain the temperature dependence of reaction kinetics, can be adapted to explain the dependence of diffusion on temperature as follows:

$$D(T) = D_o \exp\left(-\frac{E_D}{RT}\right) \qquad \text{(Eqn. 4.3)}$$

where $D(T)$ is the temperature dependent diffusion coefficient, D_o is a pre-exponential constant, and E_D, R, and T are the same as in Eqn. 4.2. According to Eqn. 4.3, if the natural logs (*ln*) of the diffusion coefficients in Table 4.1 are plotted versus inverse bake temperature, a linear curve should result. The negative of the resulting line slope should correspond to E_D/R, while $ln(D_o)$ will be the value of the curve extrapolated to infinite temperature (the y-intercept). Figure 4.6 shows the linear fits to plots of $ln(D)$ versus inverse temperature for D's calculated at various intervals during the PEB. The corresponding activation energies and pre-exponential factors are given in Table 4.2. The apparent activation energy of diffusion and the pre-exponential factor both decrease when calculated for longer bake times. Since diffusion rates are slowing at longer times, it is slightly counterintuitive that apparent activation energy would decrease for longer bake times. Slowing would seem to suggest that diffusive "jumps" are getting more difficult and, thus, would require more energy, but the entire decrease in diffusion coefficient with time is accounted for by decreases in pre-exponential factor. In reaction kinetics the pre-exponential factor is often referred to as the *frequency factor* and is said to relate to the frequency of molecular collisions. If the analogy between kinetics and diffusion is to hold, the results of Table 4.2 would have to be interpreted to mean that acid diffusion movements or "jumps" become easier (require less energy) over the course of the bake, but are attempted less often. That interpretation is not necessarily outlandish, but it is also not apparent what molecular level process would account for this behavior. It is more likely that the simple Arrhenius relation does not

capture all of the complexities of the system. In the actual system, thermal deprotection and autocatalysis from deprotected polymer are present as well as other complicating factors related to polymer relaxation dynamics and material property changes.

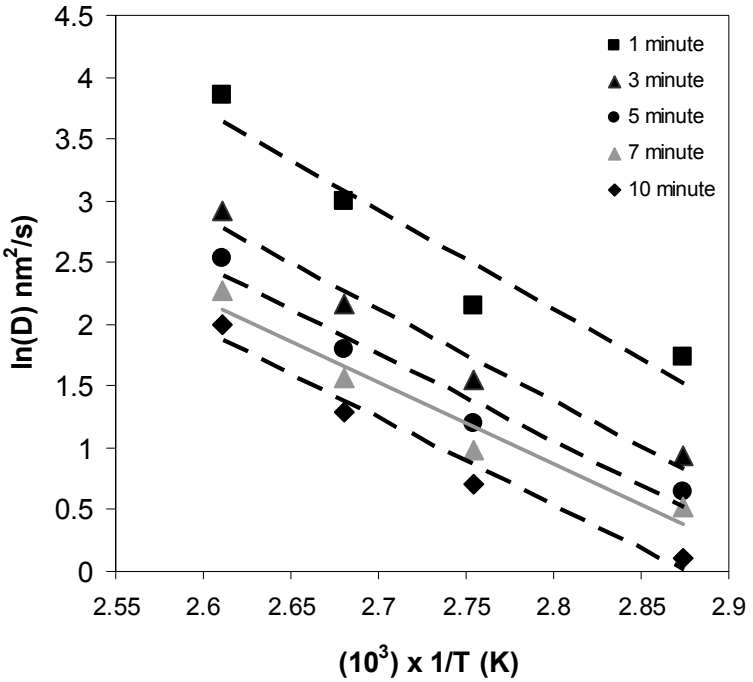

Figure 4.6: Arrhenius Plot ln(D) vs. 1/T at different bake times.

Table 4.2: E_D and D_o calculated at different times during PEB

	Bake Time				
	1 minute	3 minute	5 minute	7 minute	10 minute
E_D (kJ/mol)	66.9	61.5	59.2	54.6	58.9
D_o (nm^2/s)	5.0×10^{10}	4.0×10^{9}	1.3×10^{9}	2.3×10^{8}	7.1×10^{8}

IBM has reported[14] Arrhenius diffusion factors for the very system discussed above. For PTBOC, they report E_D = 152.7 kJ/mol and D_o = 1.9 x 10^{22} nm^2/s. They also report Arrhenius factors for diffusion in PHS (the deprotection reaction product) of E_D = 92.5 kJ/mol and D_o = 9.0 x 10^{11} nm^2/s. IBM's E_D for PTBOC is about 2.5 - 3 times larger than our estimated value and their D_o is over ten orders of magnitude larger. The values in Table 4.2 are apparent values and result from simplistic estimates of the diffusion coefficient which convolves diffusion and reaction effects into single number. IBM's values purport to be "intrinsic" diffusion values, that is, reaction effects are not included in their determination. In reality, their diffusion coefficient values are adjustable parameters in a rather complex simulation method. Thus, it is not surprising our estimates do not agree particularly well because, not only are the "measurements" made by different techniques, conceptually different things are being measured.

ACID MOLECULE SIZE DEPENDENCE

Several models are capable of predicting that diffusion rate will be affected by penetrant size. Intuitively, it would be odd if penetrant size did not affect diffusion rates in polymers, since the larger the penetrant molecule, the larger the void that must be created to accommodate it when it moves. In the gas phase there are relations that can be used to estimate diffusion coefficients based on diffusant sizes. One of these relations is the Chapman-Enskog[15] equation, shown below in simplified form for a binary system:

$$D_{AB} = K\left(\frac{1}{\sigma_{AB}^2 \Omega_D}\right)\left(\frac{1}{M_A} + \frac{1}{M_B}\right)^{1/2} \qquad \text{(Eqn. 4.4)}$$

where K is a temperature and pressure dependent constant, σ_{AB} is the Lennard-Jones collision diameter, Ω_D is the LJ collision integral, and M_A and M_B are the respective molecular weight of the diffusants. The LJ collision diameter is measure of molecular size and, according to Eqn. 4.4, D decreases with increasing size. As always, diffusion in the gas phase is easier to understand than in condensed phases and models for predicting diffusion coefficients based on molecular size in liquids or solids tend to be less general and less accurate. Liquid phase models for predicting diffusion coefficients tend to be variations on the Stokes-Einstein equation:

$$D = \frac{kT}{6\pi r \mu} \qquad \text{(Eqn. 4.5)}$$

where k = Boltzmann's constant, T is temperature, r is the radius of the diffusing particle, and μ is viscosity of the surrounding media. Several semi-empirical relationships based on Eqn. 4.5 (such as the Wilke-Chang equation) have been proposed for various systems and, like Eqn. 4.5, they predict decreased diffusion with increased penetrant size. Relationships developed to predict diffusion in solids tend to be limited to crystalline materials, but diffusion in polymers is somewhat like diffusion in liquids so perhaps a Stokes law model would not be completely inappropriate. The Glasstone, Laidler, Eyring equation (Eqn. 4.2) put forth to explain temperature dependence is actually, in a manner, linked to the molecular size-dependent Stokes models by the entropy term ($\Delta S^{\ddagger}$). The entropic

term implicitly considers penetrant size because it is clear that forming a large void requires more system ordering (decreasing entropy) than forming a small void.

It is fairly easy to use bilayer experiments to study the effect of acid anion size on diffusion simply by formulating the acid feeder layer with different PAGs. An initial experiment was conducted to study the effect of PAG size and type on measured diffusion distances with five different PAGs. The PAGs were tested at constant weight% loadings of 10 percent. Measurements were made at 100 °C with a PTBOC thickness of approximately 320 nm. The experimental diffusion curves measured for the five PAGs are shown below in Figure 4.7. The five PAGs can be divided into two different groups based on their chromophore (the photo active part of the PAG) type. The chemical structures of the five PAGs are shown in Figure 4.8 below. The PAG cation acts as the chromophore while after exposure the PAG anion becomes the conjugate base of the photoacid. All these PAGs produce strong acids as exposure products.

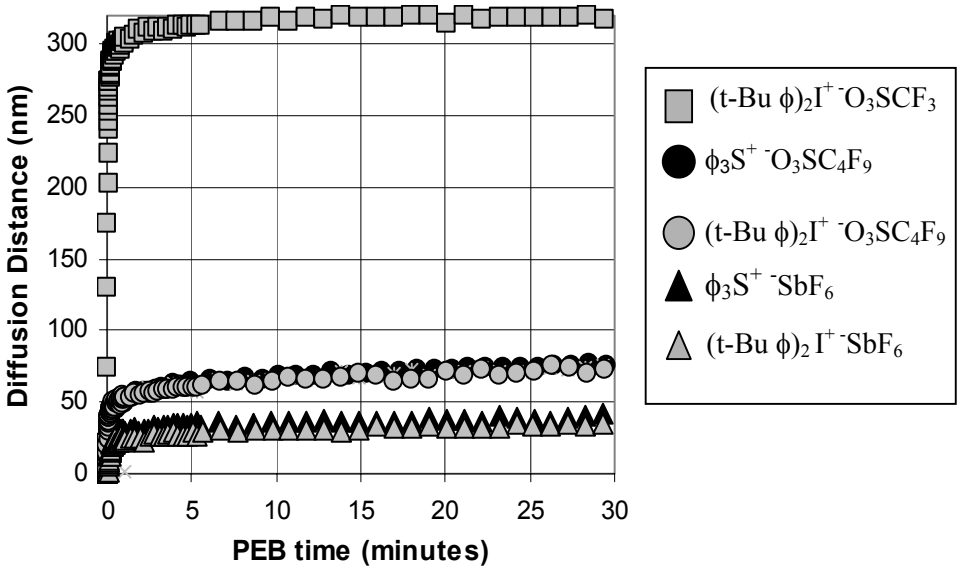

Figure 4.7: Diffusion Distance vs. PEB time for various PAGs at constant 10wt% loading. T = 100 °C, PTBOC: 320 nm, PMOS: 420 nm

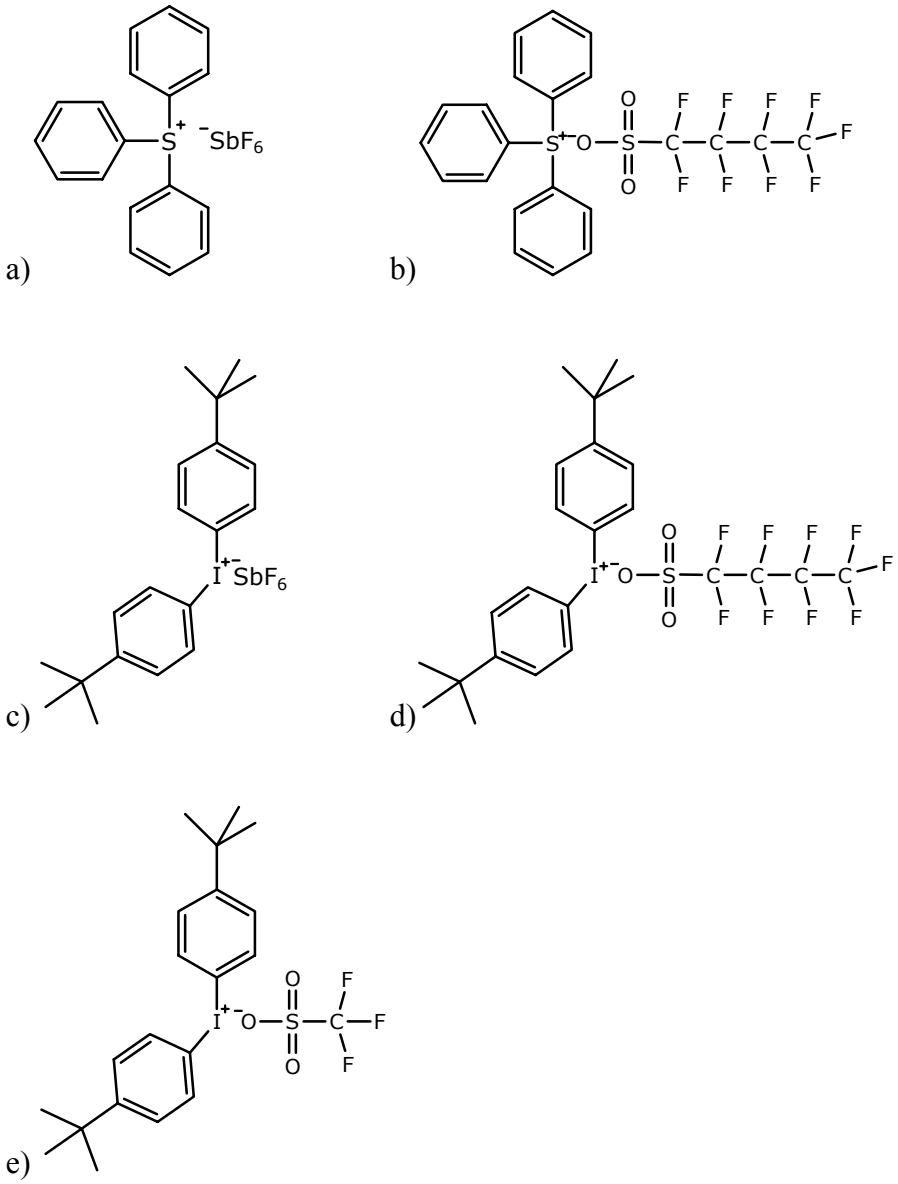

Figure 4.8: PAG Structures: a) triphenylsulfonium hexafluoroantimonate, b) triphenylsulfonium perfluorobutanesulfonate, c)bis(tert-butylphenyl)iodonium hexafluoroantimonate, d) bis(tert-butylphenyl)iodonium perfluorobutanesulfonate, e) bis(tert-butylphenyl)iodonium trifluoromethanesulfonante

The results in Figure 4.7 show that increasing conjugate base size decreases diffusion distances. The hexafluoroantimonate molecule is the largest molecule (acid molecular weight = 317 g/mol) and its diffusion rate is very slow. The nonaflate molecule is the second largest molecule (acid molecular weight = 300 g/mol) and it has the second slowest diffusion rate. The triflate molecule is the smallest (acid molecular weight = 150 g/mol) and it is, by far, the fastest. Not just the diffusion rate, but the distance at which diffusion plateaus is also affected by conjugate base size. The plateau seen for the triflate PAG is only an apparent plateau since the triflate actually appears to stop only because the 320 nm thick detector layer has been completely deprotected. The trifluoromethanesulfonic (triflic) acid generated by the triflate PAG is unusual in the data set in that it alone has an appreciable vapor pressure. Triflic acid also has solvent-like qualities, such that it could act as a film plasticizer, further increasing it diffusivity. Also, apparent in Figure 4.7 is that chromophore type does not seem to have a significant impact on acid diffusion. The main function of the chromophore is to absorb incident photons and then fragmentize to generate the acid. Once the chromophore fragments, it is no longer involved directly with the PAG anion, so it would not be expected to influence diffusion. There have been anecdotal reports from industry that chromophore type does influence diffusion, presumably by either the whole PAG or the photolysis fragments acting as plasticizers or inhibitors. This effect would likely not been seen in our experiments because acid diffuses into a clean polymer as the unexposed PAG molecules and photolysis fragments are initially confined to the feeder layer. Chromophore type does

control the quantum yield of acid generation, but, in these experiments, very high exposure doses were used to assure high conversion levels so the effect of quantum yield differences would be minimized.

For the purpose of easy, compact comparison between experiments Eqn. 2.5 ($D = L^2/2t$) was used to calculate apparent diffusion coefficients from the results seen in Figure 4.7. A single bake time of 1 minute was used in the calculation, and results are given in Table 4.3.

Table 4.3: Apparent Diffusion Coefficients at 1 minute for PAGs used in constant wt% loading experiment

	DTPI-Triflate	TPS-nonaflate	DTPI-nonaflate	TPS-antimonate	DTPI-antimonate
D (nm^2/s) at 1 minute	≥725	22.5	25.2	7.5	5.6

In many ways the previous experiment was poorly designed. Constant weight% PAG loadings are not really a fair method to compare photoacid performance. Differences in PAG molecular weights mean that for a given weight% in the feeder layer there are almost twice as many moles triflate as there are nonaflate. The previous experiment was redone with constant molar loadings of PAG in the feeder layer. Five PAGs were measured in this experiment, three from the previous experiment and two new ones. Based on the previous experiments, it was deemed unnecessary to test PAGs with the same anion but different chromophores. The structures of the two new PAGs (DTPI-hexaflate and polyPAG) are shown in Figure 4.9. The molecular weight of the generated

acid is 232 g/mol for DTPI-hexaflate. The polymeric PAG produces acid that is covalently linked to a macromolecule, effectively generating an acid with an enormous conjugate base. The DTPI-triflate, DTPI-nonaflate, and DTPI-antimonate from the previous experiment were used again in this experiment. Diffusion distance curves are shown in Figure 4.10.

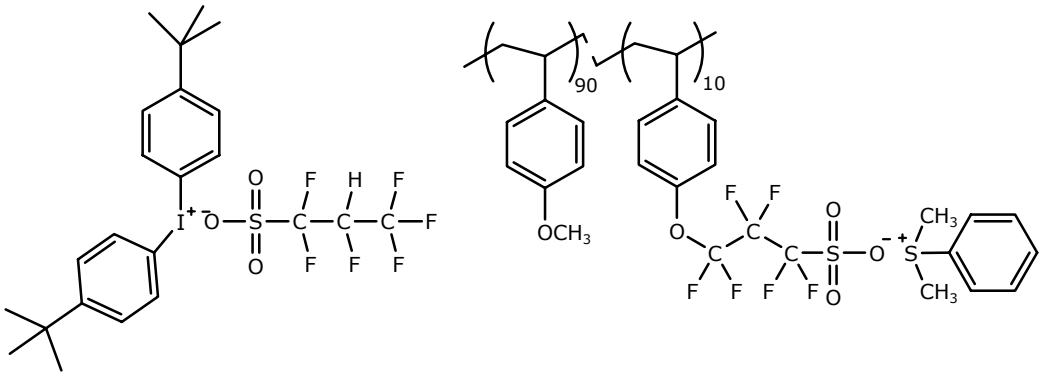

Bis(tert-butylphenyl) iodonium - 1,1,2,3,3,3 hexafluoropropanesulfonate

polyPAG

Figure 4.9: DTPI-Hexaflate and polyPAG chemical structures

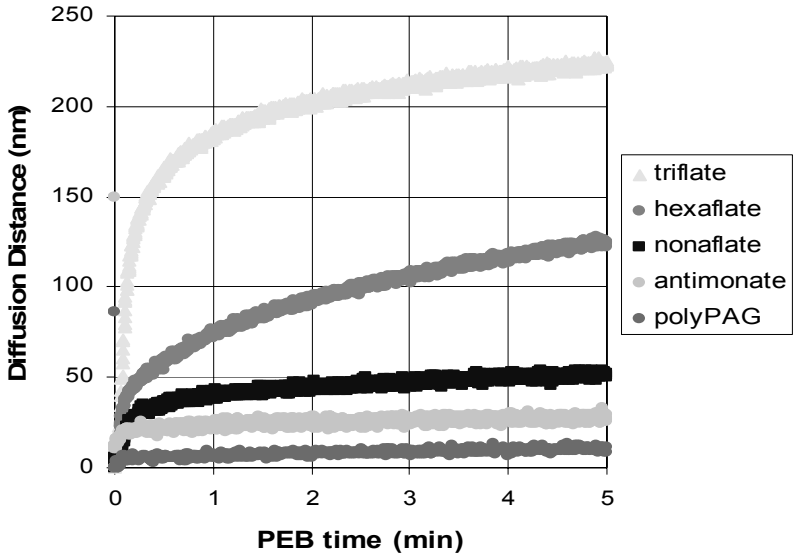

Figure 4.10: Diffusion distance vs. PEB time for various PAGs at constant 2.3% molar loadings. T = 90 °C, PTBOC: 300 nm, PMOS: 230 nm.

The results shown in Figure 4.10 are once again as expected; acid diffusion slows with increasing conjugate base size. For comparison, calculated (for a 1 minute PEB) diffusion coefficients are shown in Table 4.4 for each of the PAGs used to generate Figure 4.10.

Table 4.4: Apparent Diffusion Coefficient at 1 minute for PAGs used in constant molar loading experiment.

	DTPI-Triflate	DTPI-hexaflate	DTPI-nonaflate	DTPI-antimonate	PolyPAG
D (nm^2/s) at 1 minute	285.2	45.6	13.3	4.6	0.3

A very interesting part of Figure 4.10 is the presence of the so called polymeric PAG or polyPAG. The polyPAG is a new type of PAG developed by Willson Group chemists[16]. The polyPAG generates an acid with an anion that is covalently bound into the polymer background. The polymer-bound anion in effect becomes an enormous conjugate base. This would be expected to limit diffusivity of the polyPAG and Figure 4.10 shows that this is case. The polyPAG is a very interesting new molecule and it is discussed in greater depth in Appendix A.

From the standpoint of an acid diffusion investigation, perhaps the most significant interpretation of results in Figure 4.10 is simply that conjugate base size affects diffusion distances. This implies that acid diffuses as a proton-conjugate base pair and the acidic proton does not separate significantly from its counter ion. If the proton was able to separate significantly from its counter ion, diffusion would not correlate strongly with acid size - that it does, implies that coulombic attraction between the proton and its companion anion is strong enough to prevent significant separation. Xuelong Shi[17] has analyzed coulombic forces in exposed photoresists and reached the conclusion that the movement of the acid and its anion must be strongly correlated and, in fact, is *ambipolar* in nature. Ambipolar diffusion requires that oppositely charged species move in a coordinated manner, together or not at all, thus overall diffusion rate is controlled by the slower partner (the anion in this case). In addition to Shi's analysis, quantum mechanical simulations have been performed that suggest that separation of the proton/anion pair in media with dielectric constants similar to resist

materials is unlikely to be more than a nanometer.[18] If, as it appears, the proton is tied closely to its anion, chemical amplification in photoresist must occur by movement of the acid/anion pair and not just by proton migration.

BASE ADDITIVE EFFECT

Commercial photoresists are more complex than just a mixture of resin, PAG, and casting solvent. A commercial photoresist formulation may contain almost any number of extra additives. Just which additives, and in what amounts, are usually closely guarded trade secrets. Secrets must be kept because often there is no fundamental scientific understanding of the role the additives play in lithographic performance. Typically all that is known is an accumulated set of heuristics, the costly product of numerous trial and error experiments. Companies are usually unwilling to give away their hard won knowledge for free and one of the most closely guarded secrets is the type and amount of alkaline additives included in the resist formulation. One of the main reasons base is added to resist formulation to control resist sensitivity. Adding base controls resist sensitivity by reacting with some fraction of generated photoacid. A less sensitive resist is, amongst other things, less prone to atmospheric contamination problems. Another common reason to add base to a photoresist is to limit feature width changes caused by acid diffusion. When acid molecules from exposed areas begin to diffuse into unexposed areas, they will encounter base molecules and be destroyed (neutralized). The base acts as an acid scavenger in unexposed areas and, thus, limits linewidth spreading. Base additive effects are fairly complex

since the base molecules do not necessarily stay immobile, and can diffuse through the photoresist as well and will need to be studied separately.

The bilayer method provides a useful method for investigating the effect of base additives on changes in linewidth. The upper layer, simulating the unexposed resist, can be doped with base prior to spin casting. Figure 4.11 presents some diffusion distance versus PEB time curves for varied levels of the base 1-piperidineethanol in the PTBOC upper layer. Listed ratios are moles PAG to moles base, calculated on the basis of a hypothetical PAG loading of 1 mol% in the PTBOC layer (no PAG was actually included in the upper layer). As expected, increasing base loading reduces extent of acid diffusion, but diffusion was not completely suppressed even when PAG:Base ratio went below 1:1. A loading of 1:2 (PAG:BASE) would not be possible in an actual functioning resist because all acid would presumably be destroyed and none would be available to deprotect the resist in exposed regions, but this case can be simulated in the bilayer experiment even if it is not a realistic example. The diffusion distance seen for "excess" base loading suggests that base diffusion must also be considered when trying to predict final linewidths. The 1:2 base loading sample still has a measurable diffusion distance. This suggests that base even at high loadings is not capable of fully suppressing diffusion. This might be because the local base concentration was overwhelmed by local acid concentration. The base concentration is not necessarily uniform throughout the PTBOC layer, several people have proposed that the spin coating process does not necessarily produce a uniform distribution of resist components in the film. An extreme gradient in

additive distribution is not expected, but this could be a factor. Some early work has suggested it is also possible that the acid-base reaction does not completely "annihilate" the acid and the acid remains partially available for deprotection catalysis such that even "neutralized" acid may cause linewidth spreading.[19]

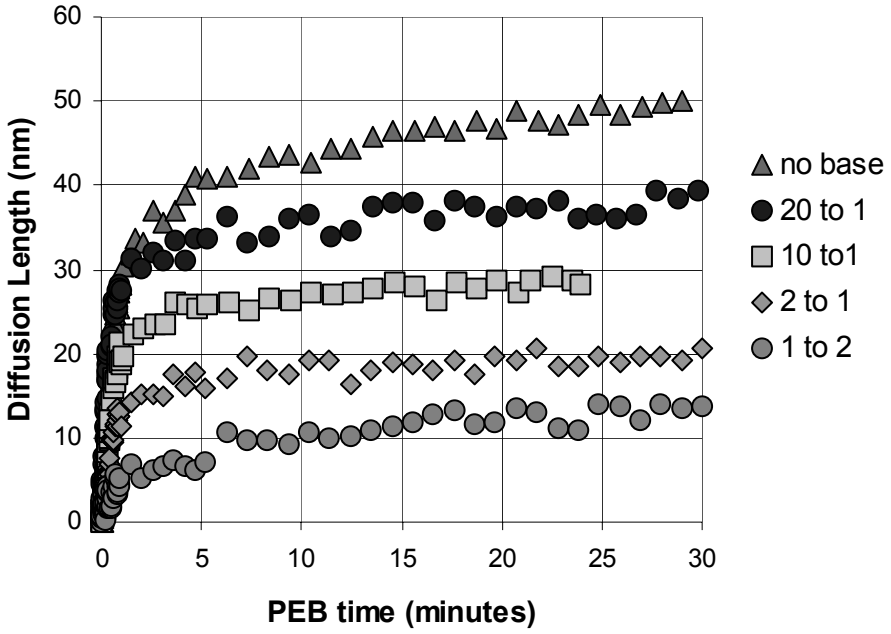

Figure 4.11: Diffusion Distance vs. PEB time for different base additive loadings. T = 90 °C, PTBOC: 320 nm, PMOS: 420 nm, Base: 1-piperidineethanol, PAG: TPS-nonaflate (5wt%)

ANALYSIS OF RESULTS

Using Eqn. 2.5, an apparent diffusion coefficient can be calculated for every point in time of the PEB. If the diffusion process is simply Fickian, a plot of apparent diffusion coefficient as a function of time would be a horizontal line.

In Figure 4.12 the calculated, apparent diffusion coefficient is plotted as a function of PEB time for one representative data set at 110 °C. Other data sets at other temperatures produce similar plots with lower temperatures being less extreme version in magnitude, but not form.

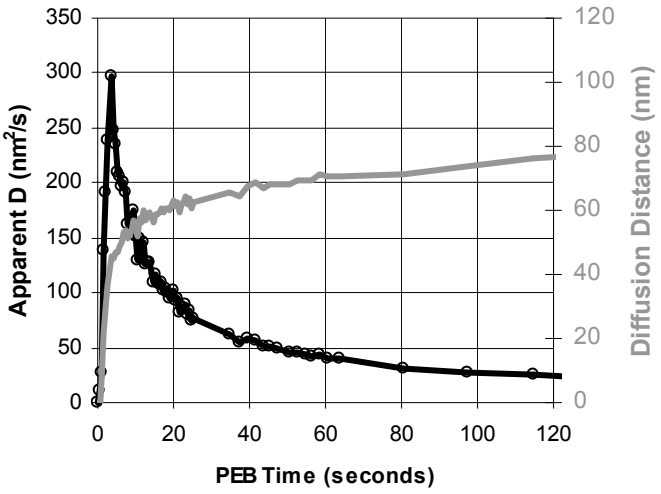

Figure 4.12: Apparent diffusion coefficient change during the PEB. T = 110 °C

In Figure 4.12 above, the apparent diffusion coefficient is seen to be a function of time. The apparent diffusion coefficient increases rapidly to approximately 300 nm^2/s in the first 3-5 seconds, then begins a power law-like decay approaching zero at long times (not shown). The initial jump in diffusion coefficient is likely the result of a startup temperature transient. The sample wafer when placed on the hotplate has a finite heating rate from room temperature to the hotplate temperature. The startup transient for this experiment type has

been measured previously and is on the order of five seconds.[1] The decay process is less clearly explainable and is the topic of discussion.

First, solving of the traditional Fickian model, then plotting penetration distance of acid (at some low concentration level) will demonstrate its inability to match our results. For the case of an infinite slab with a constant penetrant surface concentration (infinite supply), solution of Fick's law yields the following result:

$$\frac{C(x,t)}{C_o} = \frac{1}{2}\left[1 - erf\left(\frac{x}{\sqrt{4Dt}}\right)\right] \qquad \text{(Eqn. 4.6)}$$

where $C(x,t)$ is penetrant concentration, C_o is the initial surface concentration, D is the diffusion coefficient, x is depth into the slab, and t is diffusion time. This equation can be used to generate penetration distance in to film as a function of time for a fixed concentration level or concentration profiles at some fixed time. In Figure 4.13 below, the penetration of a low acid concentration threshold of C/C_o = 5% is plotted as a function of time. The diffusion coefficient (D) was set at 100 nm^2/s in attempt to match the short-time behavior. As seen below, the short time behavior is matched reasonably well, but at the price of matching the long term. The experimental data shown in Figure 4.13 was collected at 110 °C, 10 wt% TPS-nonaflate.

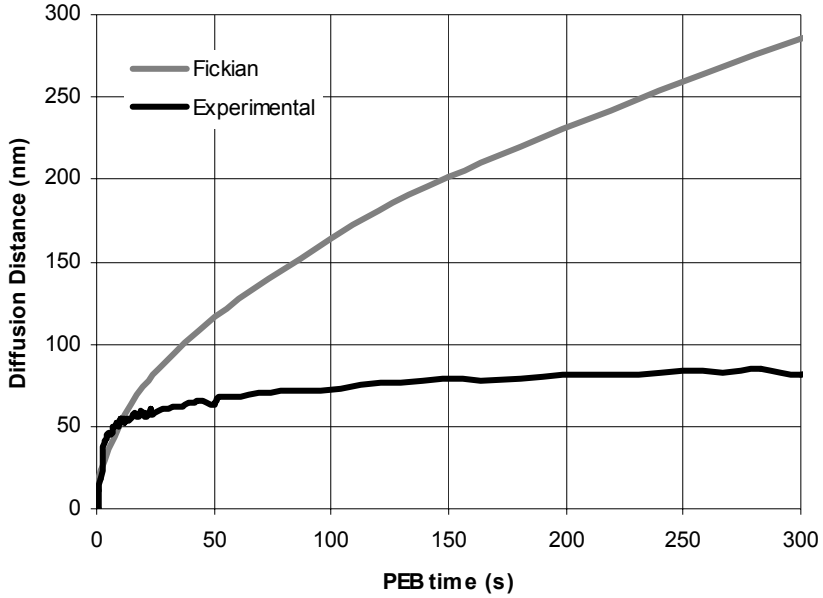

Figure 4.13: Single, constant coefficient Fickian model match to experiment data.

In the experimental diffusion distance curves, the dramatic slowing in rate of diffusion seen after an initial rapid period is particularly difficult to understand. A modified Fickian diffusion model might be able to approximate this behavior, but it would require a large diffusion coefficient (to explain the rapid initial rate) and either an acid loss mechanism or a significant drop in concentration due a limited acid supply. A loss mechanism, such as base trapping, can not be completely ruled out, but in experiments when the film was intentionally doped with base additives far above natural levels, the curve shapes and diffusion distances were not dramatically altered. By design, the issue of finite supply can probably also be discounted in these experiments. The acid feeder layer in bilayer

experiments is usually roughly the same thickness as the overlayer and the PAG loading in several cases above is 10wt%. If the acid completely redistributed homogeneously throughout both layers of the film stack, its overall concentration would not drop below roughly 5wt%. That level of PAG (after exposure) would completely deprotect the PTBOC film in about one second at 90 °C.[1] The feeder layer (PMOS) is close to its glass transition temperature at 90 °C and thus acid should readily diffuse out of that layer unless photoacid has some preference for PMOS polymer that results in a significant partition coefficient between the layers. The chemical similarity between PMOS and PTBOC does not suggest any obvious reasons for an acid molecule to have a dramatic preference for PMOS over PTBOC, so it seems unlikely that the acid concentration is significantly depleted by an approximately 15% (50 nm diffusion distance/350 nm PMOS layer thickness) increase in volume.

TWO DIFFUSION COEFFICIENTS

In the above discussion, reaction effects were not explicitly included in the single diffusion coefficient model, but reaction effects are implicitly convolved with diffusion in the single term model. It was a simplifying assumption that the reaction is diffusion limited and thus the acid front is approximately co-located with deprotection front. Others[20,21] have solved the full reaction-diffusion model including complex kinetics of reaction and have found that single coefficient model can not explain all observations. Because the chemical reaction produces a material change (and Chapter 3 showed that the material change results in

significant transport property changes) it seems probable that at least one other diffusion coefficient is needed in the model to account for reaction effects. The actual linewidth spread observed in experiment and manufacturing is, at the minimum, likely a function of both the reacted and unreacted material diffusion coefficient. The reacted material has a much smaller diffusion coefficient than the starting material and this will act to impede diffusion. If the reacted material had a larger diffusion coefficient a situation more like Case II or anomalous non-Fickian diffusion might result. Multiple methods for accounting for material change have been proposed including a linear mixing rule and exponential free volume dependent models. Figure 4.14, below, shows results from a simulation which features two distinct diffusion coefficients, one for reacted and one for unreacted. In this simulation, the chemical reaction kinetics are taken to be much faster than the diffusion time scales and the chemical switch is taken as automatic and full when catalyst concentration reaches a minimum threshold value. The minimum threshold value is an adjustable simulation parameter set to give a final conversion equal to the experimental value. The simulation is unable to fit the observed experimental results with diffusion coefficients based on our measurements in Chapter 3 ($D_{PHS} = 5 \times 10^{-16}$ cm^2/s, $D_{TBOC} = 2.5 \times 10^{-14}$ cm^2/s). It would seem that a much larger D_{TBOC} and/or a smaller D_{PHS} are required to fit the form of actual experimental data.

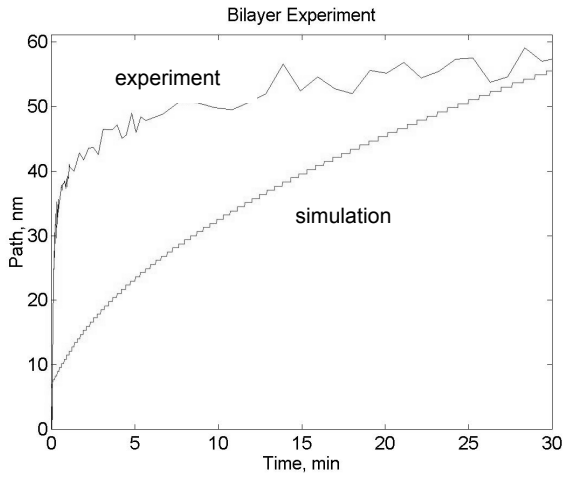

Experimental T = 90 °C
D_{tboc} = 2.5 x 10^{-14}
D_{PHS} = 5 x 10^{-16} cm^2/s

Figure 4.14: Comparison of experimental data to simulation with material dependent diffusion coefficients.

TRANSIENT REACTION-ENHANCED DIFFUSION

There is no reason to suspect that D_{TBOC} estimates are low by several orders magnitude. And, there is no reason to suspect the already small D_{PHS} is actually much smaller than estimated. The use of material-based diffusion coefficients are an attempt to account for the effect of chemical reaction on diffusion, but it is quite possible that reaction effects include more than just material composition change. The D_{TBOC} estimated in Chapter 3 is an intrinsic diffusion coefficient, that is, it does not include reaction effects; it is based on the pre-reaction diffusivity. The diffusion coefficient estimates from lithographic processes or the bilayer experiments of this chapter are typically much larger than the non-reactive D_{TBOC} or D_{PHS} estimates from Chapter 3. This suggests that acid

diffusion might somehow be increased or enhanced by the presence of the deprotection reaction. A reaction-enhanced diffusivity would effectively result in an apparent D_{TBOC} that is larger than the non-reactive estimate (D_{ao} in the notation of Chapter 3).

In Chapter 2, a Reaction Front Propagation model was discussed as an explanation for observed behavior. A key assumption of this model is that that the deprotection reaction causes a local, transient enhancement to acid diffusivity. Because D_{ao} estimates from Chapter 3 for PTBOC are seemingly too small to explain observed initial diffusion rates, some type of transport enhancement becomes necessary. Possible diffusion enhancement mechanisms might be excess free volume generated by the evolution of gaseous deprotection by-products or plasticization of the polymer caused by lingering of the gaseous by-products. Another possibility is local resist heating by exothermic reaction. Because diffusion slows, it is necessary that any enhancement be temporary and all three of the proposed mechanisms can be transient in nature. Excess free volume will collapse as the polymer relaxes, gaseous by-products diffuse away and desorb from the film, and any reaction-generated temperature gradients in the film will eventually equilibrate. The next chapter is a discussion of experiments designed to probe the existence and nature of a transient state in reacting photoresists.

GLOBAL VS. LOCAL DIFFUSION

In chemically amplified photoresists, it is assumed that there is some trade-off between acid diffusion-induced image blurring and catalytic

amplification. Chemical amplification requires the acid to be mobile enough to move to catalyze reactions at several sites, but not so mobile as to allow significant catalyst migration into unexposed regions. The estimated intrinsic (non-reactive) diffusion coefficients are believed too small to explain experimentally observed amplification. Researchers at IBM have reached a similar conclusion; to explain observed diffusion behavior they have invoked two different acid diffusivity rates, one local diffusivity to account for amplification and another long-scale, global diffusivity to account for translational diffusion resulting in diffusion bias, or linewidth spread.[14] It is not particularly satisfying to have macroscopic diffusivity disassociated from microscopic diffusivity in such a manner. The possible mechanisms to explain the apparent disconnect between local and global diffusivity have not been fully elucidated. To state that amplification occurs because the reaction has a long catalytic chain length is simply tautological, and ignores an important point: an acid's catalytic chain length can not be greater than the number of reaction sites it can access. In a glassy polymer, movement of the polymer chains is basically precluded on the time scales we are studying, so the number of accessible reaction sites must be governed by the distance the acid can migrate. In order to explain the catalytic chain lengths observed experimentally, the acid/anion complex must have higher than expected mobility, at least temporarily. The local enhancement of mobility postulated in the reaction front propagation model to explain line width spread in reactive systems can also be used to explain the anomalously high amplification. Reaction-enhanced diffusion, thus, reconnects global and local diffusivities.

According to the reaction front propagation model, the deprotection reaction causes a local enhancement in acid mobility in the regions where the reaction is in progress. This enhancement effect allows for a temporary increase in the acid/anion mobility, which in turn allows a larger number of reaction sites to become accessible to the acid for some short, finite time. Because the enhancement is transient and not recoverable in reacted regions, acid mobility eventually drops back to the slower intrinsic diffusion rates.

REFERENCES

1. Sergei V. Postnikov, *Ph.D. Dissertation*, The University of Texas at Austin, 1999.

2. E.K. Lin, C.L. Soles, D.L. Goldfarb, B.C. Trinque, S.D. Burns, R.L. Jones, J.L. Lenhart, M. Angelopoulos, C.G. Willson, S.K Satija, W. Wu. *Science*, 2002; **297**, 372.

3. S.J. Whitlow, R.P. Wool. *Macromolecules*, 1989; **22**, 2648.

4. D. Hall, J. Torkelson, *Macromolecules*, 1998; **31**, 8817.

5. E. Lin, W. Wu, S. Satija, *Macromolecules***,** 1997; **30,** 7224**.**

6. A. Karim, B.H. Arendt, G.P. Felcher, T.P. Russell. *Thin Film Solids,* 1991; **1202**, 345.

7. D.S. Fryer, S. Bollepali, J.J. de Pablo, P.F. Nealey. *J. Vac. Sci. Technol. B*, 1999; **17**, 3351.

8. D.L. Goldfarb, M. Angelopoulos, E.K. Lin, R.L. Jones, C.L. Soles, J.L. Lenhart, W. Wu. *J. Vac. Sci. Technol. B*, 2001; **19**, 2699.

9. M. Zuniga, A.R. Neureuther. *J. Vac. Sci. Technol. B*, 1995; **13**, 2957.

10. L. Schlegel, T. Ueno, N. Hayashi, T. Iwayanagi. *Jpn. J. Appl. Phys.* 1991; **11B**, 30; L. Schlegel, T. Ueno, N. Hayashi, T. Iwayanagi. *J.Vac. Sci. Technol. B*, 1991; **9**, 278.

11. J. Sturtevant, S. Holmes, P. Rabidoux, *Proc*. *SPIE*, 1992; **1672**, 114.

12. M.A. Zuniga, G. Wallraff, E. Tomacruz, B. Smith, C. Larson, W.D. Hinsberg, A.R. Neureuther. *J. Vac. Sci. Technol. B,* 1993; **11**, 2862.

13. S. Glasstone, K.J. Laidler, H. Eyring, *The Theory of Rate Processes*, McGraw-Hill: New York, 1941, p524.

14. F.A. Houle, W.D. Hinsberg, M. Morrison, M.I. Sanchez, G.M. Wallraff, C. Larson, J. Hoffnagle. *J.Vac. Sci. Technol. B*, 2000; **18**, 1874.

15. A.L. Hines, R.N. Maddox, *Mass Transfer Fundamentals and Applications*, Prentice Hall: Englewood Cliffs, NJ, 1985.

16. Hoang Vi Tran, *Ph.D. Dissertation*, The University of Texas at Austin, 2002.

17. X. Shi. *J. Vac. Sci. Technol. B*, 1999; **17(2)**, 350.

18. G.M. Schmid, V.K. Singh, L.W. Flanagin, M.D. Stewart, S.D. Burns, C.G. Willson. *Proc. SPIE*, 2000; **3999**, 675.

19. Private Communication: Timothy Michaelson and C. Grant Willson, The University of Texas at Austin.

20. E. Croffie, M. Cheng, A. Neureuther. *J. Vac. Sci. Technol. B*, 1999; **17**, 3339.

21. A.A. Krasnoperova, M. Khan, S. Rhyner, J.W. Taylor, Y. Zhu, F. Cerrina. *J. Vac. Sci. Technol. B, 1994*; **12**, 3900.

Chapter 5: Transient Experiments

As discussed in Chapters 2 and 4, the existence of a reaction-promoted, transient enhancement to acid mobility has been postulated to explain various experimental observations. The proposed mechanisms for the generation of transient enhancement were plasticization by reaction by-products, temporary free volume increases caused by volatile by-product evolution, and a local temperature increase caused by the exothermicity of deprotection. Possible sources for the transient enhancement have been suggested, but no conclusive evidence has been put forth to demonstrate that a transient physical environment actually exists in the reacting photoresist. The experiments in this chapter were designed to investigate the chemical-physical nature of a reacting photoresist to determine if a transient state triggered by by-product generation and evolution exists. The possibility of local heating is not explored in this method.

In tBOC based photoresists, the solubility switching deprotection reaction (Figure 1.5) results in the generation of gaseous by-products, carbon dioxide and isobutylene. It could be reasonably expected that the presence (and then subsequent desorption) of these by-products might alter the film properties in some manner. The deprotection reaction is certainly changing the photoresist chemically, but the effect (if any) an on-going chemical reaction has on acid mobility is not known in detail. The ultimate result of the completed chemical reaction is a large decrease in acid mobility in reacted regions, but the transitioning from reacted to unreacted material, not the overall chemical change

itself, is the suggested source of mobility enhancement. A schematic depiction of reaction-generated enhancement is presented in Figure 5.1.

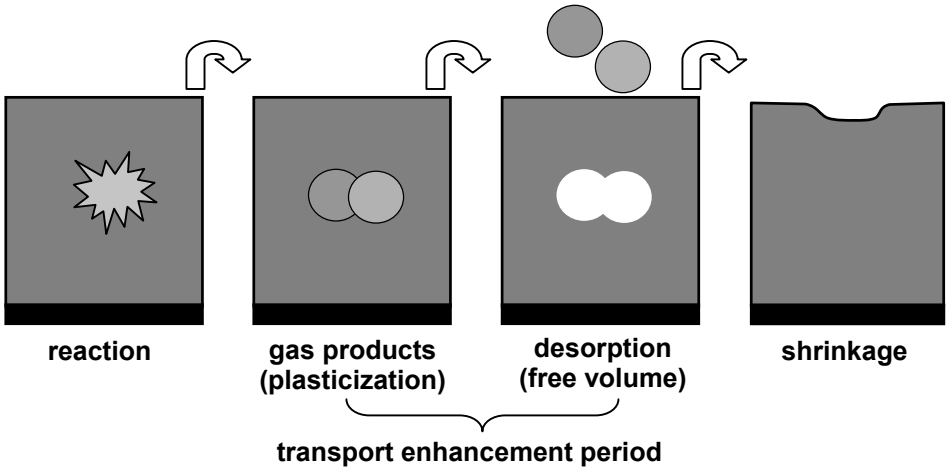

Figure 5.1: Mechanisms of reaction-generated transient enhancement

Because the deprotection reaction generates gaseous by-products, it would be expected that immediately after the deprotection of a TBOC reaction site that a fairly unusual environment would exist locally; where once just polymer and acid existed, it is now polymer, acid and gas molecules altogether. In an instant, the PTBOC unit looses approximately half its mass as gaseous by-products. According to IR analysis and thermogravimetric analysis (TGA) studies[1], the vast majority of those generated gas molecules apparently desorb fairly quickly from the resist film, but it seems entirely possible that the presence (short though it may be) and then subsequent desorption of these by-products might alter the film properties. One of the proposed mechanisms for mobility enhancement is local

plasticization and carbon dioxide, in particular, is a well known, well studied[2,3] plasticizing agent. If these reaction by-products remain in the film, they might act as plasticizers and, therefore, provide mobility enhancement to the acid. Even after these by-products leave the vicinity of reaction, the reaction area might still be in an unsettled, low density, state for some finite time. The atoms in the gas by-products account for about half the mass of the initial TBOC repeat unit and also about half its initial volume. When the gas products diffuse away from the reaction site they might leave a significant void in the matrix at their initial location. While these voids exist, they increase polymer free volume (or lower viscosity). Increasing free volume in the polymer would offer increased opportunities for diffusion. The effect of increasing free volume by void creation would be similar to increasing free volume by temperature increase – diffusivity would go up.

A transient state almost certainly exists, it is really only a matter of how long it exists and whether that time is long enough to actually alter diffusivity. The experiments described in this chapter were designed to determine if a lag exists between the generation of reaction by-products and film shrinkage. If seen, a lag would be indicative of a reaction-generated transient state. Based just on the existence of a lag it would not be possible to distinguish between mechanisms of plasticization of free volume void creation, but the two are fairly similar in concept and consequence. If a lag was seen, other experiments might be designed to distinguish specific root causes. The other proposed enhancement

mechanism is local thermal increases due to exothermic reaction; the experiments designed for this chapter do not attempt to look for this effect.

EXPERIMENTAL METHOD

It is well known that the PTBOC film loses considerable thickness upon reaction[4], but the exact relationship between reaction kinetics and rate of thickness loss is not known. A time lag between generation of by-products and film thickness change would indicate that for, at least the period of the lag, a non-equilibrium state exists in the photoresist film. A gap might be caused by either the by-products remaining in the film or the film not relaxing instantaneously to fill the space left by desorbing by-products. If the rate of by-product generation could be measured and linked to measurements of film shrinkage, the existence of a lag could be determined.

The extent of reaction in the film can be monitored quite easily via IR absorbance of the film. For tBOC-based resists, the strong carbonyl peak (near 1760 cm^{-1}) can be monitored to determine when and at what the rate by-products are being generated in the film. Film thickness can be measured by any of several methods, but the method of this chapter relies on spectroscopic ellipsometry. Spectroscopic ellipsometry can determine both the film's thickness and the refractive index simultaneously. Because the film is changing chemical composition, it is possible that index will be changing along with thickness, so ellipsometry is useful in this regard. The apparatus of this experiment has gone through several design iterations.[5] Initially, reflectometry (multi-wavelength interferometry) was used in place of ellipsometry, but reflectometry requires the

index of the sample to be known. Accounting for refractive index changes requires making assumptions about how index changes with time during the reaction, which is, to a large degree, related to exactly what the experiment was purporting to measure. Ellipsometry removes the need to make any assumptions about refractive index changes and is thus preferred.

The current experimental design (depicted in Figure 5.2) uses a "flash" exposure technique. The sample wafer is placed on a hotplate, controlled at the experimental temperature, and allowed to equilibrate (~ 1 minute). Then the sample, while being monitored by IR and ellipsometry, is exposed to generate the acid by a short pulse (~100 milliseconds) of DUV laser energy. The flash method removes the startup temperature transient associated with placing a silicon wafer on a hotplate. The reaction kinetics are very temperature dependent, and at several temperatures of interest, the time to reaction completion is about the same order of magnitude as the warm-up period (~5 seconds). The laser flash method removes a needless complication from the analysis. Results from a previous iteration using a separate (off hotplate) exposure step and interferometry where previously reported.[5]

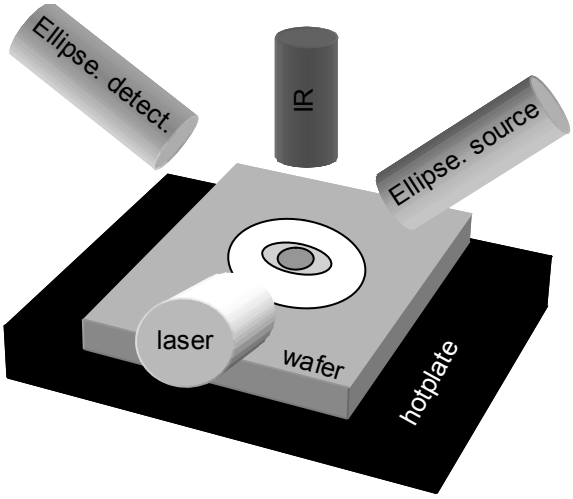

Figure 5.2: Transient experiment experimental setup.

MATERIALS AND SAMPLE PREPARATION

A simple photoresist consisting of homopolymer of *tert*-butyloxycarbonyloxystyrene (PTBOC), 2.5wt% (solids) bis(*tert*-butylphenyl)iodonium perfluorobutanesulfonate (DTPI-nonaflate) and PGMEA casting solvent was formulated. The resist formulation was spin cast onto the silicon side of a double-polished, aluminum-coated silicon wafers. Resist films were then post apply baked for two minutes at 90 °C. The films received extra baking at the experimental temperature when placed on the apparatus hotplate prior to the flash exposure. This extra, pre-exposure baking time was not closely controlled, but is estimated to have varied in the 3-5 minute range.

EQUIPMENT SETUP

The FT-IR used in these experiments is the same Nicolet 550 Magna IR equipped with an external detector described in previous chapters. As depicted in Figure 5.2, the IR beam must be perpendicular to the sample to collect data. The ellipsometer is a J.A. Woollam Co., Inc. M-2000V variable angle spectroscopic ellipsometer. The spectroscopic range is 350 nm – 1000 nm. This model does not produce light in the deep ultraviolet and, thus, does not expose the PAG and create acid during measurements. The ellipsometer beam angle can be varied from 30° to 90° (from normal to the wafer plane). Data collected in these experiments used a 70° degree angle on the ellipsometer. As shown in Figure 5.2, the IR and ellipsometer beams were aligned to sample the same spot on the wafer. As the two beams are different in size and shape, the spots did not coincide exactly, but were centered on the same point. Flash exposure was generated by a Cymer ELS-5400 Krypton-Fluorine (248 nm) excimer laser. The laser energy was passed through a non-solarizing fiber optic cable and was aligned to be incident to the wafer plane at 30° from normal. The end of the fiber optic cable was approximately six inches from the sample wafer. Exposure doses of approximately 100 mJ/cm^2 were delivered at pulse rate of 100 Hz and pulse energy of 1 mJ/cm^2.

DATA SYNCHING

IR and Ellipsometry data were collected by separate instruments attached to separate computers. Synchronization of the two data sets is critical if useful information is to be obtained. Prior to flash exposure, data collection was started

by both instruments and the unexposed sample was monitored. During this pre-exposure period a shutter was placed in front of the sample such that both instruments collect only noise. The shuttering was repeated multiple times (typically three). After the experiment was finished data from each instrument is separately analyzed, and synchronization is accomplished by matching up gaps in the data created by shuttering. The data collection rate for the FT-IR and ellipsometer is 8 Hz and 12 Hz, respectively. Based on the data collection rates the uncertainty in data synching should be approximately 210 milliseconds.

RESULTS AND DISCUSSION

With the data collection methods properly synchronized, it still remains to decide how the results should be combined. The working hypothesis behind this experiment is that there is a temporal difference between the deprotection reaction (IR measured) and the film shrinkage (ellipsometer measured). When the two data sets are plotted on the same time axis, they have y-values with different scales and units making comparison between the two meaningless. The IR data is on a scale of arbitrary absorbance units, proportional to concentration of reactant (tBOC carbonyl) remaining in the film. The ellipsometry data is in nanometers. To make the relation meaningful, the two must be on related scales. This can be accomplished by normalization of both sets to a percent change coordinate. The film has an initial IR absorbance value A_o corresponding to the unreacted film and an absorbance value at any time during the experiment of A. The absorbance of

the film normalized to the initial absorbance corresponds to the percentage of initial tBOC remaining in the film, which gives:

$$NA = A/A_o \qquad \text{(Eqn. 5.1)}$$

where NA is the normalized IR absorbance (1 - 0 scale), or also the percent tBOC unreacted. The film has an initial thickness value, T_o, and a thickness at any time during the experiment of T. For proper normalization, it is also necessary to know the final thickness for a completely reacted ($NA = 0$) film, T_f. A scale normalized just to T_f would not be bounded between one and zero and would not correspond to percent complete or remaining. In analogy with the IR normalization corresponding to percent unreacted, it would be preferred that the ellipsometry normalization correspond to percent "unshrunk", that is percent of total film thickness change remaining. The correct normalization, which is correctly bounded and corresponds to percent film shrinkage uncompleted, is as follows:

$$NT = \left[1 - \frac{(T_o - T)}{(T_o - T_f)}\right] \qquad \text{(Eqn. 5.2)}$$

where NT is the normalized thickness change. In practice this normalization is most simply accomplished by plotting NA and T on separate y-axes and adjusting the scale of the T-axis to y-max = T_o and y-min = T_f.

Once proper normalization has been conducting, the goal of the experiment is to determine if there is a temporal lag between reaction and film shrinkage. A lag would manifest itself as a gap on the time axis between the two plotted curves, NA and NT, at any time during the experiment. A gap between

curves at any time *t* can be used to measure a lag persistence by determining at what time, *t'*, the upper curve (presumably *NT*) equals the value of the bottom curve at time *t* (presumably *NA(t)*). The lag persistence would equal *t'* minus *t*. This process is illustrated on an idealized data set in Figure 5.3 below.

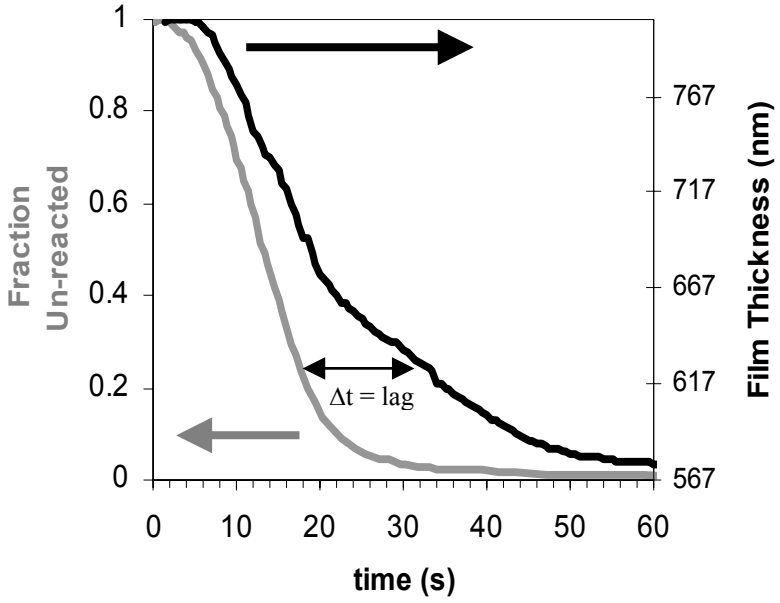

Figure 5.3: Determination of time lag between reaction and film shrinkage on an idealized data set.

Experiments were carried out at three different temperatures (75 °C, 90 °C, 100 °C) using laser flash exposure. The results are given in Figures 5.4-5.9 below, two sample runs at each temperature. The different temperatures were used to see if any effect of temperature on polymer relaxation dynamics could be seen. The range chosen was dictated by the reaction kinetics of the resist formulation. At temperatures below 75 °C, the reaction is too slow to permit full

reaction of the film in a reasonable time; at temperatures above about 100 °C, the reaction is too fast to allow capturing of more than a few data points. Also, at temperatures above 100 °C, the uncatalyzed resists deprotection rate begins to become noticeable.

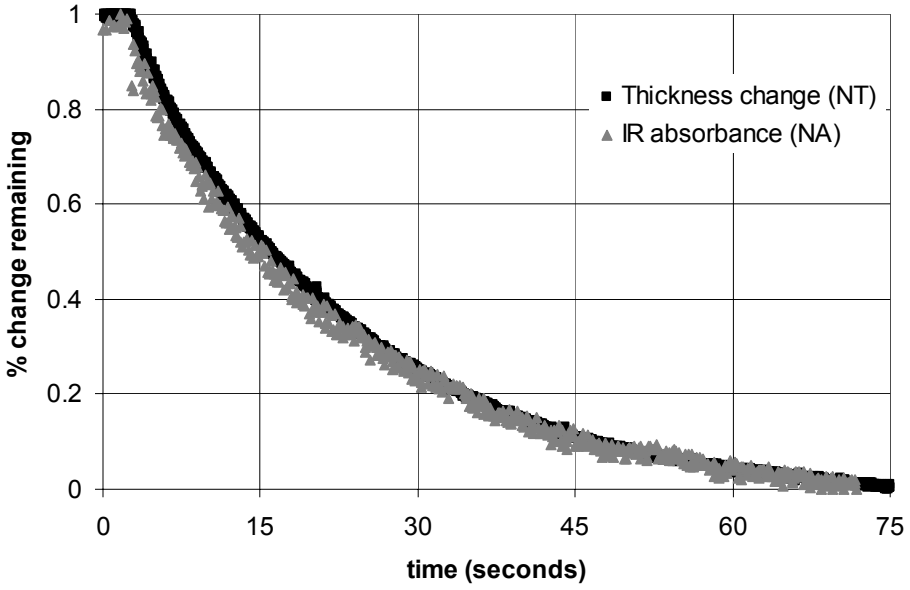

Figure 5.4: Flash exposure transient experiment at 75 °C (Sample #1).

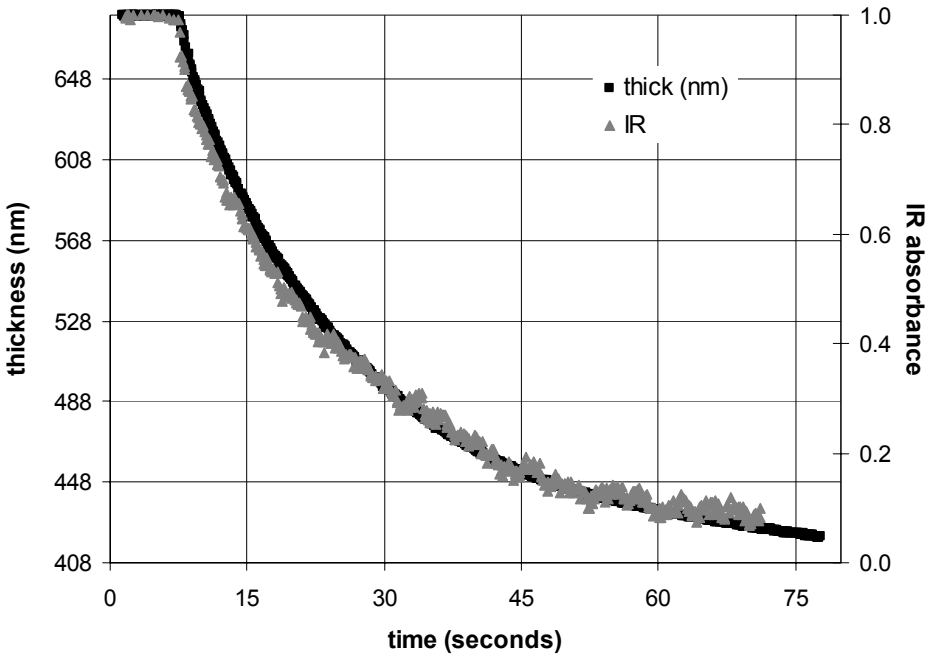

Figure 5.5: Flash exposure experiment at 75 °C (Sample #2), Axis scaling normalization method.

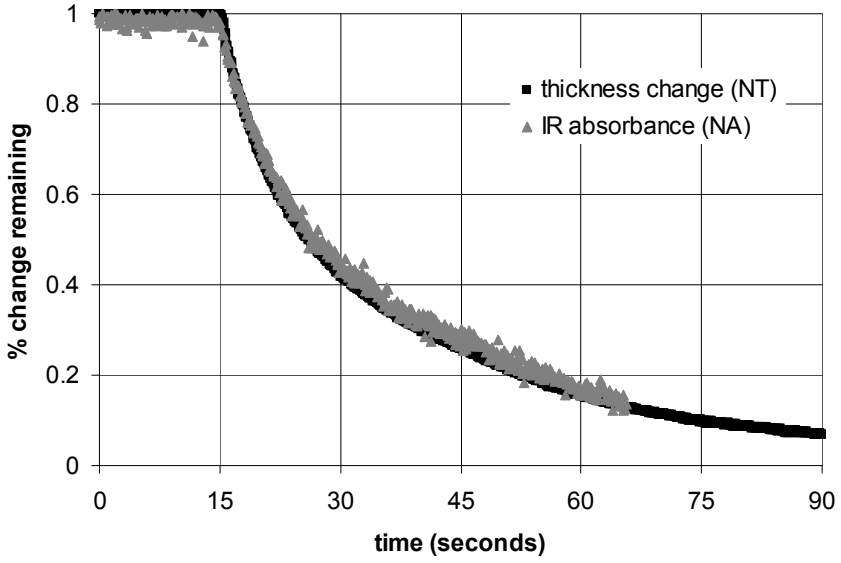

Figure 5.6: Flash exposure transient experiment at 90 °C (Sample #1)

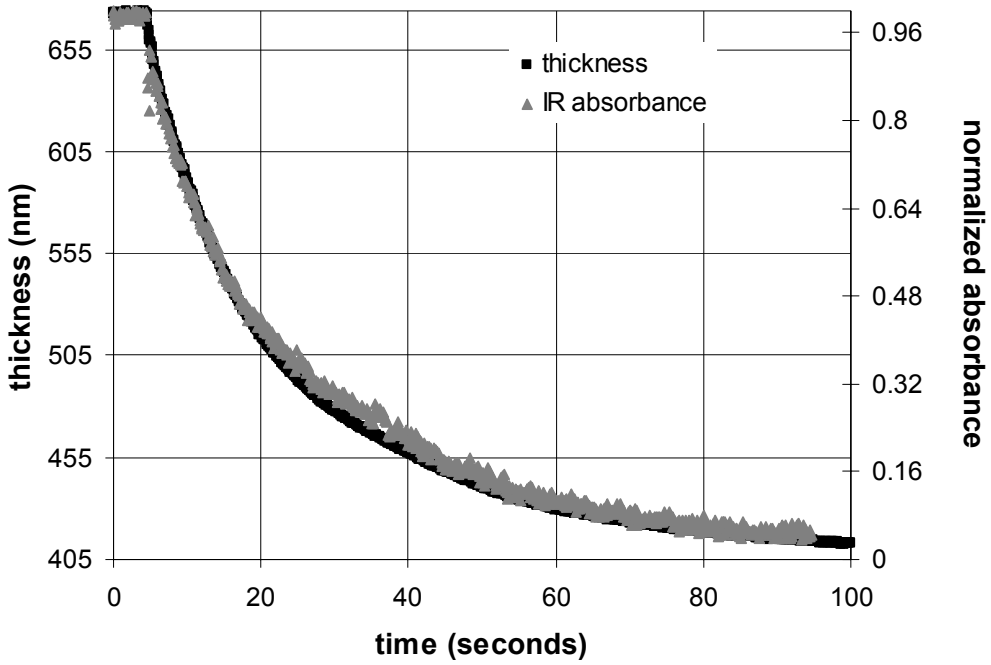

Figure 5.7: Flash exposure experiment at 90 °C (Sample #2), Axis scaling normalization method.

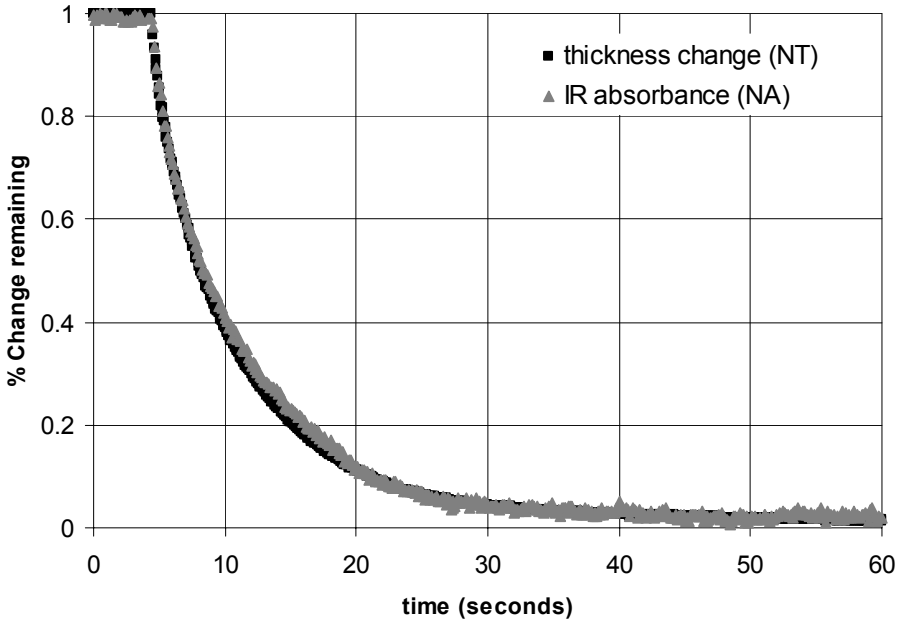

Figure 5.8: Flash exposure transient experiment at 100 °C (Sample #1).

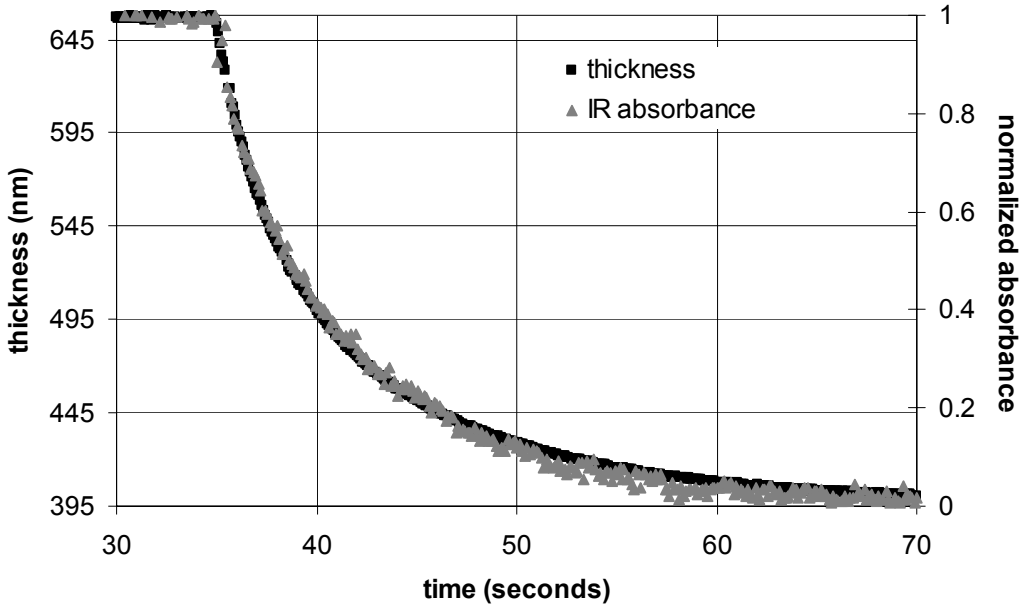

Figure 5.9: Flash exposure experiment at 100 °C (Sample #2), Axis scaling normalization method.

Experimental results at 75 °C appear to show the existence of a lag at early bake times of almost 1 second. As the rate of reaction slows, the lag appears to eventually dissipate and after 30 seconds of reaction no lag remains. With an estimated lag time it is possible to calculate corresponding diffusion coefficients necessary for by-product evolution (using $\theta = L^2/6D$). For an initial film thickness of 700 nm and a max lag time of 1.0 seconds, a max diffusion coefficient for gas evolution on the order of 8×10^{-10} cm^2/s results. The apparent self diffusion coefficient for the polymer chains is on the order of 10^{-12} cm^2/s for a thickness change of approximately 265 nm over a bake time of 75 seconds.

Results at 90 °C and 100 °C (Figures 5.6 through 5.9) do not show the presence of any measurable lag between reaction and relaxation over the course of the experiment. This does not necessarily imply that no time lag exists between the generation of reaction by-products and film shrinkage, but it does make clear that, if such a lag exists, it is less than about 200 milliseconds in lifetime. This maximum lifetime value results from the uncertainty in the synching error, which is related to the data collection rate of the two collection methods as discussed above.

Using an estimated maximum lifetime, it is possible to calculate corresponding minimum diffusion coefficients necessary for by-product evolution (again using $\theta = L^2/6D$) at the higher temperatures. For the average initial film thickness of 650 nm and a max lag time of 0.2 second, a diffusion coefficient on the order of 10^{-9} cm^2/s results. This is not outside the range expected for CO_2 in a polymer membrane especially a swollen membrane. For relaxation of polymer chains, a corresponding self diffusion coefficient can be calculated based on the thickness change over a given time. For overall thickness changes, the apparent self diffusion coefficient (assuming movement equal to thickness change) is on the order 10^{-12} cm^2/s at all three temperatures. This is much larger than a literature value[6] given for polystyrene (MW = 100,000) self-diffusion of 10^{-15} cm^2/s for a 11 wt% CO_2 swollen film at 63 °C or the literature[7] value for unswollen polystyrene (MW = 111,000) at 125 °C of 10^{-16} cm^2/s. It is possible the values are larger than expected because resist polymer molecular weights are lower (PTBOC ~ 50,000) or the film is temporarily more swollen with plasticizers

than 11 wt%. The atoms that are lost as gas molecules make up almost 50% of the initial mass of the film, during some short time periods when the film is reacting rapidly the film could be in a highly swollen state (especially locally near reaction sites), more like a foam or a gel than a glassy polymer. Of course, this "foamed" state with temporary excess free volume has, according to the experimental results at 90 °C and 100 °C, a lifetime of less than 200 milliseconds. The lifetime (if any) of reaction-generated excess free volume is apparently very short, but it is still possible that even with such a short lifetime, acid diffusion might be transiently enhanced enough to account for experimentally measured diffusion distances. Free volume based equations, such as Fujita-Doolittle, predict a diffusion coefficient with an exponential dependence on free volume changes, thus even small increases in free volume may have a large impact on diffusivity. So even with a short enhancement lifetime the effect might still be substantial.

REFERENCES

1. L.F. Thompson, C.G. Willson, M.J. Bowden. *Introduction to Microlithography*, American Chemical Society, Washington D.C., 1994.

2. M. Wessling, S. Schoeman, T.v.d. Boomgaard, C.A. Smolders. *Gas Sep. Purif.* 1991; **5**, 222.; J.D. Wind, S.M. Sirard, D.R. Paul, P.F. Green, K.P. Johnston, W.J. Koros. *Macromolecules*, 2003, **36**, 6433.

3. A. Bos, I.G.M Punt, M. Wessling, H. Strathmann. *J. Membr. Sci.* 1999; **155**, 67.

4. G.M. Wallraff, W.D. Hinsberg, F.A. Houle, M. Morrison, C.E. Larson, M. Sanchez, J. Hoffnagle, P.J. Brock, G. Breyta. *Proc. SPIE*, 1999; **3678**, 138.

5. S.D. Burns, M.D. Stewart, J.N. Hilfiker, R.A. Synowicki, G.M. Schmid, C. Brodsky, C.G. Willson, "Determining free volume changes during the PEB and PAB of a chemically amplified resist", *12th International Conference on Photopolymers*, 2000.

6. R.R. Gupta, K.A. Lavery, T.J. Francis, J.R.P. Webster, G.S. Smith, T.P. Russell, J.J. Watkins. *Macromolecules*, 2003; **36**, 346.

7. S.J. Whitlow, R.P. Wool. *Macromolecules*, 1989; **22**, 2648.

Chapter 6: Scanning Electron Microscope Experiments

Experiments were designed such that acid transport distances could be measured using a scanning electron microscope (SEM). This approach is complementary to the FT-IR approach as it gives information about the actual spatial distribution of deprotected sites. Spatial information can only be inferred from the FT-IR method as it samples both a large area and the complete depth of the film. The SEM method is based on a silylation "staining" or "decoration" technique that allows deprotection caused by the acid to be visualized using scanning electron microscopy. This method was used to corroborate conclusions drawn from FT-IR results discussed previously. SEM results also strengthen the case for the reaction front propagation model by showing that deprotection is confined to a reasonably sharp band and not distributed throughout the bulk film.

EXPERIMENTAL

Materials:

Poly(4-methoxystyrene) (PMOS) was synthesized from the reaction of poly(4-hydroxystyrene), potassium carbonate, and methyl iodide in acetone. The photoacid generators used in this study were bis(4-t-butylphenyl)iodonium perfluorobutane-1-sulfonate (nonaflate) and triphenylsulfonium trifluoromethanesulfonate (triflate). The nonaflate PAG was obtained from Midori Kagaku Co. The triflate PAG was prepared according to standard procedures in our labs. Poly(4-t-butyloxycarbonyloxystyrene) (PTBOC) used in

the SEM experiments was prepared from the polymerization of 4-t-butyloxycarbonyloxystyrene monomer using AIBN. This monomer was obtained from Triquest Chemical Co. The spin-casting solvent for the layers was propylene glycol methyl ether acetate (PGMEA), which was obtained from Aldrich Chemical Co. The silylating agent, dimethylsilyldimethylamine, used in the decoration technique was obtained from Silar Laboratories.

Sample preparation:

Film stacks for the SEM experiments were created using methods similar to those previously described for IR experiments. Feeder layers of PMOS with PAG were spin cast onto silicon substrates and then post apply baked at 90 ºC for two minutes. The t-BOC detector layer was spin cast on a glass microscope slide, then floated onto de-ionized water after a ten second, 90 ºC bake. The film was then picked up on a silicon substrate coated with the feeder layer. A two-minute bake a 40 ºC was used to evaporate residual water. The bilayer stack consisting of both feeder and detector layer was then baked at 90 ºC for two minutes. Samples with nonaflate PAG in the feeder layer were exposed with 100 mJ/cm^2 of 248 nm light. Samples with triflate PAG in the feeder layer were exposed with 15 mJ/cm^2. After exposure, samples were baked for 35 minutes at 60 ºC, 75 ºC, or 90 ºC while being monitored by IR. The sample wafer pieces were then cleaved into two halves to expose the layer profile. Samples containing triflate PAG were then placed under vacuum at 20 mTorr for ten hours to remove volatile triflic acid. One half of each cleaved sample was silylated for one minute at 90 ºC with dimethylsilyldimethylamine (DMSDMA) at a pressure of 50 mTorr. Figure 6.1

shows the silylating reaction that results in the incorporation of silicon atoms into deprotected phenolic regions. Silylated samples were then etched, edge-on, in a Plasma Technology Oxford μ80 reactive ion etch chamber for twenty seconds in oxygen plasma. The etcher settings were 10 standard cubic cm per minute of O_2, 30 mTorr pressure and 45 watts RF power. These settings and the etcher configuration were set to maximize etching in the vertical direction while minimizing isotropic etching. Etched samples were then prepared for the SEM by coating with gold/palladium. A Hitachi 4500 SEM was used to generate all micrographs.

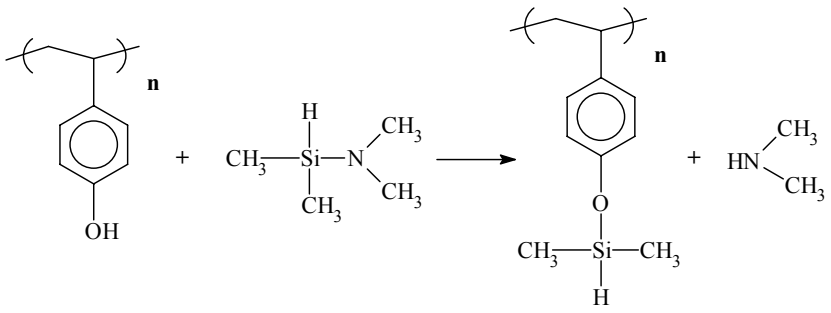

Figure 6.1: Reaction of PHS with DMSDMA

RESULTS AND DISCUSSION

The silylation/SEM method relies on the digital silylation scheme developed by MacDonald, *et al.*[1] for use as lithographic patterning technique. Under this digital silylation scheme the silylating agent reacts only with phenolic sites. Protected phenolic sites (t-BOC sites) do not react with the silylating agent,

thus silicon is only incorporated into deprotected regions. Once silicon is incorporated in phenolic regions, oxygen plasma etching can be used to "burn" away unsilylated areas, which produces a relief structure that can be seen in the SEM. In polymer regions where silicon has been incorporated the oxygen plasma generates silicon dioxide. This method can be used readily to show where acid deprotection has occurred in the film stack. Simple IR measurements can not give information about the spatial distribution of the deprotection sites because the IR beam interrogates the entire film stack thickness. The IR method is unable to distinguish partial deprotection homogeneously distributed throughout the film from deprotection that is localized to a specific band. Those two possibilities would be readily distinguishable with the silylation/SEM method.

The silylation/SEM method was developed to confirm that the acid migration distances inferred from IR experiments on bilayer (PTBOC on acid feeder layer) samples were accurate and that acid was indeed confined to a definite region and not distributed throughout the entire PTBOC layer. Figure 6.2 shows SEM micrographs of a bilayer sample with nonaflate PAG in the PMOS feeder layer that was exposed and baked at 90 ºC for 35 minutes. Figure 6.3 shows SEM micrographs of a control experiment sample that was not exposed to UV light, but otherwise was processed exactly like the exposed sample. Two distinct layers are evident in Figure 6.3 and the interface between the two layers is sharp, showing that the two layers did not mix during sample preparation. In Figure 6.2, a third layer is present that is not evident in the control experiment. The new middle layer corresponds to the PHS layer generated as the acid catalyst

migrated into the PTBOC layer from the feeder layer. As the acid migrated, it catalyzed the conversion of t-BOC sites into PHS. As measured in the SEM, the thickness of the deprotected region is 60 nm; this corresponds well with the 65 nm thickness determined by IR experiments. The grains or beads seen in the micrographs are thought to be an artifact of the decoration process and unrelated to diffusion or deprotection.

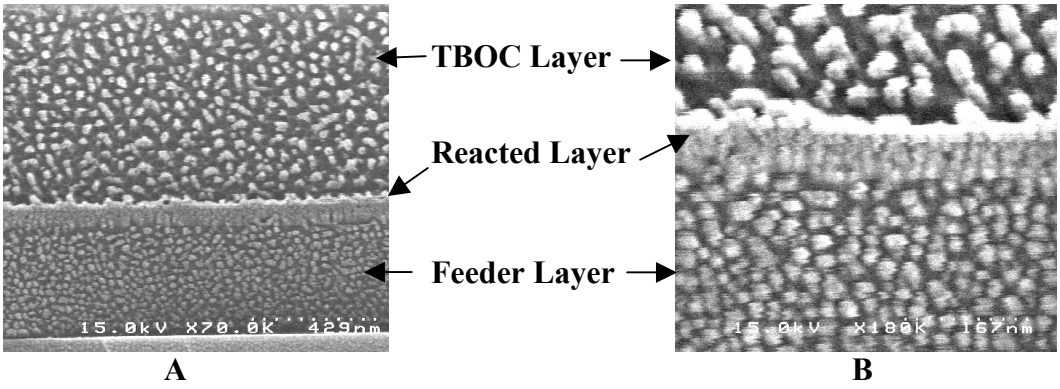

Figure 6.2: SEM micrographs of an exposed bilayer sample. Picture B is a close-up of the interface region between feeder and detector layers.

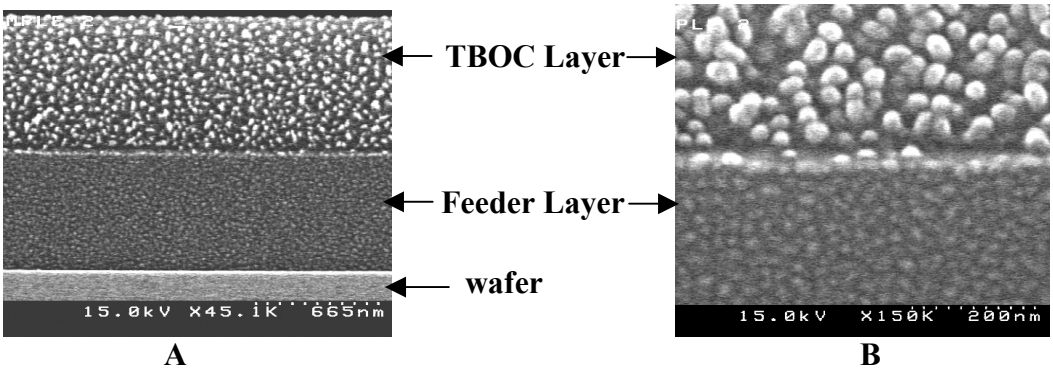

Figure 6.3: SEM micrographs of unexposed bilayer sample. Picture B is a close-up of the interface between feeder and detector layers.

The acid transport distance expected and observed in the nonaflate bilayer samples is small which means that measurement errors are significant in the estimate of total transport distance. When a triflate PAG is used in the acid feeder layer, transport distances increase significantly, making measurement errors relatively less significant. The triflate PAG was therefore chosen for an experiment designed to compare the distances measured in the SEM to the distances estimated from the IR method. Bilayer samples were constructed on mirror-backed silicon wafer pieces. Samples were exposed, then placed on a FT-IR equipped bake plate and monitored continuously for 35 minutes at three different temperatures. Acid transport distances were measured as a function of bake time and temperature. Final acid transport distances determined by IR at bake temperatures of 60 ºC, 75 ºC, and 90 ºC were 120 nm, 176 nm, and 334 nm, respectively. IR method results for the three samples are shown in Figure 6.4. At the end of the 35-minute post exposure bake, the samples were promptly removed from the silylating chamber and cooled. Samples were then cleaved and decorated according to the procedures given in the Experimental section. Figure 6.5 shows the SEM profiles for each of three different sample temperatures. Acid transport distance measured in SEM for bake temperatures of 60 ºC, 75 ºC, and 90 ºC were 129 nm, 230 nm and 415 nm, respectively.

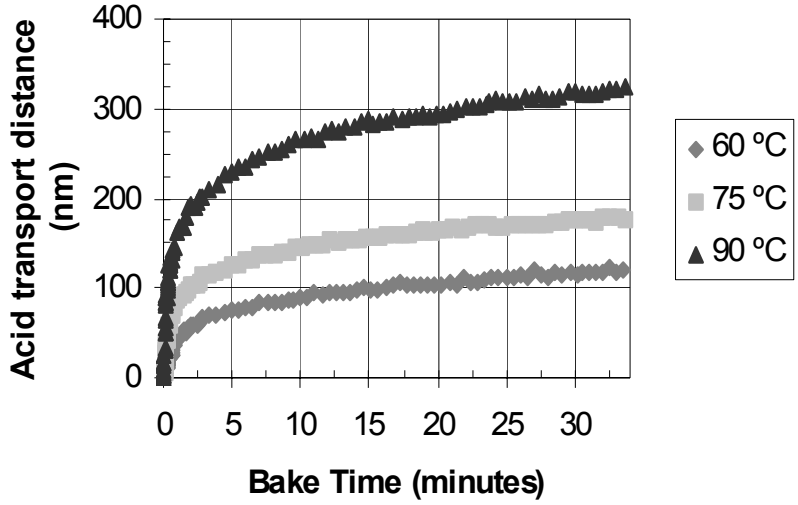

Figure 6.4: Transport distances as estimated by IR measurements.

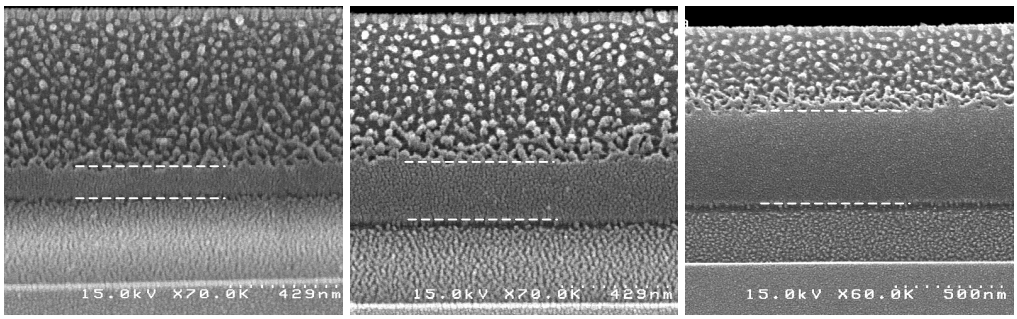

Figure 6.5: Transport distances of triflic acid into PTBOC after 35 minutes at three different temperatures. Picture A: T_{bake}= 60 ºC, Picture B: T_{bake}= 75 ºC, Picture C: T_{bake}= 90 ºC.

A comparison of results from the two different methods shows that the SEM method gives consistently higher values for acid transport distances. The difference between measured values from SEM and IR at 60 ºC was about 7%.

At 75 ºC and 90 ºC the difference between the two methods amounted to 26% and 22%, respectively. This difference likely arises from extra, unmonitored diffusion occurring during the silylation bake of the decoration procedure. The samples were held under vacuum for extended periods to remove the triflic acid, but it is possible that this did not completely accomplish complete removal of the acid. Also, the film shrinkage that occurs as a result of the deprotection reaction and the swelling that occurs when the silylating agent is incorporated into the film was not accounted for rigorously in the SEM measurements, but previous experiments by Somervell *et al*.[2] have shown that the shrinkage caused by deprotection is almost exactly balanced by the swelling caused by the particular silylating agent used in this work.

CONCLUSIONS

The silylation/SEM method confirms that deprotection in our bilayer experiments is confined generally to a definite band and is not distributed throughout the entire detector film. Transport distances measured by SEM are typically larger than distances determined by IR methods, but this discrepancy likely results from incomplete removal of acid from the film stack prior to the silylation bake step of the SEM decoration process. Micrographs of unexposed control wafers show a sharp layer interface which demonstrates that the film floating sample preparation process does not lead to layer mixing, which is also an important finding in of itself.

REFERENCES

1. S.A. MacDonald, H. Schlosser, N.J. Clecak, C.G. Willson, J.M.J Fréchet. *Chem. Mater*. 1992; **4**, 1364.

2. Mark H. Somervell, *Ph.D. Dissertation*, The University of Texas at Austin, 2000.

Chapter 7: Advanced Lithography Issues

In this chapter, acid diffusion is related to some advanced lithographic issues that are of specific interest to industrial applications. The first topic to be investigated is line end shortening (LES). LES is thought to be largely an optical phenomenon, but it does contain some contribution related acid diffusion. The second topic is line edge roughness (LER). The term "LER" is somewhat poorly defined in industrial usage, but, in general, it refers to variations in feature width within a single feature. Sometimes this variation is defined with respect to some nominal, average feature edge, other times it defined as variation in edge to edge widths. LER is also a matter of the size-scale under investigations. Long-scale (low frequency) roughness over feature lengths of microns is likely less directly related to acid diffusion than short-scale (high frequency) roughness which manifest itself on nanometer lengths.

LINE END SHORTENING

Line end shortening has emerged as a serious problem in microlithography. In some manner, LES can be overcome simply by biasing the mask dimensions, that is making the mask line longer relative to the desired printed length, but this limits achievable circuit density on the mask. Optical proximity correction (OPC) can also be used, but compensating for LES in mask design is complicated by the fact the causes of the LES phenomenon are poorly understood. This chapter section attempts to separate the causes of LES into

individually understandable mechanisms that might eventually be recombined in a lithography simulation program. The causes of LES include aerial image formation, simple pattern geometry considerations, and diffusion effects. This chapter will address each of these contributors in turn. The effect of exposure gradients on acid diffusion is described, and results of experiments designed to study gradient effects are presented.

OPTICAL EFFECTS

A significant portion of the LES problem is the result of aerial image formation. When an imaging system is operated near its resolution limit, the physics of diffraction dictate that narrow lines show LES if printed to mask width. Even large features experience corner rounding as the higher-order information about the pattern is lost in diffraction. Figure 7.1 shows the aerial image of an isolated line end simulated in PROLITH™, a lithography simulation package used widely in industry, with the mask pattern overlaid in outline form. This aerial image demonstrates the problem: a line with dimensions near the resolution limit of the imaging system cannot be simultaneously printed to both the mask width and the mask length. Clearly, there can be a significant LES problem prior to the image even being deposited into the photoresist. In addition, there is no obvious way for the photoresist to compensate for this problem. Even a perfect threshold-switching, no bias photoresist could only replicate the isoenergy profiles of the available aerial image.

While this aerial image line shortening is really unavoidable when operating near the diffraction limit, OPC enhancements and other imaging "tricks" can work to mitigate the problem. Improving resolution by moving to smaller λ or higher numerical aperture will also improve LES for a given feature dimension, but this is equivalent to moving away from the diffraction limit. A fuller description of the optical causes of LES and how optical system parameters affect LES can be found in the work of Mack.[1, 2] An experimental investigation of the relationship between imaging system parameters and LES has also been reported by Shi *et al*.[3]

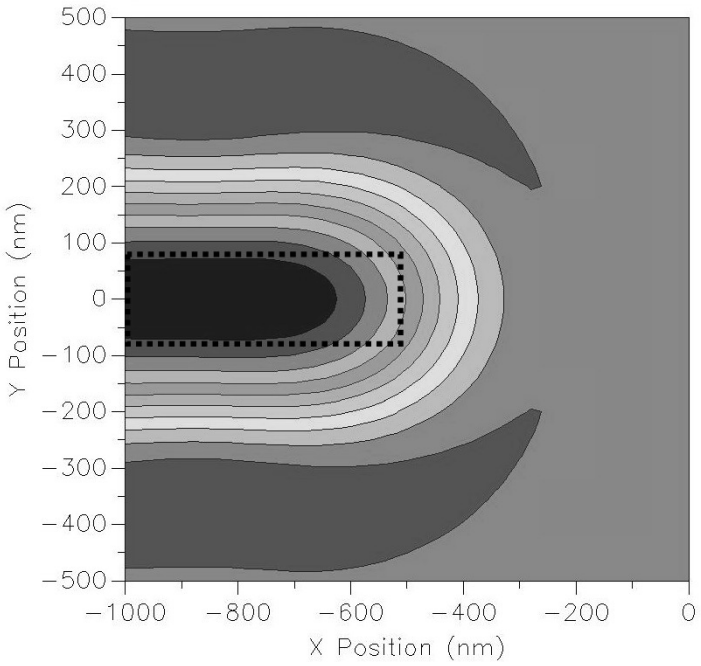

Figure 7.1: PROLITH simulated aerial image of 150nm isolated line end. Outline of mask is overlaid. (λ=248nm,σ=0.5, NA=0.5)

FEATURE GEOMETRY EFFECTS (SHAPE CONSIDERATIONS)

Even if a perfectly modulated image could be deposited into the photoresist (say by contact printing) LES might still be problem. At feature corners, diffusion of photoproducts from multiple directions works to round corners. If diffusion lengths at corners are sufficient to overlap adjacent corners, corner rounding becomes line end shortening. Differences in LES distances based on pattern shape have been reported in the work of Cheng *et al*.[4] In Cheng's work, it was found that the post exposure bake simulator STORM did not fully capture the effect of multi-dimensional diffusion as its one-dimensional diffusion estimates under predicted the actual diffusion distances for 2-D mask patterns such as posts (circle shaped exposures).

Diffusion from multiple directions can greatly enhance the photoproduct diffusion distances and must be accounted for to accurately predict lithography results. Fortunately, textbook diffusion analysis can be used to predict 2-dimensional diffusion distances in many cases. In 2-D diffusion, two general cases are possible: convergent and divergent. In the convergent case, the unexposed region is, more or less, surrounded by exposed regions. In the divergent case, the opposite is true. In the positive tone, convergent cases include printing of posts and line ends. Divergent cases in positive tone include printing of contact holes and the inside corner of line elbows.

The difference between convergent and divergent cases can be seen clearly in the printing of posts and holes. Figure 7.2 shows the initial and final conditions of a post (unexposed in the center) and hole (exposed in the center),

the overlaid arrow indicates the general direction of diffusion. Finite element analysis incorporating Fickian diffusion equations was used to determine photoproduct movement over the course of a PEB. The diffusion coefficient was set to 10^{-5} $\mu m^2/s$, a typical value estimated for photoresists at short bake times.

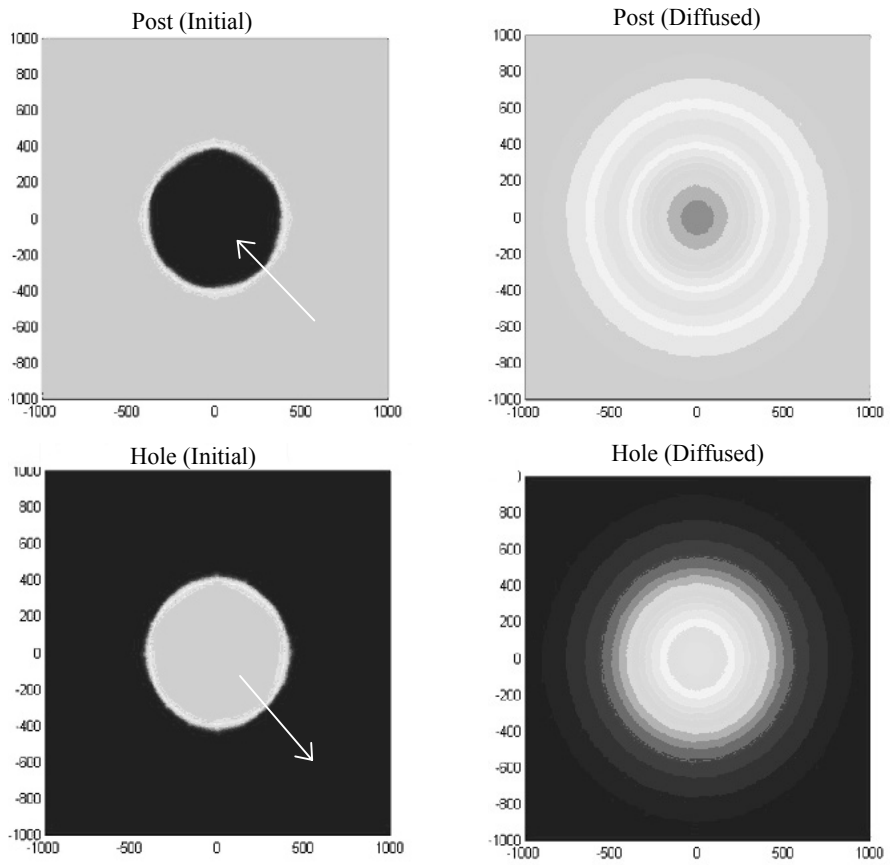

Figure 7.2: Diffusion simulation of post and hole exposure cases. Lighter regions correspond to higher acid concentrations.

Figure 7.3, below, plots the movement of an arbitrary concentration (30% of initial concentration) contour. Assuming a threshold development model (threshold = 0.3), the absolute change in radius is plotted for both the post and the hole case shown in Figure 7.2. The decrease in radius of the post is much greater in extent and faster than the increase in radius of the hole. In fact, in this case the post would completely disappear over the course of the PEB. This effect can be explained by simple volumetric arguments. For a given change in radius the increase in occupied volume is less for the post than for the hole, and thus the photoproduct concentration dies out more slowly. A line end, especially with rounded corners from the aerial image, can be thought of as sort of half post, which leads directly to the expectation that diffusion will shorten the line by more than the one-sided line width diffusion bias distance.

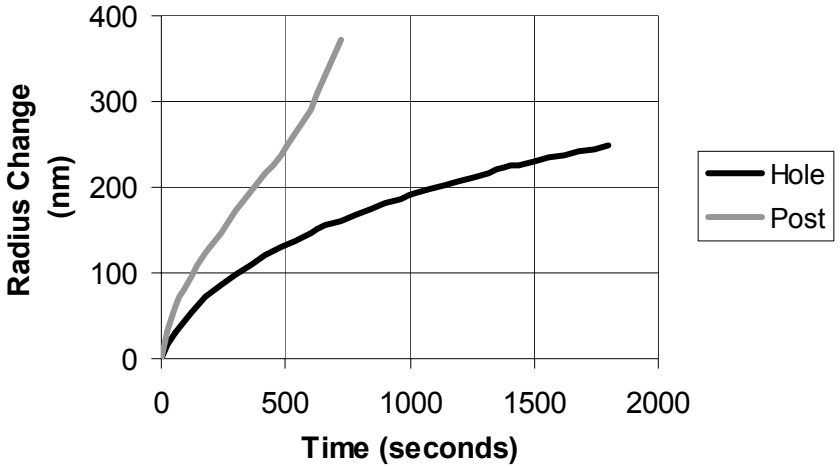

Figure 7.3: Plot of absolute radius change vs. time for post (convergent) and hole (divergent) diffusion cases.

DIFFUSION EFFECTS

Analysis in the previous section assumed diffusion of photoproducts obeyed simple Fickian diffusion rules, that is the photoproducts and the photoresist matrix resin were non-reactive. This is the case in non-chemically amplified system like DNQ/novolac I-line resists, but in chemically amplified systems the diffusing species is a photogenerated acid that catalyzes reactions as it moves through the matrix resin. As a result, acid transport occurs by a coupled reaction-diffusion mechanism which complicates analysis.

Previous chapters have discussed a transiently enhanced, reaction-diffusion mechanism to explain observed experimental results. An additional complication to reaction-diffusion analysis is the presence of exposure gradients at the feature edge, rather than sharp, step function differences in exposure. These gradients arise due to diffraction and cannot be avoided in conventional lithography. This exposure gradient, in turn, generates a gradient of acid concentration. Another factor complicating analysis is that the slope of concentration gradients at the line end can be different from the slope at the line edge. Shown in Figure 7.4 is the exposure intensity versus position for the indicated crosscuts on an isolated line end aerial image, corresponding to the line end and line edge. Note that the aerial image slope is shallower at the line end than at the line edge.

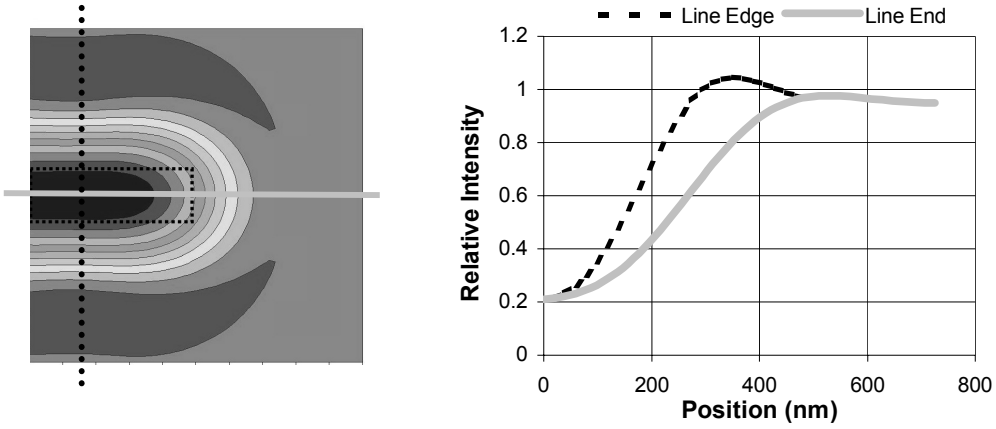

Figure 7.4: Aerial image of isolated line end. Intensity profiles are shown for indicated crosscuts at the line edge and line end. (nominal feature width: 150nm, λ=248nm,σ=0.5, NA=0.5)

Acid gradients can affect the reaction-diffusion system in two ways. A shallow acid gradient means there is less need for diffusion; that is, higher levels of acid are already present ahead of the threshold acid concentration front so less total movement of acid is required. The effect of these low levels of acid reacting while waiting for the threshold acid concentration levels to arrive also needs to be considered. As the acid reacts prior to the arrival of the threshold front, it removes matrix reactivity. Removing matrix reactivity removes mobility enhancement opportunities. In a sense there are competing mechanisms - less diffusion is required, but less mobility will be available. On first consideration, it is not clear which effect will dominate.

Experiments designed to investigate the reaction depletion effect were based on a bilayer technique. A high acid concentration feeder layer was used

while the tBOC blocking ratio of the upper resist polymer was varied. Different copolymer ratios, varied from 15% blocked to 100% blocked, were synthesized. A FT-IR based analysis was used to evaluate acid transport distances.

EXPERIMENTAL - LES

Copolymers of 4-tert-butyloxycarbonyloxystyrene (TBOC) and 4-hydroxystyrene (PHS) were prepared by partial thermolysis of TBOC homopolymer. The homopolymer, poly(4-tert-butyloxycarbonyloxystyrene) (PTBOC), was prepared by free radical initiated polymerization of TBOC monomer supplied by Triquest Chemical. Azobisisobutyronitrile (AIBN) initiator in 150:1 mole ratio (monomer:initiator) was used and the polymerization was carried out at 70 ºC for 18 hours in toluene solvent. Resulting polymer was precipitated into petroleum ether and collected by filtration. Heating of the PTBOC polymer powder to 160 ºC in a Kugelrohr (Buchi) for varying lengths of time caused some fraction of the TBOC units to convert into PHS units. By varying heating times, different ratios of protected and unprotected sites were obtained. Copolymer ratios were determined by thermo-gravimetric analysis and confirmed by IR analysis. It has been reported[5] that the thermolysis reaction that converts TBOC units into PHS units does not proceed perfectly cleanly in the solid state, but rather various side-products are also produced in small amounts. This thermolysis approach to copolymer synthesis captures the effect of the side reaction products on polymer transport properties where as other synthetic approaches would not.

The photoacid generator used in these experiments was bis(p-tert-butylphenyl)iodonium perfluorobutanesulfonate (DTPI-nonaflate). Polymer film stacks were formed by floating techniques described in previous chapters. Acid feeder layers consisting of poly(4-methoxystyrene) with a 5wt% (dry) PAG loading were spin cast onto silicon wafers from propylene glycol methyl ether acetate (PGMEA). These feeder layers were approximately 300 nm thick after a 120 second, 90 ºC post apply bake (PAB). In this set of experiments, the upper films were copolymers of TBOC and PHS with a varying TBOC:PHS ratio. These copolymer films were floated from sodium chloride crystals and were approximately 300 nm thick after processing. Figure 7.5 depicts the layer construction used in these experiments. Completed film stacks were exposed to a 248 nm wavelength dose of approximately 90 mJ/cm^2 prior to the PEB step.

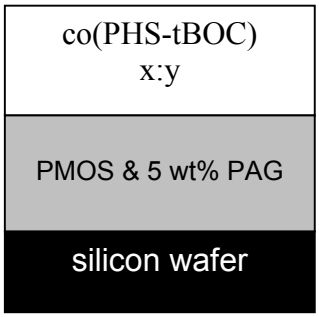

Figure 7.5: Layer construction for the reaction depletion experiment. The x:y copolymer ratio between PHS and TBOC is varied.

REACTION DEPLETION

By varying the concentration of reactive sites in the upper layer and monitoring disappearance of an IR absorption band characteristic of the reactive species, acid diffusion distance can be determined as a function of copolymer blocking fraction. Lowering the blocking fraction is equivalent to depleting reactive sites available in the resist. Polymers with blocking fractions of 100%, 90%, 80%, 50% and 15% were prepared. Figure 7.6 presents the results of the IR experiments. And as in Chapter 4, IR absorbance data was converted into acid diffusion distances by using the initial layer thickness and assuming that reaction is confined to a reasonably sharp band. Diffusion distances are for a 90 ºC PEB. Figure 7.7 presents diffusion distances as a function of blocking fraction for a fixed PEB time of 90 seconds. The effect of blocking fraction on diffusion distance is quite pronounced when going from 100% to 90% or 80%, but eventually this observed effect levels out somewhat. For example, decreasing blocking from 80% to 15% decreases the measured diffusion distance by less than 10 nm.

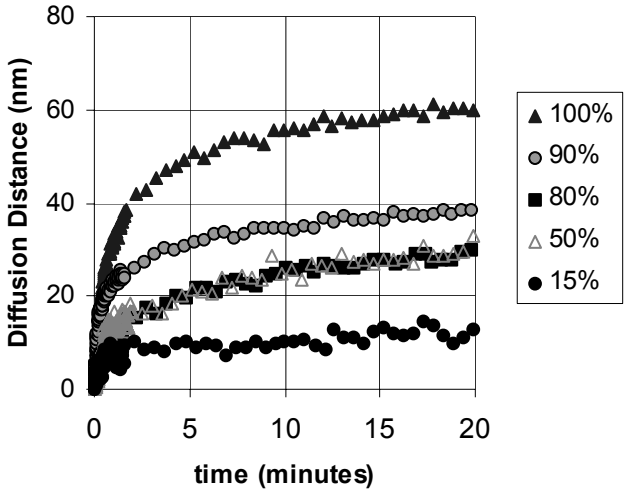

Figure 7.6: FT-IR traces of reaction progress in bilayer experiments (T = 90 ºC) with various blocking of the upper layer.

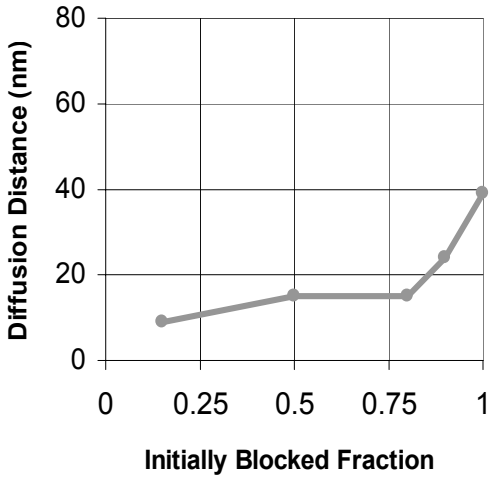

Figure 7.7: Blocking fraction vs. diffusion distance after a 90 second/90 °C PEB

LES - CONCLUSIONS

Contributors to LES include aerial image formation, 2-D convergent diffusion at the line end, and the relative shallowness of the exposure gradient at the line end. Shortening in the aerial image results from operating near the resolution limit of the imaging system. Only by improving resolution of the imaging system can LES contributed by the aerial image be reduced. LES resulting from geometry effects cannot be avoided in positive-tone systems. At the line end in positive-tone systems diffusion will be convergent and photoproduct concentration will decrease more slowly than in the 1-D diffusion case present at the line edge. As a result, diffusion will be faster and, thus, farther over the course of a post exposure bake. In addition to the shape effect present at the line end, diffusion can also be affected by the exposure gradient present at the line end. Typically this gradient will be shallower at the line end than at the line edge. In a chemically amplified system, transport occurs by a reaction-diffusion mechanism, which complicates any attempt to simulate the process. In other locations[6,7] these experimental results were used as checks on, and compared to, mesoscale computer simulations, which incorporate transiently enhanced diffusion, and were found to be in general agreement with the simulation model.

LINE EDGE ROUGHNESS

As feature dimensions shrink, line edge roughness has become an increasing concern in semiconductor fabrication. There are numerous potential contributors to line edge roughness throughout the lithographic process and any

measured roughness value on a printed device feature is, like the feature itself, a convolved function of every processing step. When the full lithographic process is used to study line edge roughness, it can be difficult to isolate the contribution to final roughness from any individual processing step or factor. To gain a more fundamental understanding of roughness generation that is specifically related to photoresist chemistry and formulation, it is necessary to design experiments that separate out exposure related issues like mask dimension variation or local dose variation ("shot noise"). This can be accomplished using the previously discussed experimental protocols for bilayer film stack creation. The bilayer experimental approach has been used to study the effect of variations in such factors as post exposure bake time, photoacid generator loading, and developer concentration on roughness generation. Surface roughness of the developed film stacks is measured via atomic force microscopy. Surface roughness of developed bilayer film stacks may be considered analogous to sidewall roughness of printed features. An acrylate-based 193 nm photoresist resin and TBOC resin are used in these experiments.

Required tolerances on feature dimensions are fast approaching the molecular scale. Line edge roughness (LER) control is seen as one of the most difficult challenges to be overcome in sub-100 nm lithography. Maintaining LER below 5% of the critical dimension at the 65 nm node implies tolerances of about 3 nm. These dimensions are on the size order of a single polymer molecule.[8] The ITRS roadmap predicts the need for 5 nm (3σ, single-sided) LER control in 2003, decreasing at a rate of a half nanometer a year for the next four

years.[9] Such tight manufacturing tolerances will be difficult to achieve without a clearer understanding of LER. Much previous work has been done to develop an understanding of line edge roughness and several possible sources have been examined as possible contributors to roughness formation. Roughness in the mask feature edge has been examined as a source of top down LER in resist features.[10] Imaging and exposure issues like local dose variation[11] and aerial image contrast[8,12,13] have been investigated. Roughness sources more directly related to the resist such as the possibility of polymer aggregates[14,15], extent of acid diffusion[8,16], amount of base quencher in resist formulation[17,18], and resist-developer interaction[19-21], have been previously studied. The effect of processing conditions, such as post exposure bake time and temperature, on resist surface roughness have also been studied.[22,23]

It is probable that all these factors contribute in some way to overall roughness formation, but to understand the full process it is necessary to understand the factors individually. To gain a more fundamental understanding of roughness generation specifically related to photoresist chemistry and formulation, it is necessary to separate out the imaging and exposure based issues. Using a bilayer film stack as an experimental model of the interface between exposed and unexposed resist, resist performance can be isolated. Bilayer film stacks are flood exposed so there are no contributions from the mask or aerial image to final roughness. In these experiments, the bilayer film stack consists of an insoluble underlayer of resist resin and an upper layer of base soluble polyhydroxystyrene and photoacid generator (PAG). This orientation is the

opposite of sample construction described in the previous section and chapters. The resist underlayer is equivalent to the unexposed regions of a patterned resist, while the upper layer is equivalent to exposed regions. Surface roughness of developed bilayer film stacks can be considered analogous to sidewall roughness on printed features. This bilayer experimental approach has been used to study the effect of variations in such factors as post exposure bake time, developer concentration, and PAG loading on roughness generation.

This experimental approach convolves all the post exposure processing steps (post exposure bake, development, and drying) into one roughness value. It is not fully clear how further separation of the contributions from resist processing steps could be accomplished cleanly in experiment, but it is possible through use of computer simulation to investigate these factors separately. Insight into processing steps has been gathered from the use of a mesoscale lithography simulator described elsewhere.[6,8,24,25]

EXPERIMENTAL-LER

Materials:

An acrylate-based photoresist resin (ARP) was provided (additive free) by JSR Microelectronics. A poly(4-tert-butyloxycarbonyloxystyrene) (PTBOC) homopolymer was prepared by free radical polymerization of 4-tert-butyloxycarbonyloxystyrene monomer donated to UT-Austin by Triquest Chemical, Co. Poly(4-hydroxystrene) (PHS) used as acid feeder layers was obtained from Triquest as well. The photoacid generator di(tert-butylphenyl)

iodonium perfluorooctanesulfonate (PFOS) was purchased from DayChem. Casting solvents 3-pentanone, propylene glycol methyl ether acetate (PGMEA), and 1-butanol were purchased from Aldrich Chemical, Co. and used as received. The developer was Shipley CD-26 (TMAH 0.26 N, surfactant-free).

Instrumentation:

Initial and final film thicknesses of the samples were measured using reflectometry (n&k Analyzer, n&k Technology, Inc.). The interference fringes from the UV-visible reflectivity spectrum were fit using a four parameter model based on Forouhi-Bloomer equations. Roughness measurements were made using atomic force microscopy (DI 3100 AFM, Digital Instruments) in tapping mode with standard TESP tips. Topographic profiles were subject to a second-order plane fit before calculating the root-mean-squared (rms) roughness with standard DI software.

Sample Processing:

The method of sample preparation is based on a previously reported method described more fully elsewhere.[26] The sample processing steps, in brief summary, are first spin coat the photoresist resin layer onto a hexamethyldisilazane primed silicon wafer. The first layer was post apply baked at 130 °C for 60 s. After initial first layer thicknesses are measured, the second layer consisting of PHS and PAG was spin coated from 1-butanol over the first layer. The alcohol solvent does not dissolve the underlayer to any measurable extent. The film stack was post apply baked again at 130 °C for 60 s. Samples were exposed to broadband UV light to very high doses (~1000 mJ/cm^2) to ensure

high PAG conversion. After exposure, samples were post exposure baked according to experimental design. Bilayers were immersion developed in TMAH solutions for 30 s, followed by a rinse in de-ionized water and drying by blown nitrogen. The thickness of the remaining underlayer was measured, and then AFM measurement was carried out.

LER-RESULTS AND DISCUSSION

It is necessary to explore several processing and formulation variables in order to determine their possible effect on roughness. The bilayer method allows this to be done relatively cheaply. Some of the factors explored were PEB time, developer concentration, and base addition to the resist resin. These variables were explored in two different resin types, ARP and PTBOC. In Figure 7.8 below, the effect of PEB time on measured developed distance (d_{dev}) and root-mean-square surface roughness is shown for both the tested resins. These measurements were made using a fixed PAG loading (5 wt%) and constant development time (30 s). Over these bake times, d_{dev} can be shown to scale with the square-root of PEB time and thus be said to be consistent with Fickian-type diffusion (diffusion coefficient ~ 2.5 $x10^{-6}$ $\mu m^2/s$). Measured surface roughness of both resins appears to plateau after about thirty seconds of post exposure baking. For PTBOC, roughness plateaus at about 2.0 nm (rms). For ARP, it plateaus at a slightly higher value of 2.5 nm (rms). The different plateau values are not necessarily significant as measured root-mean-square roughness values result from a convolution of the AFM tip size and the surface morphology.

Variations in the absolute measured roughness values are expected when different AFM tips are used. Nevertheless, trends in roughness as a function of processing conditions were reproducible. Bilayer samples that experienced no PEB had surface roughness values (≈ 0.6 nm (rms)), which are very close to those measured for as-cast films.

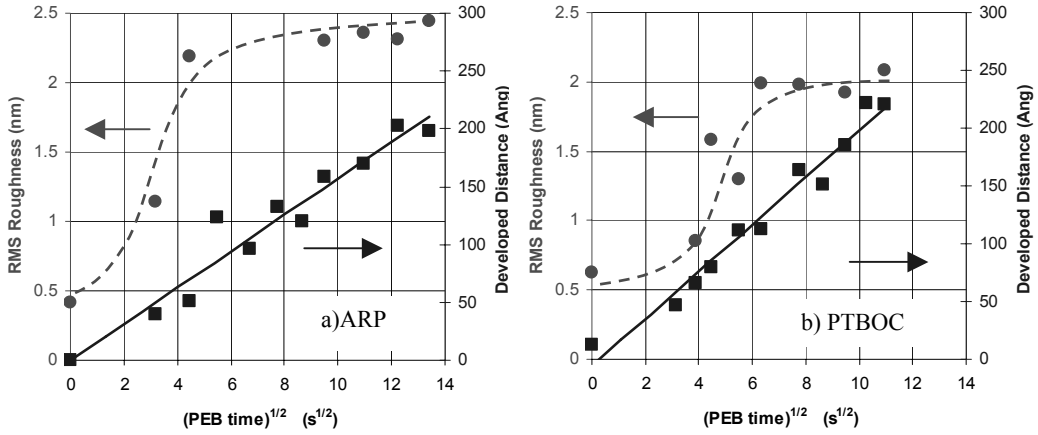

Figure 7.8: Roughness and diffusion length as a function of PEB time. PFOS PAG, T = 130C, 30s development. Dotted line is to draw the eye only and is not a fitted function.

The images shown in Figure 7.9 below illustrate the evolution of the surface morphology, representative of a feature sidewall, as PEB time increases. Inspection of the AFM images suggests the possible presence of polymer aggregates on the surface of the developed bilayers with an average size of ≈ 20 nm. The existence of polymer aggregates in photoresist materials and the link between their size and the number average molecular weight of the resin has been reported before.[15] The actual size of such features is unclear due to the finite size

of the AFM probe (nominal tip radius of curvature 5 to 10 nm) and its interaction with the polymer substrate and many dispute even the existence of polymer aggregates in photoresist films.

In these experiments on developed surfaces, the diffusion front moves deeper into the film with increasing PEB time and thus the developed distances also increases, but no matter how deep into the film the "line edge" moves, it is probable that the development stops at a position of constant resin protection level. It has been shown that for PTBOC films this level of protection is around thirty percent.[27] Due to the nature of the diffusion process as acid advances deeper into the film the fixed level of deprotection that leads to solubility is achieved locally by differing numbers of acid molecules. At short distances into the film, deprotection is achieved by relatively high acid concentrations. The further into the film the deprotection front moves, the fewer acids available at the front to catalyze reactions. This means individual acids at the leading edge must react with more protected sites on average as diffusion progresses. It is expected that the stochastic nature of reaction and diffusion would lead to greater roughness when fewer acid molecules are involved in achieving the solubility-switching deprotection levels. In chemically amplified photoresists, any given level of deprotection can be achieved by multiple pathways by trading between post exposure bake times and temperatures. Higher temperatures can be used for shorter times or lower temperatures for longer times. Previously, it has been shown by mesoscale simulation that roughness increases when a given deprotection level is achieved by fewer acids.[8] He and Cerrina have also shown

experimentally that surface roughness is dependent on the resist processing pathway with generally greater measured roughness when longer PEB bake times are used to achieve equivalent deprotection levels.[22] The results presented here can be taken as further confirmation of the expectation that diffusion induced roughness will depend on the local "deprotection burden" of acid molecules in the resist.

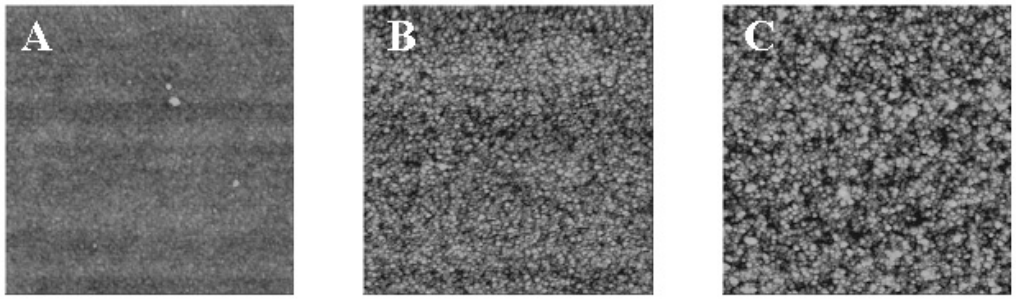

Figure 7.9: AFM scans (1 micron x 1 micron, height-scale: 20 nm) of developed PTBOC bilayers post-exposure baked for variable times: A) 0 s, B) 20 s, C) 120 s. Images are typical of samples of both PTBOC and ARP.

In Figure 7.10 below, measured surface roughness and developed distance as a function of developer concentration is shown. In this series of experiments the samples were all baked for the same time at the same temperature, so they have the same nominal latent deprotection profile. For the PTBOC film, increasing developer concentration increases d_{dev} and, correspondingly, increases rms roughness. For the ARP film, developer concentration has no effect on either d_{dev} or rms roughness.

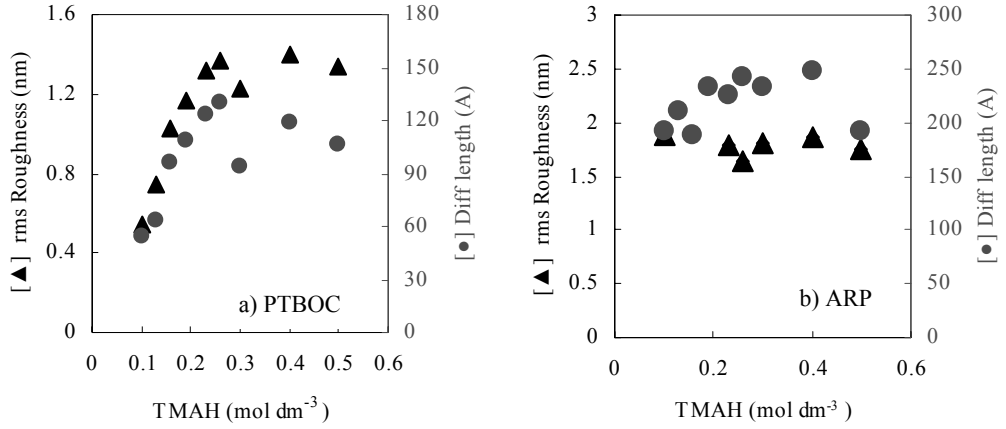

Figure 7.10: Effect of developer concentration on developed distance and surface roughness.

It appears that the two resins are affected very differently by changes in developer. The different chemistries of the two resins must be considered to understand these results. In one sense varying developer concentration and developing for a fixed time is equivalent to holding developer concentration constant and changing development time. Above a certain (fairly low) developer concentration, whether a particular chain is soluble or not depends entirely on the level of blocked sites on the chain. As long as the requisite number of sites is deprotected, say greater than ~75% for PTBOC, the chain is ultimately soluble and it is simply a matter of kinetics as to when it will actually enter solution. In the simplest model, lowering the developer concentration simply lowers the rate of dissolution and does not change which polymer chains ultimately dissolve, given enough time. In Figure 7.10 for PTBOC, roughness and d_{dev} both increase

from a baseline until reaching a plateau value after 0.26M in PTBOC. It is quite possible that at lower developer concentrations some soluble chains remained undissolved due simply to lack of time. Once developer concentration reaches a level high enough to dissolve all the soluble chains during the fixed development time both roughness and d_{dev} stop increasing. After all soluble chains are removed, it would seem that developer concentration does not change surface morphology (at least rms roughness) significantly in the case of PTBOC.

As the ARP resin was designed for 193 nm lithography, it is likely that its solubility switching functional group is not based on a phenolic group like PTBOC, but likely it generates a carboxylic acid group when it deprotects. Due to a lower pKa, the rate at which a carboxylic acid based polymer dissolves is rather insensitive to changes in developer concentration. The lower pKa polymer functional group also tends to make dissolution very rapid. The results in Figure 7.10 for ARP suggest that for all tested developer concentrations most developable material was removed during the development time. For ARP, the roughness and d_{dev} are largely unchanged by increasing developer concentrations.

If the increasing roughness shown in Figure 7.10a results from soluble material remaining undissolved, then that roughness is not a result of the diffusion process, but, rather, results from the dissolution process. Simulations by Flanagin *et al*.[19] predicted and experiments by Burns *et al*.[20] have shown that for films of completely soluble material (novolac or PHS) surface roughness increases linearly with developed distance into the film until some steady-state, bulk value is reached, after which surface roughness is constant until the film begins to clear

the substrate. The results shown in Figure 7.10a are ambiguous because it seems possible that the films were not developed long enough to remove all reacted resin. If not all reacted resin was removed the interaction of diffusion induced roughness and the development process can not be judged, but for developer concentrations above 0.26N no differences in surface roughness were observed with increasing developer concentrations. Once developed distance was no longer increasing (i.e. once all soluble material was removed) changes in developer concentration did not appear to affect surface roughness.

From a sharp interface, the randomness of the dissolution process alone should result in roughness generation. It seems unlikely that all the measured roughness in these bilayer samples results simply from development, but if the results shown in previous graphs (along with other results from IBM[29]) are replotted as roughness vs. d_{dev} (see Figure 7.11 for PTBOC and Figure 7.12 for ARP) it can be seen that roughness is minimum related to developed distance. Even with significant variation in process variables like PEB time, developer concentration or feeder layer PAG loading, roughness seems to depend most strongly on the final developed distance. A plateau in roughness of about 2 nm (rms) is reached in both resins after they have developed about 100 Angstroms. This value can be compared to the measured bulk value of Burns *et al.* of 2.5 nm (rms) for single layer, fully soluble novolac films developed for different times.

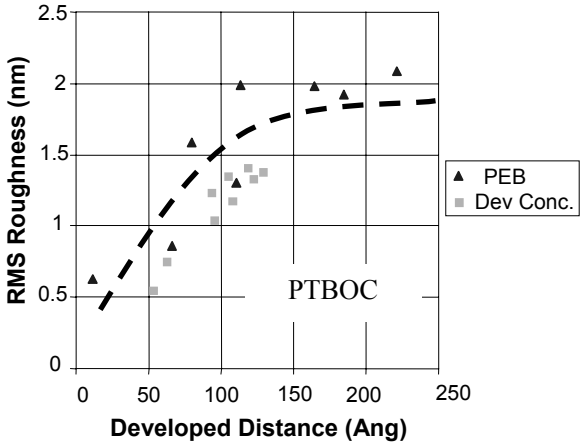

Figure 7.11: Measured PTBOC roughness versus developed distance for various process and formulation variable.

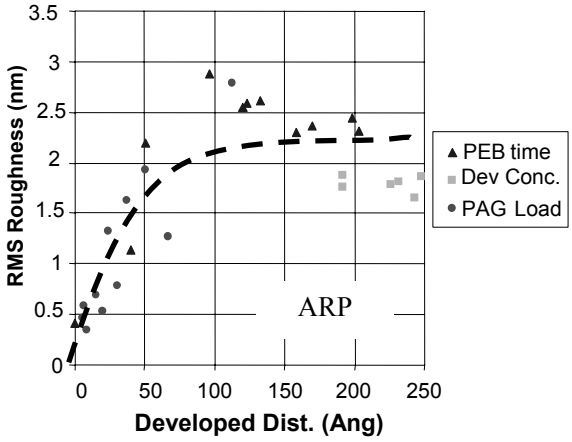

Figure 7.12: Measured ARP roughness versus developed distance for various process and formulation variables.

CONCLUSIONS - LER

An experimental method was used to emulate the interface between exposed (de-protected) and unexposed (protected) regions in a positive-tone resist pattern. The present approach is applicable to the study of the materials origins of sidewall roughness. This methodology uses a flood exposure on bi-layer films of protected and de-protected resist analogs to remove contributions from the mask and the aerial image to the spatial distribution of acid in the latent resist image. The remaining factors that affect the spatial extent of de-protection events that characterize the bi-layer interface are exclusively materials related. Limiting resist roughening by informed processing and formulation choices is possible and the main lesson appears to be things that work to limit critical dimension spreading also work to limit high frequency roughness generation. It would be expected that adding of base into the resist film should serve to lessen roughness. The expectation arises because, at the minimum, adding base into the resist should reduce overall diffusion distances. Base molecules might also work to smooth the diffusion stochastics by scavenging the rare "far traveling" acid molecules. At the molecular level, diffusion is a random process; statistical expectations are such that some acid molecules will advance more quickly than others. With the addition of base into the formulation, fast moving acid molecules will be sequestered by base before they can cause many reactions. Short bake times and addition of base into the resist formulation which can work to limit diffusion also appear effective means to limit resist roughness. Simulations and experiments suggest positioning the line edge at regions of high acid concentration (high

imaging contrast) also mitigates roughness. The roughness values here are analogous to feature sidewall roughness values. As this work concentrated on resist sidewall roughness, it should be made clear that sidewall roughness and top down line edge roughness are not directly equivalent as top down roughness is a projection of sidewall roughness. It should also be noted that resist roughness does not necessarily directly translate into post-etch feature roughness. Post-etch feature roughness is the real issue in device performance, not resist roughness.

REFERENCES

1. C.A. Mack, *Microlithography World*, **9-2**, 25-26 (Spring 2000)
2. C.A. Mack, *Microlithography World*, **9-4**, 25 (Autumn 2000)
3. X. Shi, B. Socha, J. Bendik, M. Dusa, W. Conley, B. Su. *Proc. SPIE*, 1999; **3678**, 777.
4. M. Cheng, E. Croffie, A. Neureuther. *Proc. SPIE*, 1999; **3678**, 867.
5. H. Ito, M. Sherwood. *Proc. SPIE*, 1999; **3678**, 104.
6. Gerard M. Schmid, *Ph.D. Dissertation*, The University of Texas at Austin, 2003.
7. M.D. Stewart, G.M Schmid, S.V. Postnikov, C.G. Willson. *Proc. SPIE*, 2001; **4345**, 10.
8. G.M. Schmid, M.D. Stewart, V.K. Singh, C.G. Willson. *J. Vac. Sci. Technol. B*, 2002; **20**, 185.
9. Technology Roadmap for Semiconductors (2001 Edition).
10. G.W. Reynolds, J.W. Taylor, C.J. Brooks. *J. Vac. Sci. Technol. B*, 1999; **17**, 3420.
11. N. Rau, F. Stratton, C. Fields, T. Ogawa, A. Neureuther, R. Kubena, G. Willson. *J. Vac. Sci. Technol. B*, 1998; **16**, 3784.

12. M.I. Sanchez, W.D. Hinsberg, F.A. Houle, J.A. Hoffnagle, H. Ito, C. Nguyen. *Proc. SPIE*, 1999; **3678**, 160.

13. J. Shin, G. Han, Y. Ma, K. Moloni, F. Cerrina. *J. Vac. Sci. Technol. B*, 2001; **19**, 2890.

14. T. Yamaguchi, H. Namatsu, M. Nagase, K. Kurihara, Y. Kawai. *Proc. SPIE*, 1999; **3678**, 617.

15. T. Yamaguchi, H. Namatsu, M. Nagase, K. Yamazaki, K. Kurihara. *Appl. Phys. Lett.* 1997; **71**, 2388.

16. T. Yoshimura, Y. Nakayama, S. Okazaki. *J. Vac. Sci. Technol. B,* 1992; **10**, 185.

17. T. Ushirogouchi, K. Asakawa, M. Nakase A. Hongu. *Proc. SPIE*, 1995; 2438, 160.

18. E. Shiobara, D. Kawamura, K. Matsunaga, T. Koibe, S. Mimotogi, T. Azuma and Y. Onishi, *Proc. SPIE*, 1998; **3333**, 313.

19. L.W. Flanagin, V.K. Singh, C.G. Willson, *J. Vac. Sci. Technol. B*, 1999; **17**, 1371.

20. S.D. Burns, A.B. Gardiner, V.J. Krukonis, P.M. Wetmore, J. Lutkenhaus, G.M. Schmid, L.W. Flanagin, C.G. Willson. *Proc. SPIE*, 2001; **4345**, 37.

21. G.W. Reynolds, J.W. Taylor. *J. Vac. Sci. Technol. B*, 1991; **17**, 334.

22. D. He, F. Cerrina. *J. Vac Sci. Technol. B*, 1998; **16**, 3748.

23. H.P Koh, Q.Y. Lin, X. Hu, L. Chan. *Proc. SPIE,* 2000; **3999**, 240.

24. G.M. Schmid, V.K. Singh, L.W. Flanagin, M.D. Stewart, S.D. Burns, C.G. Willson. *Proc. SPIE*, 2000; **3999**, 675.

25. G.M. Schmid, M.D. Smith C.A. Mack, V.K. Singh, S.D. Burns, C.G. Willson. *Proc. SPIE*, 2001; **4345**, 1037.

26. D.L. Goldfarb, M. Angelopoulos, E.K Lin, R.L. Jones, C.L. Soles, J.L. Lenhart, W. Wu. *J. Vac. Sci. Technol. B*, 2001; **19**, 2699.

27. E.K. Lin, C.L. Soles, D.L. Goldfarb, B.C. Trinque, S.D. Burns, R.L. Jones, J.L. Lenhart, M. Angelopoulos, C.G. Willson, S.K. Satija, W. Wu, *Science*, 20002; **297**, 372.

28. Private Communication, Dario Goldfarb, IBM T.J. Watson, Research Center, Yorktown Heights, NY. 2002.

Chapter 8: Diffusion in Acetal-protected Resist Systems

Most work discussed in previous chapters focused on "APEX-like" photoresists, a class of photoresists known more generally as high activation energy photoresists. There exists another class of photoresists referred to as low activation energy photoresists. Low activation energy photoresists have not been studied to the same extent as high activation energy photoresists and they remain poorly understood in the microlithography community. In general, low activation energy resists seem less sensitive to processing variations, but no clear explanation for this observation has been developed. Acetal-based photoresists have been shown to react readily at room temperature, and this is typically offered as an explanation for their better process stability, but this is not a full, mechanistic explanation.

Structurally, the difference between high and low activation energy photoresists lies in the type of protecting group used to block the resin's aqueous base soluble groups. The high activation energy resists use t-butyl carbonate groups or, sometimes, t-butyl ester groups that require high temperatures to undergo thermolysis even when in the presence of strong acids. The low activation resists rely on acetal and ketal-based protecting groups which, in the presence of water, react at room temperature. Structures of general acetal and ketal groups are shown in Figure 8.1. Structures of some typical examples of typical acetal-based photoresist polymers are shown in Figure 8.2.

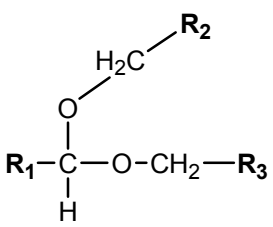

acetal group

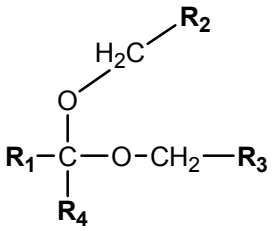

ketal group

Figure 8.1: General structures of acetal and ketal groups.

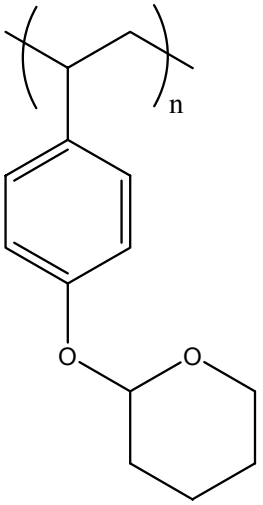

poly(1-tetrahydopyranoxystyrene)

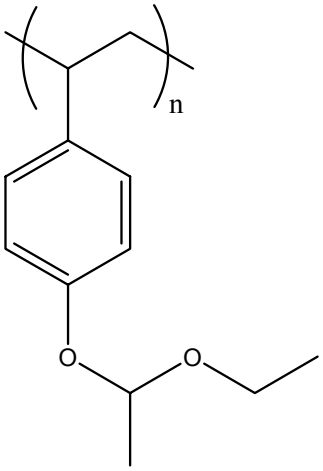

poly(1-ethoxyethyloxystyrene)

Figure 8.2: Specific examples some acetal-based photoresist materials.

The generally accepted reaction pathway for acetal/ketal low temperature (room temperature) deprotection with acidic catalysis and stoichometric amounts of water is shown below in Figure 8.3.

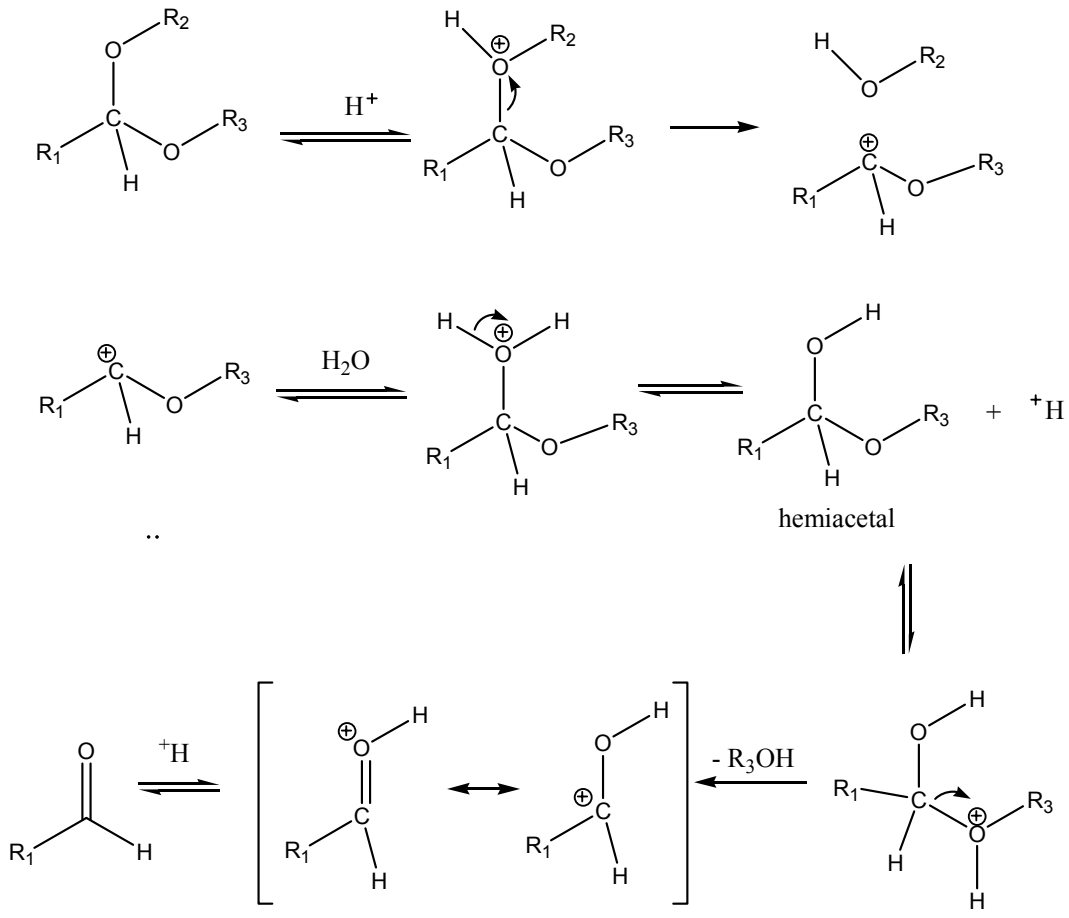

Figure 8.3: Room temperature deprotection pathway for acetal/ketal groups.

It may not be readily apparent what, if any, advantage a low activation energy photoresist has over a normal high activation photoresist system, but for

some applications they are actually preferred. The low activation energy resists are typically used when processing stability is essential. The apparent stability of acetal resists is believed to be the product of the room temperature deprotection reaction; soon after exposure, most of the reaction is complete, leaving less opportunity for variations that occur in high activation systems. In high activation systems, since the majority of resist deprotection does not occur until a high temperature bake step, variation in resist performance can come with variation in the time between exposure and bake processing, so called post exposure delay (PED) instability, as well as variations in baking times and temperatures. For high activation systems, often even the small variations in bake temperatures across a wafer hotplate (less than 1 °C) can have noticeable effects on feature widths. Manufacturing users suggest that low activation energy resists show less sensitivity to process variations in post exposure delay times and post exposure bake conditions[1-4], but the reasons for this behavior has not been conclusively explained.

Because of their PED stability, low activation energy resists have been investigated[5,6] for use in the production of photomasks for microlithography. Mask writers typically use direct, serial writing exposure systems rather than projection imaging systems, so complex mask patterns often take many hours to write out. With write times sometimes approaching a full day, post exposure delay between the first written pattern pieces and last written pattern pieces can be significant, making PED stability crucial in this application.

Another processing variation tries to provide an additional level of post exposure stability by using the low temperature reaction pathway's requirement for stoichometric amounts of water to limit reaction. IBM's electron beam resist KRS-XE is designed to be exposed in the water-free, vacuum environment of an e-beam tool.[7] Electron beam exposure generates acid, but with no water available the resist is unable to react. In a dry environment the entire mask may be written before significant reaction occurs. When the mask blank is removed from the ebeam tool and exposed to ambient humidity, the KRS-XE resists begins to react. This method reportedly has less process variation than high activation energy resists, presumably because even at low temperatures high activation energy resists have a finite rate of deprotection, while the low activation energy resists cannot react without water. It is also possible that the acid is partially sequestered by partial reaction with the resin further limiting diffusion. The sequestering of the acid catalyst can be seen in Figure 8.3, the acid combines with the acetal in the first step, but is not regenerated until either subsequent reaction with water occurs or the initial reaction reverses.

ACETAL PHOTORESIST PERFORMANCE

The fundamentals of acetal-based photoresist performance have not been widely investigated, at least not to the extent of APEX-type photoresists. One of the few fundamental experimental studies of an acetal-based photoresist the work of Sekiguchi *et al.*[1] In Sekiguchi's work, the extent of deprotection was monitored by FT-IR spectroscopy while exposure is carried out at various

temperatures. Reproduced in Figure 8.4 is graph of extent of acetal resist protection versus exposure dose at various temperatures from Reference 1. For comparison purposes a similar graph, also from Reference 1, for an APEX-type resist is presented in Figure 8.5. Dotted lines in Figure 8.4 and Figure 8.5 are simulation fits from the original work and are not of particular significance to this discussion. Because the exposure dose in these experiments was provided by a UV lamp (irradiance 1 mW/cm^2), it is not possible to easily deconvolve the effect of longer baking times from increased exposure dose, but the trends in data are more important than the specific numbers.

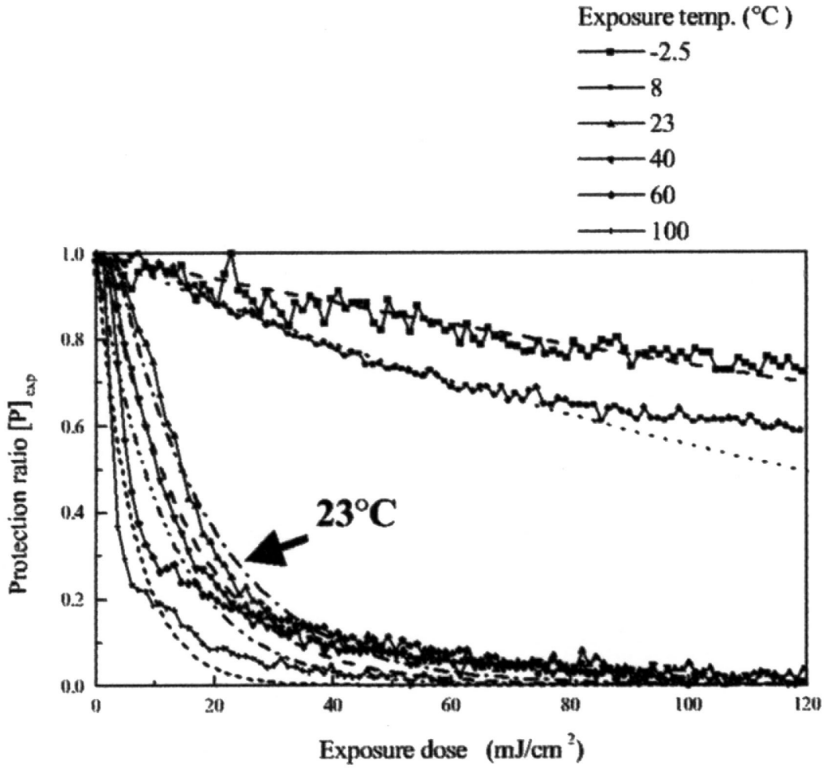

Figure 8.4: Ethyl acetal deprotection at various exposure temperatures. (Reproduced from Reference 1)

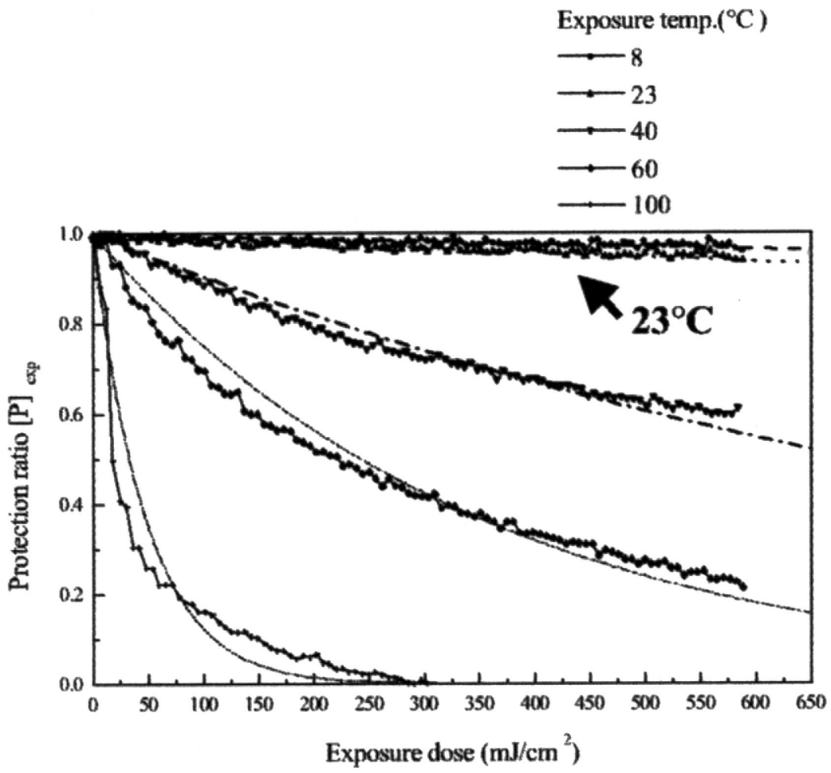

Figure 8.5: APEX resist deprotection at various exposure temperatures. (Reproduced from Reference 1)

Presented below in Figure 8.6 and Figure 8.7 are contrast curves from Sekiguchi *et al*. for an acetal-based photoresist and an APEX-type photoresist, respectively. Figure 8.6 shows for an acetal resist that there is very little difference in resist performance whether the resist is post exposure baked or not. This is a very strong example of stability to process variation for a low activation energy resist. Figure 8.7 demonstrates that the post exposure bake is critical for

APEX resist function. A high activation energy resist will not be able to produce an image without a post exposure bake.

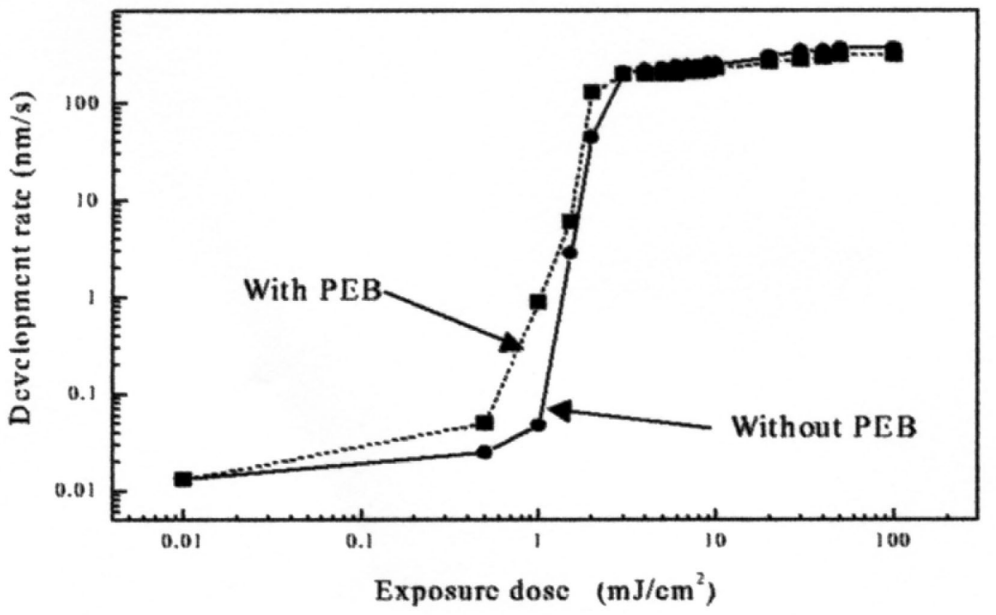

Figure 8.6: Contrast curve for an acetal-based photoresist with and without PEB. (Reproduced from Reference 1)

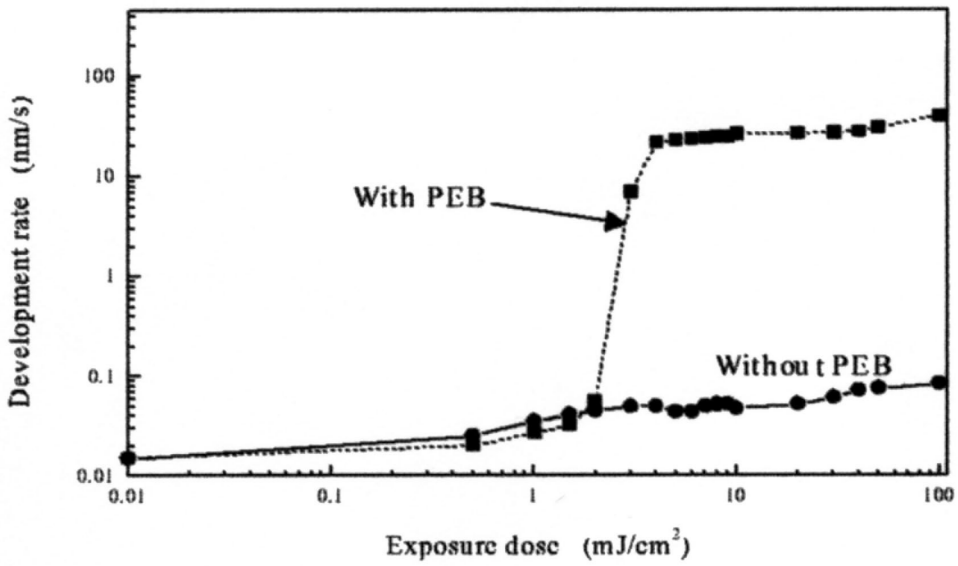

Figure 8.7: Contrast curve APEX-type photoresist with and without PEB. (Reproduced from Reference 1)

The specific stability of line widths in low activation energy photoresists to variations in post exposure bake time is demonstrated in Figure 8.8. Reproduced from Reference 2, Figure 8.8 shows variations in resist feature size (critical dimension) as a function of exposure dose at various PEB times. At a PEB temperature of 130 °C, the individual points for a range of different PEB times lay one on top of the other, indicating PEB time (over this range) has almost no effect on the final feature dimension. The insensitivity of low activation energy resists to PEB time has led some researchers[2,3] to suggest that low activation energy photoresists have an imaging behavior that more resembles non-chemically amplified photoresists, like DNQ/novolac, than the typical high

activation energy chemically amplified systems. In non-chemically amplified photoresists light directly causes the resist solubility switch and the latent image of soluble and insoluble regions is thus directly linked to exposure. In Figure 8.8, PEB bake time does not significantly affect developed feature dimensions, making it appear that that acid diffusion in low activation photoresists is extremely slow. It is possible that diffusion in low activation energy resists appears slow relative to other resists at elevated temperatures only because the low activation energy photoresists has already reacted at lower temperatures. In the case shown in Figure 8.8 the resist is an ethyl acetal compound deprotects to form polyhydroxystyrene. Diffusion in polyhydroxystyrene was shown in Chapter 3 to be extremely slow at a PEB temperature of 130 °C. The resist used in Figure 8.8 produces acetalaldehyde (b.p. 21 °C) and ethanol (b.p 78 °C) as by-products which might be expected to be quickly driven from the film.

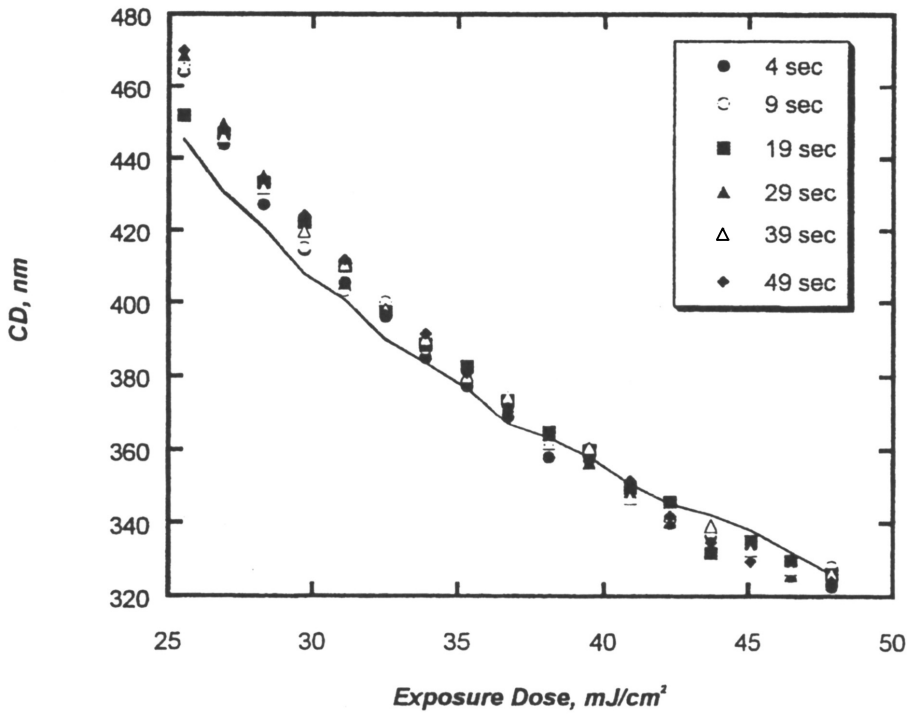

Figure 8.8: Line width insensitivity to PEB time for a acetal photoresist. (Reproduced from Reference 2)

ACETAL RESISTS AND THE REACTION FRONT PROPAGATION MODEL

For several reasons acetal photoresists do not fit cleanly into the reaction front propagation model used to explain experimental diffusion results in APEX-like, high activation energy photoresists. The main difference is that acetal photoresists do not necessarily produce small molecule, gas by-products when they deprotect. The mechanisms of transient diffusivity enhancement rely on reaction by-products being generated, then removing themselves from the resist film by desorption. With some acetal resists, relatively high molecular weight

alcohols are generated. It is quite possible that even high molecular weight alcohol by-products could act as plasticizing agents in the film, but if they do not readily desorb from the film the diffusivity enhancement might be more permanent than transient. This does not fit well with the observation that acetal photoresists actually have better feature width stability with post exposure bake time variations than other resist systems. If acetal photoresists were permanently plasticized by reaction by-products, feature widths would be expected to grow significantly over time, but this is not observed.

Some of the underlying assumptions about acetal photoresists need to be examined. First to be considered is whether alcohol reaction by-products actually plasticize the resist film. This seems a reasonably safe assumption because the base resin for the acetal photoresists (often polyhydroxystyrene) is partially soluble in most alcohol-based solvents. It was seen in the experiments of Chapter 3 and Chapter 7 that ethanol and n-butanol could be used as casting solvents for polyhydroxystyrene, so clearly polyhydroxystyrene is soluble in at least these alcohols, and presumably others as well. Solvent plasticization of resist films has been studied previously[8,9] and the presence of solvent in the resist film was found to be a significant contributor to increasing polymer free volume. Figure 8.9 below is a plot of solvent diffusivity in a polymer matrix as a function of solvent content in the film. The plot is generated using a modified Fujita-Doolittle equation using typical solvent and polymer parameters as reported by Mack[9]. Figure 8.9 shows that solvent in the resist film can significantly alter diffusivity.

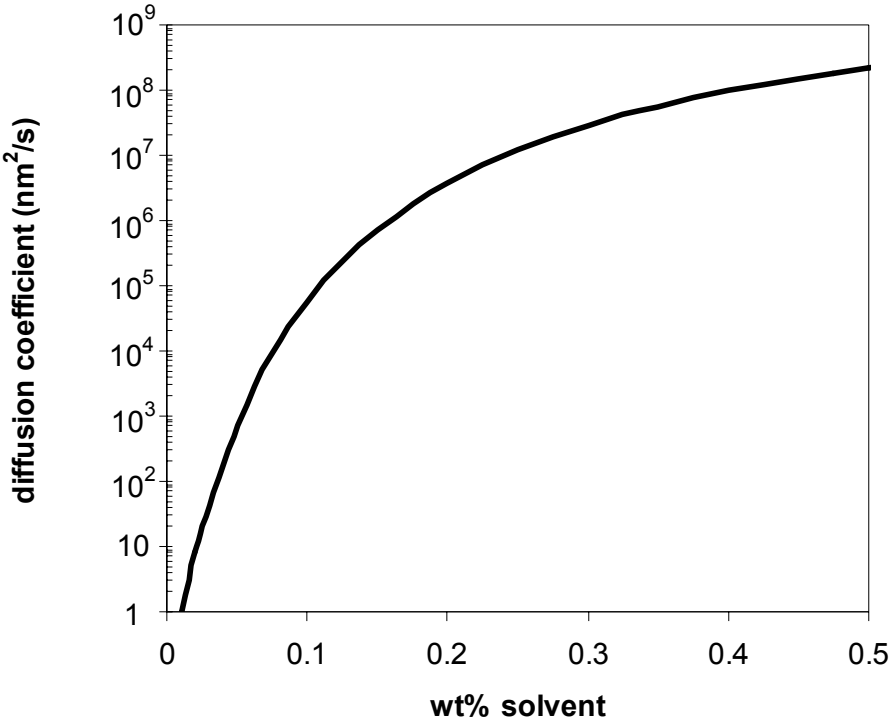

Figure 8.9: Diffusivity versus solvent wt% in the polymer film.

There is some evidence that even large alcohol by-products are not permanently trapped in the film after generation. Ellipsometry experiments with poly(1-tetrahydropyranoxystyrene) (PTHPS) resin (shown in Figure 8.2) show the film loses significant thickness during the baking step when mixed with an acid and ramped through temperature. This thickness change is presumably reaction products being driven off from the previously completed reaction, but it shows that the generated by-products can leave the film. Shown in Figure 8.10 are thickness change measurements from ellipsometry for PTHPS resin at a constant temperature of 130 °C for 10 minutes. The film loses about 20% of its initial

thickness in 10 minutes presumably indicating substantial mass loss as well. Figure 8.11 shows results from an experiment in which the PTHPS resin was ramped at 5 °C per minute from 25 °C to 175 °C and the film thickness was monitored once again by ellipsometry. The film was stable to approximately 75 °C, but then began to lose thickness. Ultimately, the film lost almost a quarter of its initial thickness over the course of the experiment. These experiments show that even large reaction by-products can leave the film during baking.

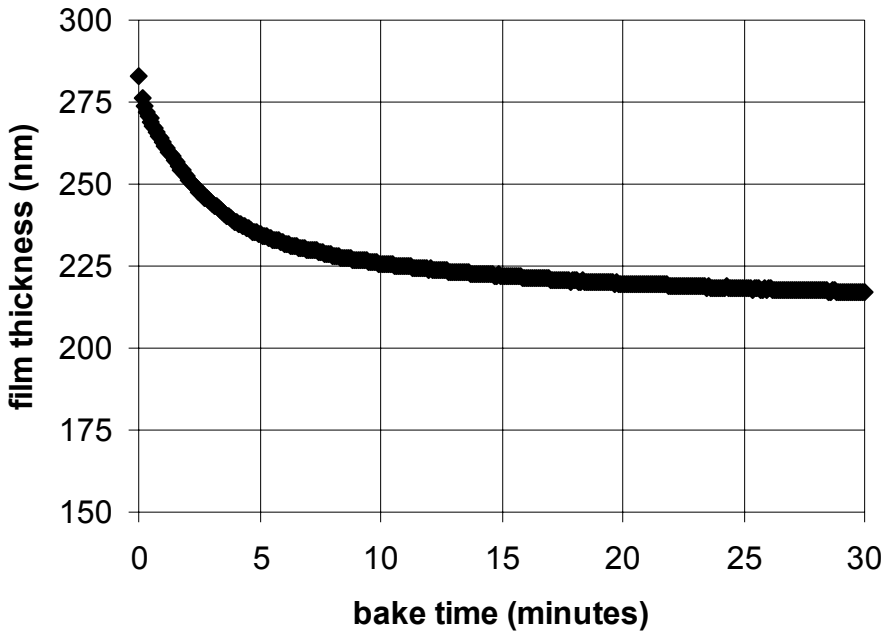

Figure 8.10: Acetal thickness change at constant baking temperature. T = 130 °C

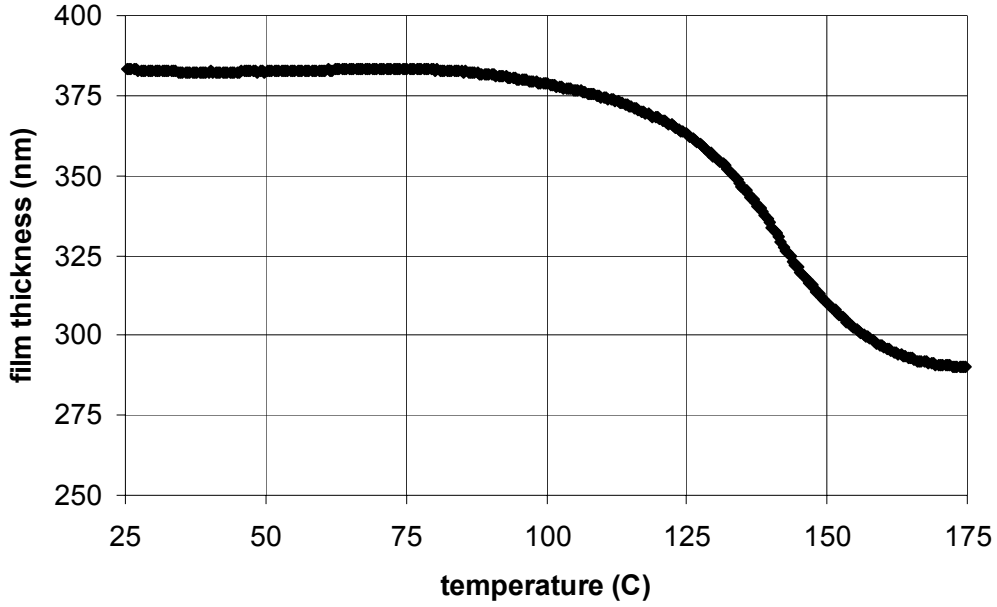

Figure 8.11: Acetal thickness change as function of temperature.

But, as shown in the work of Sekiguchi *et al.*, the majority of deprotection occurs at room temperature and at temperatures below typical alcohol boiling points (64.7 °C for methanol, 78.3 °C for ethanol and 117 °C for n-butanol). In addition, the work of Mueller[8] and Gardener[10] show that even after elevated bake processing, significant solvent can remain in the film, so that it might be expected that significant amounts of alcohol by-product would remain in the film after the ambient temperature hydrolysis reaction is complete.

If the alcohol by-product remains in the film, it is not clear how any reaction generated diffusivity enhancement resulting from the presence of by-products in the film could be transient in nature. The behavior of low activation energy photoresists needs further examination. Unlike high activation energy

systems, low activation energy systems start reacting immediately after exposure (even at room temperature). Because diffusion is temperature dependent, the photoacid is likely in a relatively slow diffusion environment (due simply to low temperature) even if the by-products linger and partially plasticize the resist film. Most acetal resists have glass transition temperatures above 100 °C, so unless by-product concentration is very high, acid molecules will still be in a glassy polymer and, therefore, will have fairly low mobility. Mack[9] gives the following relation for the solvent content effect on polymer glass transition temperature:

$$T_g(\phi_s) = T_g(\phi_s = 0) - \beta\phi_s / \alpha_2 \qquad \text{(Eqn. 8.1)}$$

where T_g is the film glass transition temperature, ϕ_s is the solvent volume fraction in the film, and β and α_2 are constants. The β constant accounts for the fraction of solvent volume that can be considered free. Mack uses a value of 0.19 for β. The α_2 constant is the related to coefficient of thermal expansion for a rubbery polymer. Mack uses a value of 4.8×10^{-4} K^{-1} as typical for most polymers. A drop of 50 °C in film glass transition temperature requires a solvent volume fraction of about 15% using Mack's typical values for the constants. Polyhydroxystyrene has a glass transition temperature of approximately 150 °C, so to lower a polyhydroxystyrene film T_g to room temperature, the solvent volume fraction would need to be over 30%. Typically acetal photoresists are no more than 20-30% protected initially, and an acetal groups like tetrahydropyran would make up at most 10-20% of the total resin volume in this type of system (smaller acetal groups would make up even less of total resin volume).

At room temperature, in a still glassy polymer, acid molecules will not be moving large distances. Because translational movement of the acid is limited by the low temperature, one can picture an acid molecule sitting in a more or less fixed position while completely deprotecting everything in its local, vibrational vicinity. By reacting with its nearest neighbors and releasing resin solvent-like by-products, the acid will have temporarily plasticized its local vicinity, increasing its mobility. But from the perspective of the reaction front model the acid is potentially generating itself something of a diffusion cage. If the by-products diffuse away from the reaction zone faster than the acid, the acid will be caged/trapped. Unlike in the APEX system, the by-products do not necessarily leave the film quickly or at all, so it is not clear how long the reaction zone remains plasticized, but with some reasonable assumptions it can be seen that the cage could close and by-product promoted diffusion would be of limited lifetime.

By-product alcohols will be fairly good resin solvents, and perhaps smaller in molecular dimension than the photoacid, so they will likely have a higher mobility than the photoacid. At the molecular level this means the alcohol by-product can move away from the reaction site faster than the acid. From a bulk perspective one would expect that the concentration of by-product in the exposed region will drop more quickly than the acid concentration. If the by-product has a larger diffusion coefficient than the acid, the reaction generated enhancement will diminish with time (especially in a patterned sample with alternating exposed and unexposed regions). Depending on how long after exposure the PEB occurs, much of the acid could have already caged itself by

reacting with the surrounding material and the local high concentrations of plasticizing by-products might have diffused away. This self caging behavior can explain the insensitivity of low activation energy photoresists to variations in post exposure bake times and temperatures and is in line with the reaction front model.

REFERENCES

1. A. Sekiguchi, Y. Miyake, M. Isono. *Jpn. J. Appl. Phys.* 2000; **39**, 1392.
2. D. Kang, S. Robinson. *Proc. SPIE*, 2002; **4690**, 963.
3. J. Lewellen, E. Gurer, E. Lee, L. Chase, L. Dulmage. *Proc. SPIE*, 1999; **3882**, 45.
4. H. Roeschert, K. Przybilla, W. Spiess, H. Wengenroth, G. Pawlowski. *Proc. SPIE*, 1992; **1672**, 33.
5. B. Rathsack, C. Tabery, J. Albelo, P. Buck, C.G. Willson. *Proc. SPIE*, 2001; **4186**, 8163.
6. C.H. Kim, C.U. Jeon, S.W. Choi, W.S. Han, J.M. Sohn. *Proc. SPIE.* 2001; **4186**, 108.
7. D.R. Medeiros, A. Aviram, C.R. Guarnieri, W.S. Huang, R. Kwong, C.K. Magg, A.P. Mahorowala, W.M. Moreau, K.E. Petrillo, M. Angelopoulos. *IBM J. Res. Dev.* 2001; **45**, 639.
8. Katherine E. Mueller, *Ph.D. Dissertation*, The University of Texas at Austin, 1998.
9. Chris A. Mack, *Ph.D. Dissertation*, The University of Texas at Austin, 1998.
10. Allen B. Gardiner, *Ph.D. Dissertation*, The University of Texas at Austin, 1999.

Chapter 9: Conclusions and Future Work

It appears from results in Chapter 3 that intrinsic (non-reactive) diffusion rates in resist materials are too small to account for observed diffusion bias. Diffusion coefficients for poly(4-t-butyloxycarbonyloxystyrene) (PTBOC) were estimated based on non-reactive analogues, but even without the analogues, it might be estimated using free volume arguments, like Williams-Landel-Ferry, that PTBOC, with a glass transition temperature of approximately 120 °C, would have fairly low diffusivity for large penetrants at temperatures in the 70 – 100 °C range. Experiments in reactive photoresist polymers, conducted as bilayer experiments in Chapter 4, demonstrate diffusion distances versus time curves with shapes that can not be easily matched with a Fickian model. Curves could not be matched with a single coefficient or with two separate coefficients (with realistic values) for reacted and unreacted material with out assuming some form of enhanced local diffusivity, or a local acid diffusivity that does not match the overall, or global diffusion rate. Unfortunately, experiments described in Chapter 5 could not conclusively show the existence of transient state at high temperatures, but at 75 °C a lag between reaction and film shrinkage of just less than 1 second was observed. For higher temperatures, the best that can be said is that if a transient state exists, it is of less than 200 milliseconds duration, which is the time resolution limit of the experimental equipment. Chapter 6 provided a simple visual confirmation that the bilayer diffusion front is relatively sharp. The SEM experiments of Chapter 6 were largely done to show that the IR based

method was valid and this was accomplished. In Chapter 7 the experimental methods designed for fundamental diffusion studies were put into service to investigate line edge roughness (LER) and line end shortening (LES). Chapter 7 demonstrates that the conceptual model of Reaction Front Propagation can be a useful framework to study some important, resist-related issues of concern to the semiconductor industry.

As for the reaction front model, it is perhaps somewhat complex and it does not lend itself to simple mathematical formulation. For lithographers in manufacturing, using a Fickian diffusion model and a single diffusion coefficient often yields sufficient accuracy, but our goal is not just to fit the experimental data to some equation, it is to try to understand the process at the molecular level. Given enough fitting parameters, the data can always be fit, but understanding is more difficult to achieve. It would be satisfying to have an equation that could be solved for arbitrary temperatures, acid sizes, bake times, *etc.* to give an image blurring distance, but resist function appears too complex for a simple equation to explain the full range of behaviors. The mesoscale modeling effort[1] in the Willson research group is an attempt to deal with the complexities of resist behavior and the mechanisms of the reaction front propagation model can be embedded in the mesoscale, post exposure bake simulator. Figure 9.1 below presents a comparison of mesoscale simulation results with experimental results for a bilayer sample (like discussed in Chapter 4). The main adjustable parameters in the mesoscale simulation are initial void fraction (free volume level) and the lifetime of reaction-generated voids. Using reaction-generated

voids is the simulation's method for modeling transiently enhanced mobility. The void lifetime was calibrated to match observed trends in measured deprotection reaction kinetics. Figure 9.1 shows that experimental observations can be matched using a simulation which incorporates the main concepts of the reaction front propagation model. Further details of the mesoscale model can be found at References 1 & 2.

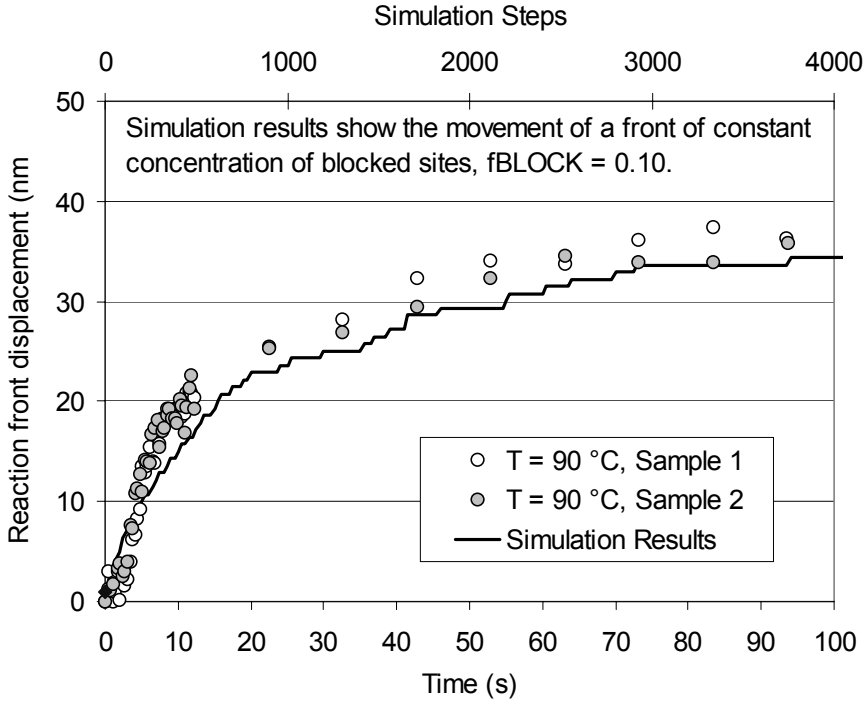

Figure 9.1: Mesoscale simulation results compared to experiment. (Reproduced from Reference 1)

In some sense, this mesoscale simulation is our (not so) simple equation. Albert Einstein once said, "Things should be made as simple as possible, but not

simpler." The reaction front model is not simple, but perhaps it is as simple as possible.

FUTURE WORK

There are always more things to be done, more data points to be collected. One might, for example, do bilayer experiments for a larger variety of PAGs or trilayer experiments with different PAGs. Different resin materials other than PTBOC and PHS might be studied, like acrylate-based or acetal-based resists. In retrospect, collecting data over a range of temperatures for a variety of PAGs would have been interesting, as it would have perhaps allowed a correlation between penetrant size and the apparent activation energy of diffusion. The correlation obtained in bilayer experiments might then be compared to non-reactive results from corresponding trilayer experiments. Other than that, there are few really interesting or untried experiments using the film stack approach to study acid diffusion in APEX-like photoresists. While acid diffusion has been well studied, there are still plenty of experiments to do in the area of base diffusion and many experiments to perform to understand acid-base interactions in formulated photoresists. The model resist used in most of these experiments simply consisted of PTBOC mixed with a small amount of PAG. Real commercial resists are typically more complex, sometimes with a mix of different PAGs and additional components like base additives and dissolution inhibitors. Diffusion of base and other components can play an important role in resist imaging, and it, in general, remains poorly understood and little studied.

As seen in Chapter 8, definite experiments remain to be done as regards to acid diffusion in low activation energy, acetal-based resists. If acetal-protected resin that is insoluble in alcohol solvents can be synthesized, bilayer experiments much like those in described in Chapter 7 for line edge roughness could be performed fairly easily. Experiments with flash exposures at elevated temperatures might be very interesting for acetal-based photoresists. No one has yet published clean data on the kinetics of deprotection for a low activation energy photoresists. Flash exposure using excimer lasers would also more closely mimic the manufacturing environment.

As for the transient state investigation, when faster tools become available the simultaneous ellipsometry-spectroscopy experiment could be repeated to see if the higher time resolution can see the transient at higher temperatures. Alternatively, other techniques, like simultaneous IR and quartz crystal microbalance (to measure mass loss with time), could be investigated.

DIRECTION OF LONG RANGE RESEARCH

More emphasis needs to be placed on the limitations of chemically amplified photoresists in the sub-50 nm regime. Examples of successfully printed sub-50 nm nested line/space patterns in positive tone chemically amplified resists are extremely rare and sub-30 nm nested positive tone lines are more or less non-existent. This may eventually change, but researchers have been probing resist resolution limits for at least 15 years and little to no progress in improving ultimate resolution has been achieved. All proposed “Next Generation

Lithography" systems for sub-50 nm imaging assume that resists will be available when needed (in the fairly near future) and these resists will be both highly sensitive to the exposure radiation and have high imaging resolution, but this should not be taken for granted. Perhaps, the most significant conclusion to be drawn from this dissertation is that image blur caused by acid diffusion into unexposed areas can only be limited, not eliminated, if high sensitivity due to chemical amplification is to be maintained. It appears that the mechanisms responsible for high sensitivity are intimately tied to the processes that result in imaging blurring, making it extremely difficult, perhaps approaching impossible, to have a highly sensitive, high resolution chemically amplified photoresist based on current design concepts. New resist design concepts that can achieve high resolution and high sensitivity need to be developed and explored. Perhaps such things as unstable catalysts with limited lifetimes or fundamentally different resist architectures could be the answer, but the existence of industry as we know it depends on developing new high performance resists.

REFERENCES

1. Gerard M. Schmid, *Ph.D. Dissertation*, The University of Texas at Austin, 2003.

2. G.M. Schmid, V.K. Singh, L.W. Flanagin, M.D. Stewart, S.D. Burns, C.G. Willson. *Proc. SPIE*, 2000; **3999**, 675; G.M. Schmid, M.D. Smith C.A. Mack, V.K. Singh, S.D. Burns, C.G. Willson. *Proc. SPIE*, 2001; **4345**, 1037; G.M. Schmid, M.D. Stewart, V.K. Singh, and C.G. Willson. *J. Vac. Sci. Technol. B*, 2002; **20**, 185.

Appendix A: Polymeric PAGs

The motivation for polymeric photoacid generators comes from the expectation that increasing the size of a photoacid's counter ion will help limit diffusion and thus also imaging blurring. There are perhaps other uses for polymeric PAGs as more general film coatings, but the main application envisioned is in photoresists. Experiments showing the effect of counter ion size on measured diffusion distances were presented in Chapter 4. By covalently attaching an acid anion to a polymer backbone the diffusional cross-section of the acid becomes enormous. Diffusion of the polymer-bound acid would be expected to be controlled by rates of polymer chain interdiffusion. Interdiffusion of glassy state polymers is extremely slow, making diffusion of a polymer-bound acid extremely slow as well. With slow rates of catalyst diffusion, the exposure sensitivity of a resist formulated with a polymeric photoacid generator would be expected to suffer, but this might be compensated by increased loadings of the PAG unit in the resist. Eventually, the PAG unit might be directly incorporated onto the photoresist resin backbone allowing higher PAG unit molar loadings before phase segregation occurs.

In addition to potential improvements in photoresist performance polymeric PAGs are likely more environmentally friendly than monomeric PAGs. Recently, the semiconductor industry has been forced to largely forego the use of one of its standard PAGs, those based on perfluorooctanesulfonates (PFOS),

because of concern over human uptake. A polymeric PAG would not be volatile, thus human exposure could on come from direct ingestion of the resist.

SYNTHESIS OF POLYMERIC PAGS AND RELATED MATERIALS

Actual synthesis of polymeric PAGs was part of the thesis work of Hoang Vi Tran[1] and Brian Trinque[2]. A full accounting of the synthetic procedures can be found at the given references. Two different versions of polymeric PAGs with different co-monomers were prepared along with some model compounds for comparison purposes. The anion-bound polymeric PAG (anPAG1) was synthesized by copolymerization of the corresponding lithium salt and polystyrene, followed by metathesis reactions on the resultant copolymer. After polymerization, the product was precipitated into hexanes and washed with water. The polymer was passed through an acidic ion exchange column, then stirred with silver carbonate to convert to the polymer to the silver salt. Final product was obtained by addition of thioanisole and iodomethane. A similar procedure was used for anPAG2, which is a polymeric PAG just like anPAG1 but with 4-methoxystyrene as the co-monomer instead of polystyrene. Elemental analysis and careful ^{19}F-NMR were used to confirm the copolymer ratios. For the synthesis of the cation-bound polymeric PAG (catPAG), the silver salt of the acid anion, along with iodomethane, was mixed with a copolymer of styrene and 4-methylthiostyrene to give the desired product. Shifting of S-CH_3 resonances in ^{1}H-NMR was used to confirm total conversion to sulfonium groups. The monomeric PAG (mPAG) was synthesized by mixing the same silver salt used to

make the catPAG with thioanisole and iodomethane, followed by recrystallization from a solution of acetonitrile and diethyl ether. The structures of the discussed compounds are shown in Figure A.1 below.

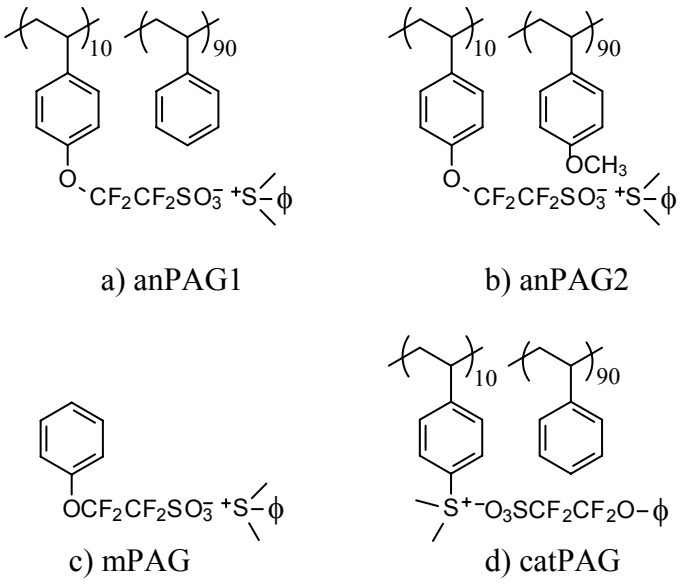

Figure A.1: Structures of polymeric PAGs and the monomeric analogue. a)anion-bound PAG (anPAG1); b) second version anion-bound PAG (anPAG2); c) monomeric PAG (mPAG); d) cation-bound PAG (catPAG)

BLEND EXPERIMENTS

In general, two types of experiments were performed to test the behavior of polymeric PAGs. The first experiment consisted simply of taking the PAGs and blending them into resist resin, then exposing them to UV radiation to test their activity. Polymeric PAGs were blended with PTBOC in a 1:1 mass ratio,

while the monomeric PAG was blended to give a roughly equivalent molar acid loading as the polymeric PAGs. Phase compatibility when blending polymers is always a concern, but the spin cast films of these solutions formed acceptable films from solutions that were slightly hazy. After spin casting, the samples were post apply baked at 90 ºC for 90 seconds, then exposed to ultraviolet light to generate acid. The samples were then placed on a 90 ºC hotplate and monitored by FT-IR. The disappearance of the carbonyl peak from TBOCST was monitored to determine extent of reaction. The results from these experiments are shown in Figure A.2. Experimental results are in line with expectations: the monomeric PAG generated the fastest deprotection rate and the greatest extent of reaction, while the PAG with polymer bound cation/chromophore approached the extent of reaction of the unbound, monomeric PAG. The PAG with polymer-bound acid anions was less reactive than either of the other two PAGs. While the monomeric PAG and the cation-bound PAG generate the same acid it is not necessarily surprising that the polymeric PAG would appear somewhat less reactive. Because of phase incompatibilities it is likely that some acid generated in the cation-bound PAG system is segregated in polystyrene rich phase areas. Any acid in polystyrene rich phase areas must first diffuse into areas with reactive groups before it can catalyze any reactions. The anion-bound PAG generates an acid with a counter ion covalently bound to the polymer backbone, so in addition to generating acid in non-reactive polystyrene rich regions, the mobility of the acid is expected to be extremely restricted.

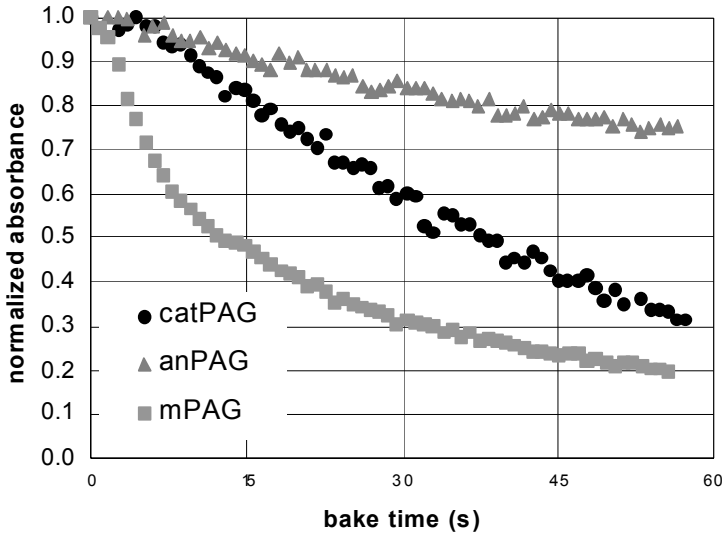

Figure A.2: Blend experiment with catPAG, mPAG, and anPAG1

Blend experiments with anPAG2, the polymer-bound PAG with improved blending behavior, show that it has deprotection curves similar to typical monomeric PAGs, but it appears either somewhat less sensitive or less effective as a catalyst. Figure A.3 shows a series of experiments with anPAG2 where the blend samples were exposed to increasing doses. Increased exposure dose speeds the reaction until saturation is achieved in the 40 – 80 mJ/cm^2 range. For comparison the deprotection curve for a typical monomeric PAG (triphenylsulfonium hexafluoroantimonate) at a similar molar loading and exposure dose is plotted with the anPAG2 result in Figure A.4. The antimonate PAG deprotects the PTBOC much faster than anPAG2 system. This could be because of differences in diffusion rates, though it might also result from poor

photochemical conversion to the acid in the polymeric system. Saturation exposure doses were used for both PAGs, but it has not yet been shown that every PAG repeat unit in a polymeric PAG is photoactive which might reduce the expected molar amount of acid.

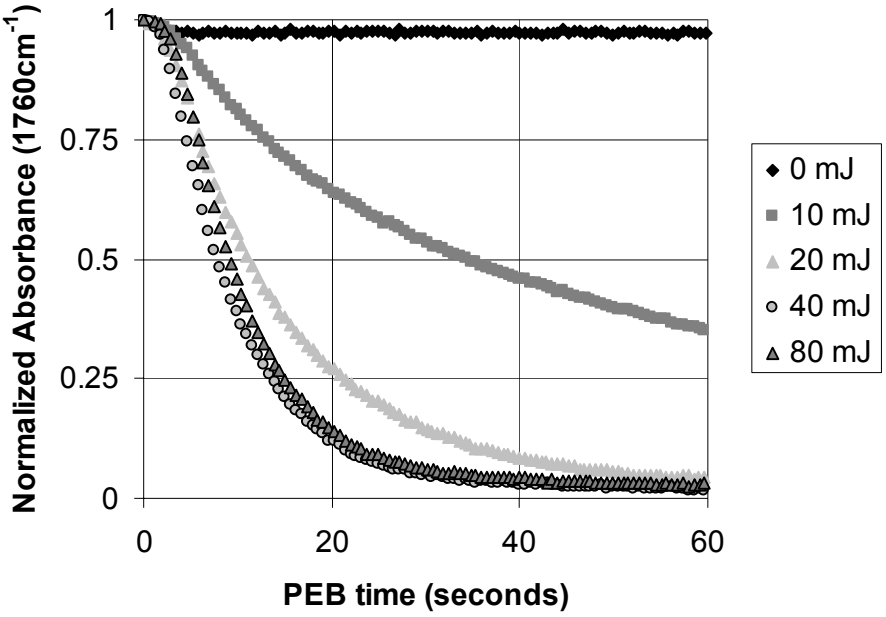

Figure A.3: Blend experiments with anPAG2 at different exposure doses.

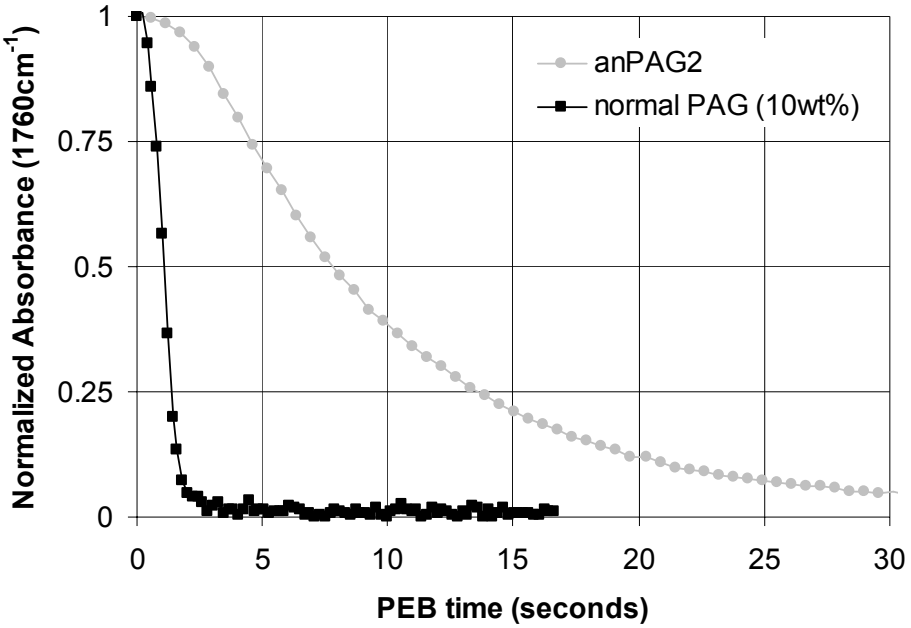

Figure A.4: Comparison of anPAG2 and a typical monomeric PAG

POLYMERIC PAG BILAYER EXPERIMENTS

The second type of diffusion experiments involving polymeric PAGs were bilayer film stack experiments like those discussed in Chapter 4. In the first bilayer experiments a film of pure polymeric PAG was spin cast onto the substrate to act as the acid feeder layer. (In previous bilayer experiments, PAGs were dispersed in polymer carrier layer, but this is not necessary with polymeric PAGs.) A PTBOC detector layer was then floated onto the sample as a second layer. Films were post apply baked at 90 ºC for 90 seconds. Films were exposed to ultraviolet light, then placed on a 90 ºC hotplate and monitored by FT-IR. Results of bilayer experiments with anPAG1, anPAG2, and catPAG are presented

in Figure A.5. Results from the bilayer experiments are shown as diffusion distance versus bake time as in Chapter 4.

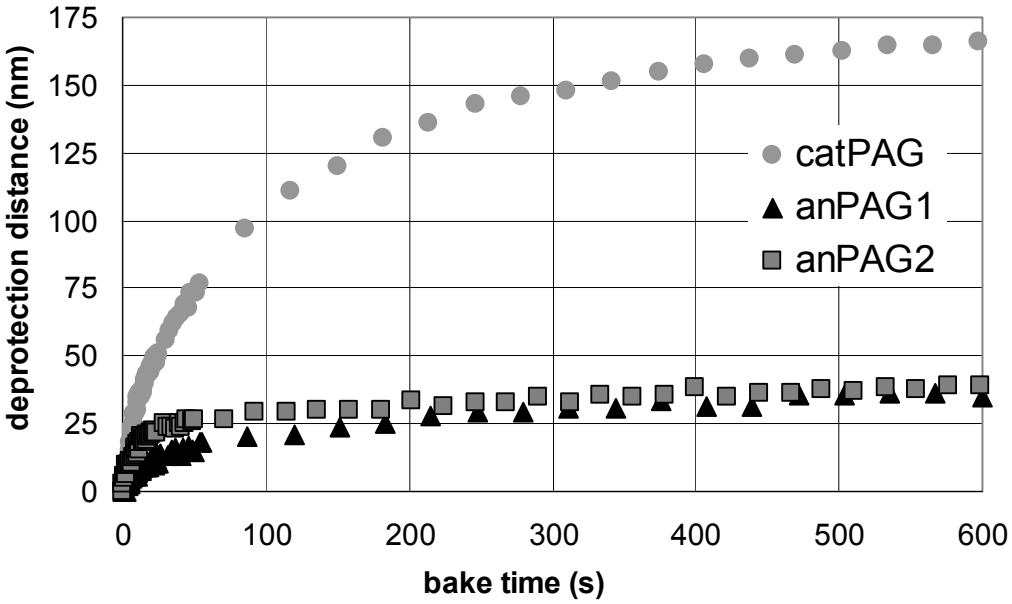

Figure A.5: Bilayer experiment results for anPAG1, anPAG2, and catPAG.

The two anion-bound PAGs produce similar results with little difference in final extent of diffusion, but some variation during in the initial period. As before, the stated diffusion distances assume that the reaction and diffusion fronts are co-located and relatively sharp. The distance reported for the unbound acid (catPAG) is approximately 160 nm over the course of a ten minute 90 ºC bake. This some 100 nm longer than seen for $HO_3SC_4F_9$ (nonaflic acid) at ~3% molar loading, but the generated acid in this case is the slightly lighter $HO_3SC_2F_4OC_6H_5$. The molar loading of the catPAG in the acid feeder layer is about 3 times as great

as the loading of nonaflic acid. Significantly higher loadings of a monomeric PAG are not readily achievable due to solubility constraints.

The results from the bound acid samples are slightly surprising. If the acid is bound to the polymer backbone, it was expected that diffusion will be extremely restricted - perhaps only to the distance the acidic proton can separate from its counter anion. Results from these bilayer experiments give a diffusion distance of 25 nm for the anPAGs. This distance is too great to be accounted for by just proton separation from the counter anion as the force required to separate the charge over that distance would be impossibly large. Some diffusion of the entire acidic polymer is necessary to explain a deprotection distance of 25 nm. An alternate explanation for the observed results is that the two layers are intermixing during sample preparation. This seems unlikely because the polymers are not extremely compatible to begin with and the sample preparation method is design to limit opportunities for mixing between layers. Another explanation is perhaps the polymeric acid is actually diffusing into upper layer due to reaction enhanced diffusion. At the initial stages of the bake the sample is in an unusual state, the presence of reaction by-products like carbon dioxide and isobutylene, perhaps along with photolysis fragments from the PAG chromophore, could create a severely plasticized film stack that could temporarily allow for interpenetration of the polymers in the upper and lower layers.

Another experiment, previously discussed in Chapter 4, shows the anPAG2 in comparison with some monomeric PAGs. This polymeric PAG is miscible with poly(4-methoxystyrene), so it can be dispersed in carrier layer, this

allows constant molar acid loadings to be used so comparison between the various PAGs is fair. Figure A.6 is a plot of diffusion distance versus PEB time for various PAGs at constant a molar loading of 2.3%. The polyPAG of this experiment is anPAG2. The anPAG2 is shown to be the least mobile of all the PAGs tested with a final diffusion distance of about 15 nm.

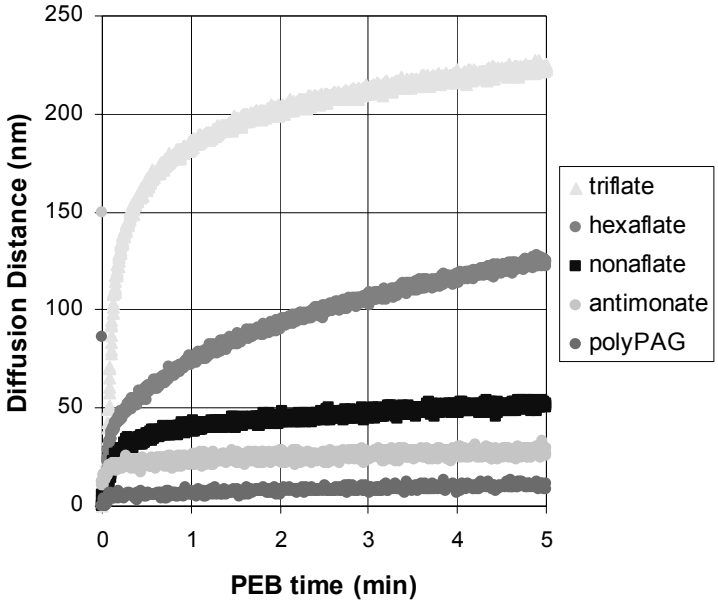

Figure A.6: Diffusion distance vs. PEB time for various PAGs at constant 2.3% molar loadings. T = 90°C, PTBOC: 300nm, PMOS: 230nm.

CONCLUSIONS

The polymeric PAGs are interesting new materials with multiple potential uses. A cation-bound PAG like the one shown in Figure A.1 could potentially limit outgassing (component volatilization) during exposure since the volatile piece (the aromatic ring) of the chromophore is covalently attached the polymer

backbone. It has been shown that much of outgassed material consists of PAG chromophore fragments generated by photodecomposition.[3] The design of these cation-bound could drastically reduce the potential for outgassing. The anion-bound PAG does not have any mechanism to limit outgassing as the chromophore is not covalently linked to the polymer backbone, but it does have a mechanism to greatly reduce acid diffusion. Any generated acid will have its conjugate base, or counter anion, covalently attached to a polymer backbone. In effect, the acid has an extremely bulky conjugate base and long distant migration will be extremely difficult. Due to columbic forces, separation of the proton and its conjugate base is also severely limited. Tethering the acid anion to the polymer backbone restricts the radius of influence a generated acid molecule can have during the course of the post exposure bake. While the polymeric PAGs have some advantages, as currently constructed these polymeric PAGs have several limitations. Synthesis is difficult, especially for the anion-bound PAG. PAGs copolymerized with polystyrene have limited miscibility when mixed into common photoresist resins. The methoxystyrene version has much improved miscibility in resins used for 248 nm lithography, but it would not be appropriate in resists for 193 nm or 157 nm lithography. It also seems that the range of possible copolymers is limited due to required synthetic routes. The polymeric PAGs, as currently synthesized, also have poor stability over time. All version of polymeric PAGs thermally decomposed to generate significant acid at room temperature over the course of about six months. The monomeric PAG does not seem to have a stability problem.

REFERENCES

1. Hoang Vi Tran, *Ph.D. Dissertation*, The University of Texas at Austin, 2002.

2. Brian Trinque, *Ph.D. Dissertation*, The University of Texas at Austin, 2003.

Bibliography

T.E. Alfrey, E.F. Gurnee, W.G. Lloyd. *J. Polym. Sci.* 1966; **C12**, 249.

K. Asakawa. *J. Photopolym. Sci. Technol.* 1993; **6**, 505.

R.M. Barrer, *Diffusion in and through Solids*, Cambridge University Press: London, 1951.

F.W. Billmeyer, *Textbook of Polymer Science, 3rd ed.*, John Wiley & Sons: New York, 1984, p321.

A. Bos, I.G.M Punt, M. Wessling, H. Strathmann. *J. Membr. Sci.* 1999; **155**, 67.

G. Breyta, D.C. Hofer, H. Ito, D. Seeger, K. Petrillo, H. Moritz, T. Fischer. *J. Photopolym. Sci. Technol.* 1994; **7**, 449.

S.D. Burns, A.B. Gardiner, V.J. Krukonis, P.M. Wetmore, J. Lutkenhaus, G.M. Schmid, L.W. Flanagin, C.G. Willson. *Proc. SPIE*, 2001; **4345**, 37.

M. Cheng, E. Croffie, A. Neureuther, *Proc. SPIE*, 1999; **3678**, 867.

C. Coenjarts, J. Cameron, N. Deschamps, D. Hambly, G. Pohlers, C. Scaiano, R. Sinta, S. Virda, A. Zampini. *Proc. SPIE*, 1999; **3678**, 1062.

J. Crank, *The Mathematics of Diffusion*, 2nd ed., Oxford University Press: Oxford, UK, 1975.

J.V. Crivello, J.H. Lam. *J. Polym. Sci.: Polym Chem. Ed.,* 1979; **17**, 977.

J.V. Crivello. *J. Polym. Sci. A,* 1999; **37***,* 4241.

E. Croffie, M. Cheng, A. Neureuther, *J. Vac. Sci. Technol. B*, 1999; **17**, 3339.

R.A. Dammel, *Diazonapthoquinone-based Resists*, SPIE Optical Engineering Press: Bellingham, WA, 1993**.**

P.M. Dentinger, B. Lu, J.W. Taylor, S.J. Bukofsky, G.D. Feke, D. Hessman, R.D. Grober. *J. Vac. Sci. Technol. B*, 1998; **16**, 3767.

D. J. Ehrlich, M. Rothschild. *Microelectronic Eng.*, 1989; **9**, 27.

T.H. Fedynyshyn, M.F. Cronin, C.R. Szmanda. *J. Vac. Sci. Technol. B*, 1991; **9**, 3380.

T.H. Fedynyshyn, C.R. Szmanda, R.F. Blacksmith, W.E. Houck. *Proc. SPIE*, 1993; **1925**, 2.

T. Fedynyshyn, J. Thackeray, J. Georger, M. Denison, *J. Vac. Sci. Technol. B*, 1994; **12**, 3888.

T.H. Fedynyshyn, J.W Thackeray, J.M. Mori. *Microelectron. Eng.*, 1994; **23**, 315.

L.W. Flanagin, V.K. Singh, and C.G. Willson, *J. Vac. Sci. Technol. B*, 1999; **17**, 1371.

J.M.J. Fréchet, H. Ito, C.G. Willson. *Proc. Microcuit Eng*., 1982; 260.

D.S. Fryer, S. Bollepali, J.J. de Pablo, P.F. Nealey. *J. Vac. Sci. Technol. B*, 1999; **17**, 3351.

H. Fujita, A. Kishimoto, K. Matsumoto. *Transactions Faraday Soc*., 1960; **56**, 424.

Allen B. Gardiner, *Ph.D. Dissertation*, The University of Texas at Austin, 1999.

S. Glasstone, K.J. Laidler, H. Eyring, *The Theory of Rate Processes*, McGraw-Hill: New York, 1941.

N. Glezos, G.P. Patsis, I. Raptis, P. Argitis, M. Gentili, L. Grella. *J. Vac. Sci. Technol. B*, 1996; **14**, 4252.

D.L. Goldfarb, M. Angelopoulos, E.K. Lin, R.L. Jones, C.L. Soles, J.L. Lenhart, W. Wu. *J. Vac. Sci. Technol. B*, 2001; **19**, 2699.

R.R. Gupta, K.A. Lavery, T.J. Francis, J.R.P. Webster, G.S. Smith, T.P. Russell, J.J. Watkins. *Macromolecules*, 2003; **36**, 346.

D. Hall, J. Torkelson. *Macromolecules*, 1998; **31**, 8817-8825.

A.L. Hines, R.N. Maddox, *Mass Transfer Fundamentals and Applications*, Prentice Hall: Englewood Cliffs, NJ, 1985.

D. He, F. Cerrina. *J. Vac. Sci. Technol. B*, 1998; **16**, 3748.

F.A. Houle, W.D. Hinsberg, M. Morrison, M.I. Sanchez, G.M. Wallraff, C. Larson, J. Hoffnagle. *J. Vac. Sci. Technol. B*, 2000; **18**, 1874.

T. Itani, H. Yoshino, M. Fujimoto, K. Kasama. *J. Vac. Sci. Technol. B*, 1995; **13**, 3026.

T. Itani, H. Yoshino, S. Hashimoto, M. Yamana, N. Samoto, K. Kasama. *J. Vac. Sci. Technol. B*, 1996; **14**, 4226.

T. Itani, H. Yoshino, S. Hashimoto, M. Yamana, N. Samoto, K. Kasama. *J. Vac. Sci. Technol. B*, 1997; **15**, 2541.

H. Ito, C.G. Willson. *Polym. Eng. Sci.*, 1983; **23**, 1012.

H. Ito, C.G. Willson. *Polymers in Electronics*; T. Davidson, Ed.; ACS Symposium Series 242, American Chemical Society, Washington D.C. 1984.

H. Ito, C.G. Willson, J. M. J. Fréchet. U.S. Patent 4,491,628, 1985.

H. Ito, G. Breyta, D. Hofer, R. Sooriyakunaran, K. Petrillo, D. Seeger. *J. Photopolym. Sci. Technol.*, 1994; **7**, 433.

H. Ito, M. Sherwood, *Proc. SPIE*, 1999; **3678**, 104-115.

D. Kang, E.K. Pavelchek, C. Swible-Keane. *Proc. SPIE*, 1999; **3678**, 877.

D. Kang, S. Robinson. *Proc. SPIE*, 2002; **4690**, 963.

A. Karim, B.H. Arendt, G.P. Felcher, T.P. Russell. *Thin Film Solids*. 1991; **1202**, 345.

C.H. Kim, C.U. Jeon, S.W. Choi, W.S. Han, J.M. Sohn. *Proc. SPIE,* 2001; **4186**, 108.

J. Kim, J. Choi, Y. Kwon, M. Hung, K. Chang. *Polymer*, 1999; **40**, 1087.

H.P Koh, Q.Y. Lin, X. Hu, L. Chan. *Proc. SPIE,* 2000; **3999**, 240.

A.A. Krasnoperova, M. Khan, S Rhyner, J.W. Taylor, Y. Zhu, F. Cerrina. *J. Vac. Sci. Technol. B,* 1994; **12**, 3900.

A. Kumar, R.K. Gupta. *Fundamentals of Polymers*, McGraw-Hill: New York, 1998.

J. Lewellen, E. Gurer, E. Lee, L. Chase, L. Dulmage. *Proc. SPIE*, 1999; **3882**, 45.

E. Lin, W. Wu, S. Satija. *Macromolecules***,** 1997; **30,** 7224-7231.

E.K. Lin, C.L. Soles, D.L. Goldfarb, B.C. Trinque, S.D. Burns, R.L. Jones, J.L. Lenhart, M. Angelopoulos, C.G. Willson, S.K Satija, W. Wu. *Science*, 2002; **297**, 372.

F.A. Long, D. Richman. *J. Am. Chem. Soc.*, 1960; **82**, 513.

B. Lu, J.W. Taylor, F. Cerrina, C.P. Soo, A.J. Bourdillon. *J. Vac. Sci. Technol. B*, 1999; **17**, 3345.

S.A. MacDonald, H. Schlosser, N.J. Clecak, C.G. Willson, J.M.J Fréchet. *Chem. Mater*., 1992; **4**, 1364.

S.A. MacDonald, W.D. Hinsberg, H.R. Wendt, N.J. Clecak, C.G. Willson, C.D. Snyder. *Chem. Mater*., 1993; **5**, 348.

S.A. MacDonald, C.G. Willson, J.M.J. Fréchet. *Accounts Chem. Res.*, 1994; **27**, 150.

C.A. Mack, *Inside Prolith*, Finle Technologies: Austin, Texas, 1997.

C.A. Mack. *Microlithography World*, **9-2**, 25-26 (Spring 2000)

C.A. Mack. *Microlithography World*, **9-4**, 25 (Autumn 2000)

Chris A. Mack, *Ph.D. Dissertation*, The University of Texas at Austin, 1998.

P.J. Meares, *J. Am. Chem. Soc.,* 1954; **76**, 3415.

D.R. Medeiros, A. Aviram, C.R. Guarnieri, W.S. Huang, R. Kwong, C.K. Magg, A.P. Mahorowala, W.M. Moreau, K.E. Petrillo, M. Angelopoulos. *IBM J. Res. Dev*., 2001; **45**, 639.

Katherine E. Mueller, *Ph.D. Dissertation*, The University of Texas at Austin, 1998.

P. Munk, *Introduction to Macromolecular Science*, John Wiley & Sons, New York, 1989.

J. Nakamura, H. Ban, K. Deguchi, A. Tanaka. *Jpn. J. Appl. Phys. Part 1*, 1991; **30**, 2619.

O. Nalamasu, E. Reichmanis, J. E. Hanson, R. S. Kanga, L. A. Heimbrook, A. B. Enerson, F. A. Baiocchi, S. Vaidya. *Polym. Eng. Sci.*, 1992; **32**, 1565.

L.E. Ocola, F. Cerrina, T. May. *J.Vac. Sci. Technol. B*, 1997; **15**, 2545.

J.S. Petersen, C.A. Mack, J. Sturtevant, J.D. Byers, D.A. Miller. *Proc. SPIE*, 1995; **2438**, 167.

S.V. Postnikov, M.D. Stewart, H.V. Tran, M.A. Nierode, D.R. Medeiros, T. Cao, J. Byers, S.E. Webber, C.G. Willson. *J. Vac. Sci. Technol. B*, 1999; **17**, 3335.

Sergei V. Postnikov, *Ph.D. Dissertation*, The University of Texas at Austin, 1999.

I. Raptis. *Jpn. J. Appl. Phys*., 1997; **36**, 17.

B. Rathsack, C. Tabery, J. Albelo, P. Buck, C.G. Willson. *Proc. SPIE*, 2001; **4186**, 8163.

N. Rau, F. Stratton, C. Fields, T. Ogawa, A. Neureuther, R. Kubena, C.G. Willson. *J. Vac. Sci. Technol. B*, 1998; **16**, 3784.

A. Reiser, *Photoreactive Polymers – The Science and Technology of Resists*, J. Wiley & Sons, New York, 1989**.**

G.W. Reynolds, J.W. Taylor. *J. Vac. Sci. Technol. B*, 1991; **17**, 334.

G.W. Reynolds, J.W. Taylor, C.J. Brooks. *J. Vac. Sci. Technol. B*, 1999; **17**, 3420.

H. Roeschert, K. Przybilla, W. Spiess, H. Wengenroth, G. Pawlowski. *Proc. SPIE*, 1992; **1672**, 33.

M.I. Sanchez, W.D. Hinsberg, F.A. Houle, J.A. Hoffnagle, H. Ito, and C. Nguyen. *Proc. SPIE*, 1999; **3678**, 160.

R. E. Schenker, L. Eichner, H. Vaidya, S. Vaidya, W. G. Oldham. *Proc. SPIE*, 1995; **2440**, 118.

L. Schlegel, T. Ueno, N. Hayashi, T. Iwayanagi. *Jpn. J. Appl. Phys.*, 1991; **11B**, 30.

L. Schlegel, T. Ueno, N. Hayashi, T. Iwayanagi. *J. Vac. Sci. Technol. B*, 1991; **9**, 278.

G.M. Schmid, V.K. Singh, L.W. Flanagin, M.D. Stewart, S.D. Burns, C.G. Willson. *Proc. SPIE*, 2000; **3999**, 675.

G.M. Schmid, M.D. Smith C.A. Mack, V.K. Singh, S.D. Burns, C.G. Willson. *Proc. SPIE*, 2001; **4345**, 1037.

G.M. Schmid, M.D. Stewart, V.K. Singh, and C.G. Willson. *J. Vac. Sci. Technol. B*, 2002; **20**, 185.

Gerard M. Schmid, *Ph.D. Dissertation*, The University of Texas at Austin, 2003.

A. Sekiguchi, Y. Miyake, M. Isono. *Jpn. J. Appl. Phys.*, 2000; **39**, 1392.

X. Shi. *J. Vac. Sci. Technol. B*, 1999; **17(2)**, 350.

X. Shi, B. Socha, J. Bendik, M. Dusa, W. Conley, B. Su. *Proc. SPIE*, 1999; **3678**, 777.

J. Shin, G. Han, Y. Ma, K. Moloni, and F. Cerrina. *J. Vac. Sci. Technol. B*, 2001; **19**, 2890.

E. Shiobara, D. Kawamura, K. Matsunaga, T. Koibe, S. Mimotogi, T. Azuma and Y. Onishi. *Proc. SPIE*, 1998; **3333**, 313.

Mark H. Somervell, *Ph.D. Dissertation*, The University of Texas at Austin, 2000

M.D. Stewart, S.V. Postnikov, H.V. Tran, D.R. Medeiros, M.A. Nierode, T. Cao, J. Byers, S.E. Webber, C G. Willson. *ACS Polymeric Mat. Sci. Eng.*, 1999; **81**, 58.

M.D. Stewart, G.M Schmid, S.V. Postnikov, C.G. Willson. *Proc. SPIE*, 2001; **4345**, 10-18.

M.D. Stewart, G.M. Schmid, D.L. Goldfarb, M. Angelopoulos, C.G. Willson. *Proc. SPIE,* 2003; **5039**, 415.

J. Sturtevant, S. Holmes, P. Rabidoux. *Proc. SPIE*, 1992; **1672**, 114.

N.L Thomas, A.H. Windle. *Polymer*, 1978; **19**, 255.

L. F. Thompson, C. G. Willson, M.J. Bowden, *Introduction to Microlithography*, American Chemical Society, Washington D.C., 1994.

Hoang Vi Tran, *Ph.D. Dissertation*, The University of Texas at Austin, 2002.

Brian Trinque, *Ph.D. Dissertation*, The University of Texas at Austin, 2003.

S. Uchino, J. Yamamoto, S. Migitaka, K. Kojima, M. Hashimoto, F. Murai, H. Shiraishi. *J. Photopolym. Sci. Technol*., 1998; **11**, 555.

C.P. Umbach, A.N. Broers, C.G. Willson, R. Koch, R.B. Laibowitz. *J. Vac. Sci. Technol. B*, 1988; **6**, 319.

C.P. Umbach, A.N. Broers, C.G. Willson, R. Koch, R.B. Laibowitz. *IBM J. Res. Dev.*, 1988; **32**, 454.

T. Ushirogouchi, K. Asakawa, M. Nakase and A. Hongu. *Proc. SPIE*, 1995; 2438, 160.

G.M. Wallraff, W.D. Hinsberg, F.A. Houle, M. Morrison, C.E. Larson, M. Sanchez, J. Hoffnagle, P.J. Brock, G. Breyta. *Proc.* SPIE, 1999; **3678**, 138.

H. Watanabe, H. Sumitani, T. Kumada, M. Inoue, K. Marumoto, Y. Matsui. *Jpn. J. Appl. Phys*., 1995; **34**, 6780.

M. Wessling, S. Schoeman, T.v.d. Boomgaard, C.A. Smolders. *Gas Sep. Purif.,* 1991; **5**, 222.

S.J. Whitlow, R.P. Wool. *Macromolecules*, 1989; **22**, 2648.

M.L. Williams, R.F Landel, J.D. Ferry. *J. Am. Chemical Soc*., **77**, 1955.

C.G. Willson, R.A. Dammel, A. Reiser. *Proc. SPIE*, 1997; **3051**, 28.

J.D. Wind, S.M. Sirard, D.R. Paul, P.F. Green, K.P. Johnston, W.J. Koros. *Macromolecules*, 2003; **36**, 6433.

T. Yamaguchi, H. Namatsu, M. Nagase, K. Kurihara, Y. Kawai. *Proc. SPIE*, 1999; **3678**, 617.

T. Yamaguchi, H. Namatsu, M. Nagase, K. Yamazaki, K. Kurihara. *Appl. Phys. Lett.*,1997; **71**, 2388.

T. Yoshimura, Y. Nakayama, S. Okazaki. *J. Vac. Sci. Technol. B,* 1992; **10**, 185.

T. Yoshimura, Y. Nakayama, S. Okazaki. *J. Vac. Sci. Technol. B*, 1992; **10**, 2615.

T. Yoshimura, H. Shiraishi, T. Terasawa, S. Okazaki. *J. Vac. Sci. Technol. B,* 1996; **14**, 4216.

P. Zandbergen, H.J. Dijkstra. *Microelectron. Eng.*, 1994; **23**, 299.

P.L. Zhang, S.E. Webber, J. Mendenhall, J.D. Byers, K. Chao. *Proc. SPIE*, 1998; **3333**, 794.

P.L Zhang, A.R. Eckert, C.G. Willson, S.E. Webber, J.D. Byers. *Proc. SPIE*, 1997; **3049**, 898.

M.A. Zuniga, G. Wallraff, E. Tomacruz, B. Smith, C. Larson, W.D. Hinsberg, A.R. Neureuther. *J. Vac. Sci. Technol. B,* 1993; **11**, 2862.

M.A. Zuniga, A.R. Neureuther. *J. Vac. Sci. Technol. B*, 1995; **13**, 2957.

M.A. Zuniga, A.R. Neureuther. *J. Vac. Sci. Technol. B*, 1996; **14**, 4221.

Vita

Michael Dean Stewart was born on December 2, 1974 in Augusta, GA, the youngest child of Joy Rambin and Tommy Ray Stewart. He graduated from Riverdale High School in Murfreesboro, TN in 1993. He enrolled at Vanderbilt University and graduated in 1997 with a Bachelor of Engineering degree in Chemical Engineering. He began graduate study at The University of Texas at Austin in 1998, finishing in December 2003 with Doctorate of Philosophy degree in Chemical Engineering.

Permanent address: 2110 Stratford Rd., Murfreesboro, TN 37129

This dissertation was typed by the author.